

Electronic Thesis and Dissertation Repository

9-15-2014 12:00 AM

Magnitude Estimation for Earthquake and Tsunami Early Warning Systems

Attieh Eshaghi
The University of Western Ontario

Supervisor
Dr. Kristy Tiampo
The University of Western Ontario

Graduate Program in Geophysics
A thesis submitted in partial fulfillment of the requirements for the degree in Doctor of Philosophy
© Attieh Eshaghi 2014

Follow this and additional works at: <https://ir.lib.uwo.ca/etd>



Part of the [Geophysics and Seismology Commons](#)

Recommended Citation

Eshaghi, Attieh, "Magnitude Estimation for Earthquake and Tsunami Early Warning Systems" (2014).
Electronic Thesis and Dissertation Repository. 2451.
<https://ir.lib.uwo.ca/etd/2451>

This Dissertation/Thesis is brought to you for free and open access by Scholarship@Western. It has been accepted for inclusion in Electronic Thesis and Dissertation Repository by an authorized administrator of Scholarship@Western. For more information, please contact wlsadmin@uwo.ca.

Magnitude Estimation for Earthquake and Tsunami Early Warning Systems

(Thesis format: Integrated Article)

by

Attieh Eshaghi

Graduate Program in Geophysics

A thesis submitted in partial fulfillment
of the requirements for the degree of
Doctor of Philosophy

The School of Graduate and Postdoctoral Studies

The University of Western Ontario

London, Ontario, Canada

© Attieh Eshaghi, 2014

Abstract

In this study, different magnitude estimation methods were investigated for application to earthquake early warning (EEW) and tsunami early warning systems. This integrated study is divided into two main parts. First, I used strong motion accelerograms recorded by borehole and surface stations from the Kiban Kyoshin network (KiK-net) for Japanese earthquakes with moment magnitude (M) ≥ 5.0 in order to develop ground motion prediction equations (GMPEs). I developed new GMPEs for peak ground acceleration (PGA) and peak ground velocity (PGV) using two different catalogs. The first catalog included earthquakes with $5.0 \leq M \leq 8.1$ from 1998-2010. In order to improve the determination of attenuation parameters and magnitude scaling, the second catalog included earthquakes with $5.0 \leq M \leq 9.0$ from 1998-2011, which increased the time period by only one year but added approximately twice as much data to the first catalog. The GMPEs were used to estimate the magnitude from PGA values (M_{pga}) and from PGV values (M_{pgv}) for those events in the borehole and surface databases with at least 20 available records. The results confirmed that M_{pga} and M_{pgv} strongly correlate with the moment magnitude of the event. In addition, I studied the site effect terms in the GMPEs using the shear wave velocity in the uppermost 30 meters (VS30). It was found that correcting for VS30 improved the accuracy of magnitude estimates from surface recordings, particularly for M_{pgv} . Incorporation of this parameter into the GMPEs can provide a more accurate estimate of the earthquake magnitude in EEW systems. The GMPEs also were used to estimate the magnitude of the M9.0 Tohoku event and those estimates were compared with the magnitude estimates provided by the existing EEW system in Japan. I demonstrate that, unlike the estimates provided by the existing EEW

system in Japan, the magnitude estimates from GMPEs do not saturate. The results demonstrate that M_{pgv} from borehole recordings had the smallest standard deviation among the estimated magnitudes and produced more stable and robust magnitude estimates. Based on this observation, I propose the incorporation of borehole recordings into EEW systems. This method can improve the existing EEW system in Japan or other regions that have a dense seismic network.

In the second part of this thesis, the displacement spectra of the strong ground motion recordings were used to directly estimate the magnitude of Japanese earthquakes with $4.5 \leq M \leq 9.0$, 2000 to 2011, using the first available data provided by the KiK-net and Kyoshin network stations. The source parameters were determined using the inversion of displacement spectra for available P- and S-waves windows assuming the Brune source model. I tested the application of a fixed low-cut filter, and found that it decreases the accuracy of magnitude estimation for large events ($M > 7.0$). As a result, instead of a fixed low-cut filter I applied a frequency bandwidth cutoff based on a signal-to-noise ratio criterion. The results showed that magnitude estimation using the strong motion recordings from the closest station to the source of the event provides a good early estimate for the final size of the event, which can reduce the time required to calculate final magnitude and hence provides a longer warning time (from a few seconds to a few minutes). The results also indicated that the predicted magnitude based on the P-wave window (M_P) provides a longer warning time, but with a larger uncertainty, in comparison to the estimation based on the S-wave window (M_S). The magnitude estimate based on inversion of the displacement spectra is independent of magnitude scaling relationships, as is the case with magnitude vs. early P-wave parameter

relationships or GMPEs, because it determines the moment magnitude from the estimated source parameters directly from the displacement spectra. Therefore, this method can be used in regions with sparse seismic networks where historic recordings of strong ground motion from potentially damaging earthquakes are not available to develop an empirical relationship, such as the Cascadia region of North America.

Keywords: Earthquake early warning system; ground motion prediction equation; moment magnitude; magnitude estimation; Brune source model; Japan.

Co-Authorship Statement

The materials presented in chapters 2, 3, and 4 of this thesis were previously published or submitted for publication to two peer-reviewed journals, *Bulletin of Seismological Society of America* and *Pure and Applied Geophysics*. This thesis contains only the original results of research conducted by the candidate under supervision of her mentor.

The original contributions are summarized as follows:

Strong ground-motion data acquisition from the K-NET (1998-2011) and KiK-net (2000-2011) networks ($M \geq 4.5$); data processing of the recorded earthquake waveforms for Japan region; calculation/tabulation of ground-motion parameters including peak ground acceleration, peak ground velocity and Fourier spectral amplitudes (FSA); regression analysis and derivation of a new form of ground motion prediction equation (GMPE); calculating V_{S30} for KiK-net stations; site effect studies (linear form) for all of the KiK-net stations using the estimates for V_{S30} ; statistical analysis, including of analysis of residuals and standard deviations; moment magnitude determination using the estimated GMPEs for large Japanese earthquakes; determination of the source parameters through inversion of the displacement spectra; moment magnitude determination based on the obtained source parameters.

Dr. Tiampo, Dr. Atkinson and Dr. Ghofrani were my co-authors in all of the articles presented in this thesis.

The work for this project was completed under supervision and financial support of Dr. Tiampo. She provided instruction and guidance on the challenges of the statistical analysis and interpretation of the results.

Dr. Ghofrani provided discussions/instruction on processing of seismic data and interpreting of earthquake ground-motion data.

Dr. Atkinson assisted with interpretation and suggestions, reviewing all of the papers.

An additional co-author of the paper in Chapter 4 is Dr. González, who assisted with the nonlinear inversion code and provided discussion on statistical analysis of the results.

Acknowledgments

I would like to give my heartfelt thanks to the following people. Without them, the completion of this thesis would be impossible.

First of all, I offer my sincerest gratitude to my supervisor Professor Kristy F. Tiampo for her support and advice throughout the completion of this research while giving me the freedom to work in my own way. I would also like to extend my gratitude to Dr. Hadi Ghofrani, Professor Gail Atkinson and Dr. Pablo González who are my co-authors. They generously provided me with useful information, discussion, and helpful suggestions in reviewing my articles. Their cooperation and discussions made my research move forward.

I offer my special thanks to all staff and fellow graduate students at Western University especially Marie Schell, John Brunet, Claire Mortera, and Margaret Moulton for their kindness, support and love, which made my life easier in Canada. I would also like to thank Bernie Dunn for his technical support.

I would last, but not least, thank my parents, my brothers, my sister and my friends for their encouragement, constant love and support in one way or the other throughout every adventure, including graduate school.

To my parents: *Sedigheh and Ali Asghar*

Table of Contents

Abstract.....	II
Co-Authorship Statement.....	V
Acknowledgments.....	VII
Table of Contents	IX
List of Tables	XIII
List of Figures	XIV
List of Appendices	XX
List of frequently-used symbols and acronyms	XXI
Chapter 1	1
1 General Introduction	1
1.1 Objective	1
1.2 Introduction	1
1.2.1 Front Detection	5
1.2.2 P-Wave parameters	6
1.2.3 Onsite Approach (Single station).....	8
1.2.4 Regional Approach (Network-based)	9
1.3 Earthquake Magnitude	9

1.4	Earthquake Ground Motions	10
1.4.1	Source Model	11
1.4.2	Path	13
1.4.3	Site	14
1.4.4	Ground Motion Prediction Equations (GMPEs).....	14
1.5	Japanese Data	16
1.6	Organization of thesis.....	17
1.7	References	19
	Chapter 2.....	26
2	Using Borehole Records to Estimate Magnitude for Earthquake and Tsunami Early-Warning Systems	26
2.1	Introduction	28
2.2	Strong Ground Motion Database.....	30
2.3	Strong Ground Motion Prediction Equation	34
2.4	Ground-Motion Prediction Equation for Borehole Record Database	38
2.5	Ground-Motion Prediction Equation for Surface Record Database.....	40
2.6	Magnitude Estimation	40
2.7	Site Effects Term.....	43
2.8	Conclusions	45
2.9	References	47

Chapter 3.....	52
3 Magnitude Estimation for the 2011 Tohoku-Oki Earthquake Based on Ground Motion Prediction Equations	52
3.1 Introduction	54
3.2 Performance of the Existing EEW System for the M9.0 Tohoku Earthquake... 58	
3.3 Strong Ground Motion Databases	59
3.4 New Strong Ground Motion Prediction Equation.....	61
3.5 Magnitude Estimation for M9.0 Tohoku Event	65
3.6 Results Using New GMPEs	71
3.7 Discussion and Conclusions.....	74
3.8 References:	80
Chapter 4.....	86
4 Real-Time Moment Magnitude Estimation from Displacement Spectral Inversion 86	
4.1 Introduction	88
4.2 Spectral Analysis.....	91
4.3 Data and processing	93
4.4 Results	101
4.5 Discussion and Conclusions.....	113
4.6 References:	119
Chapter 5.....	127

5	Conclusions and future studies	127
5.1	Summary and conclusions.....	127
5.2	Suggestions for future studies	131
5.3	References	133
	Appendices.....	134
	Curriculum Vitae	166

List of Tables

Table 2.1 Standard deviation for predicted magnitude.	30
Table 2.2. Epicentral Distance Cutoffs (R_c) for Each Event.....	32
Table 2.3 Data Employed in Regression Analysis.....	33
Table 3.1 Data used in this study	58
Table 3.2 Equation 1 parameters for each database.	60
Table 3.3 Equation 3.3 parameters for surface recordings.....	64
Table 3.4 Estimated magnitudes, Tohoku earthquake.	68
Table 3.5 Standard deviation for predicted magnitude	70
Table 3.6 Estimated magnitudes for Tohoku earthquake based on Catalogs 3 and 4.....	71
Table 3.7 The history of magnitude estimation in each issuance of EEW for $M_{JMA} = 7.2$ ($M = 6.9$) earthquake on 14/06/2008 (from Kamigachi et al., 2009)	75
Table 3.8 The history of moment magnitude estimation using the proposed method in this study for $M6.9$ earthquake on 14/06/2008 (Borehole database, Catalog 2).	76
Table 4.1 Mean residuals for the predicted magnitude (moment magnitude) using the single station approach.....	96

List of Figures

- Figure 2.1** Distribution of the KiK-net stations (solid triangles) that recorded the selected events. (a) The distribution of borehole stations. (b) The surface stations that recorded the selected events. Open circles are the epicenters of the earthquakes used in this study for each database. 35
- Figure 2.2** Magnitude-epicentral distance distributions for (a) borehole database and (c) surface database. Magnitude-focal depth for the (b) borehole database and (d) surface database..... 36
- Figure 2.3** Distribution of residuals versus epicentral distance for PGA and PGV for the (a and b) borehole record database and (c and d) surface record database. Different symbols show the range of magnitudes. Large square symbols show the mean value of the residuals contained in a specific distance bin, whereas bars represent ± 1 standard deviation..... 37
- Figure 2.4** The histogram of the residuals for PGA and PGV for the (a and b) borehole record database and (c and d) surface record database. σ represents the standard deviation of the residuals. Solid curves represent normal distributions with zero mean and given standard deviation. 39
- Figure 2.5** Map of KiK-net stations that recorded PGA and PGV for the 23 October 2004 M6.6 event (a) for borehole records with $PGA \geq 10 \text{ cm/s}^2$ and (b) for surface records with $PGA \geq 80 \text{ cm/s}^2$. Mpga versus time (seconds) after origin time for current (c) borehole dataset, and (d) surface dataset. Mpgv versus time (seconds) after origin time for current (e) borehole dataset, and (f) surface dataset..... 42

Figure 2.6. Map of KiK-net stations that recorded PGA and PGV for the 16 August 2005 M7.1 event for (a) borehole records with $PGA \geq 10 \text{ cm/s}^2$ and (b) surface records with $PGA \geq 80 \text{ cm/s}^2$. Mpga versus time (seconds) after origin time for current (c) borehole dataset and (d) surface dataset. Mpgv versus time (seconds) after origin time for current (e) borehole dataset, and (f) surface dataset.....	44
Figure 2.7 (a) Histograms of the site terms for magnitude estimates from PGA values. (b) Histograms of the site terms for magnitude estimates from PGV values.	45
Figure 2.8 M versus predicted magnitude (Mpga and Mpgv) for the (a, b) borehole database and (c, d) surface dataset.....	47
Figure 3.1 Spatial distribution of the epicenter of selected events (Catalog 2) used in this study (open circles). KiK-net stations (grey triangles) that registered the (a) borehole recordings with $PGA \geq 10 \text{ cm/s}^2$ and (b) surface recordings with $PGA \geq 80 \text{ cm/s}^2$. KiK-net stations that recorded the Tohoku event are identified as red triangles. The star represents the epicenter of 2011 Tohoku event.	63
Figure 3.2 Magnitude-focal depth for borehole database (a) and surface database (c). Magnitude-epicentral distance distributions for the borehole database (b) and surface database (d).	66
Figure 3.3 Distribution of residuals against epicentral distances for the borehole record database from Equation 3.1 for PGA and PGV (a and b respectively) and for the surface record database from Equation 3.2 for PGA and PGV (c and d respectively). Different symbols show the range of magnitudes. Large square symbols show the mean value of the residuals contained in a specific distance bin, where bars represent ± 1 standard deviation.....	69

Figure 3.4 The histogram of the residuals for PGA and PGV for the borehole record database (a, b) and surface record database (c, d). r represents the standard deviation of the residuals. Solid curves represent normal distributions with zero mean and given standard deviation. 72

Figure 3.5 M_{pga} and M_{pgv} versus time (seconds) after OT for **M**9.0 Tohoku event based on GMPEs obtained from Catalog 1. M_{pga} versus time for current (a) borehole dataset and (c) surface dataset. M_{pgv} versus time for current (b) borehole dataset and (d) surface dataset. EEW M is the magnitude estimated by the existing EEW system in Japan. Solid line shows the moment magnitude ($M = 9.0$)..... 73

Figure 3.6 M_{pga} and M_{pgv} versus time (seconds) after OT for **M**9.0 Tohoku event based on GMPEs obtained from Catalog 2. M_{pga} versus time for current (a) borehole dataset and (c) surface dataset. M_{pgv} versus time for current (b) borehole dataset and (d) surface dataset. EEW M is the magnitude estimated by the existing EEW system in Japan. Solid line shows the moment magnitude ($M = 9.0$) 74

Figure 3.7 Magnitude estimation history in real time given by new GMPEs along with the reported M for borehole database (left) and surface database (right) for **M**6.6 (23/10/2004), **M**6.9 (14/06/2008), and **M**5.9 (12/04/2011). Solid line represents the moment magnitude..... 78

Figure 3.8 M versus predicted magnitude (M_{pga} and M_{pgv}) for Catalog 2 for the borehole database (a and b) and surface dataset (c and d). The solid line shows the 1:1 relation and dashed lines show one standard deviation. 80

Figure 4.1 Spatial distribution of the events used in this study recorded by (a) KiK-net stations, and (b) K-net stations. Every station did not record all the events..... 94

Figure 4.2 Magnitude vs. focal depth distribution used in this study for (a) KiK-net and (b) K-net database. Magnitude vs. epicentral distance distribution for (c) KiK-net and (d) K-net database used in this study..... 99

Figure 4.3 Observed and inverted spectra of (a) P-waves and (b) S-waves of the vertical components for the October 23, 2009, **M5.0** event at a hypocentral distance of 108.2 km; the March 23, 2011, **M6.1** event at a hypocentral distance of 101.45 km; the August 16, 2005, **M7.1** event at a hypocentral distance of 110.6 km; and the September 26, 2003, **M8.1** Tokachi-Oki event at a hypocentral distance of 117 km. The inverted spectra shown are computed for the frequency range where the signal/noise ratio is larger than 3. 100

Figure 4.4 Example of observed and inverted spectra of P- and S-waves (vertical component) for the April 12, 2011 **M4.5** event at 25.44 km hypocentral distance. (a) Vertical component of the acceleration time series from the FKSH12 KiK-net borehole station; black arrows show the selected P- and S- phase windows (3 and 6 sec respectively). (b) Observed and inverted P-wave spectra; **MP** and f_c are **M5.1** and 0.76 (Hz) respectively (c) observed and inverted S-wave spectra; **MS** and f_c are **M4.9** and 0.72 (Hz) respectively..... 102

Figure 4.5 Example of observed and inverted spectra of P- and S-waves (vertical component) for the August 5, 2011 **M4.9** event at 104.57 km hypocentral distance. (a) Vertical component of the acceleration time series from the IWTH02 KiK-net borehole station; black arrows show the selected P- and S- phase windows (12.45 and 13 sec respectively). (b) Observed and inverted P-wave spectra; **MP** and f_c are **M5.2** and 0.99

(Hz) respectively and (c) observed and inverted S-wave spectra; **MS** and f_c are **M4.7** and 2.5 (Hz) respectively. 103

Figure 4.6 Example of observed and inverted spectra of P- and S-waves (vertical component) for the January 18, 2006 **M5.5** event at 115.4 km hypocentral distance. (a) Vertical component of the acceleration time series from the MYGH11 KiK-net borehole station; black arrows show the selected P- and S- phase windows (13.74 and 16 sec respectively). (b) Observed and inverted P-wave spectra; **MP** and f_c are **M5.7** and 0.46 (HZ) respectively and (c) observed and inverted S-wave spectra; **MS** and f_c are **M5.43** and 0.78 (Hz) respectively. 104

Figure 4.7 Ppredicted magnitude (**MP**, **MS** and **MPS**) versus **M** for the KiK-net borehole database (a, b and c), the KiK-net surface database (d, e and f) and the K-net database (g, h and i). The solid line is the 1:1 relation and dashed lines are one standard deviation..... 105

Figure 4.8 Distribution of magnitude residuals ($M_{\text{predicted}} - M_{\text{reported}}$) against epicentral distances. **MP** residuals vs. epicentral distance distribution for (a) KiK-net borehole, (b) KiK-net surface, and (c) K-net database. **MS** residuals vs. epicentral distance distribution for (d) KiK-net borehole, (e) KiK-net surface, and (f) K-net database. 107

Figure 4.9 Observed and inverted spectra of P- and S-waves (vertical component) for the three largest events in this study. The P- and S-waves spectra from the KiK-net borehole stations for (a) the September 26 2003 **M8.1** Tokachi-Oki event, at 111.68 km hypocentral distance, (b) the 11 March 2011 **M9.0** Tohoku event, at 139.38 km hypocentral distance, and (c) the 11 March 2011 **M7.8** Tohoku aftershock event at 71.8 km hypocentral distance. 109

Figure 4.10 Predicted magnitude (**MP** and **MS**) versus time (seconds) after the first P- and S-wave arrivals for the September 26, 2003 **M8.1** Tokachi-Oki event. **MP** and **MS** versus time using the closest station for the KiK-net borehole stations (a and b); KiK-net surface stations (c and d); and K-net stations (e and f). The solid line represents the reported moment magnitude. 111

Figure 4.11 P-phase window and S-phase windows of the vertical component of the strong ground motion record at the closest (a) MYGH12 KiK-net borehole (b) MYGH12 KiK-net surface and (c) MYG011 K-net station to the epicenter of the March 11, 2011 **M9.0** Tohoku event..... 112

Figure 4.12 Predicted magnitude (**MP** and **MS**) and **EEW M** versus time (seconds) after the first P- and S-wave arrivals for the March 11, 2011 **M9.0** Tohoku event. **MP** and **MS** versus time using the closest station for the KiK-net borehole stations (a and b); KiK-net surface stations (c and d); and K-net stations (e and f). The solid line represents the reported moment magnitude. 115

Figure 4.13 Predicted magnitude (**MP** and **MS**) versus time (seconds) after the first P- and S-wave arrivals for the March 11, 2011 **M7.8** Tohoku aftershock event. **MP** and **MS** versus time using the closest station for the KiK-net borehole stations (a and b); KiK-net surface stations (c and d); and K-net stations (e and f). The solid line represents the reported moment magnitude. The solid line represents the reported moment magnitude. 117

List of Appendices

Appendix A: Tables of Results Tables A1 and A2 show the date, moment magnitude, M_{pga} , M_{pgv} , latitude, longitude and number of records used in magnitude estimation for borehole and surface recording database in Catalog 2 respectively.

Appendix B: Table B1 compares the mean residuals and standard deviations for the predicted magnitude (moment magnitude) using filtered and unfiltered data. Figure B1 shows the predicted magnitude versus moment magnitude for filtered databases.

Appendix C: Computer Code

List of frequently-used symbols and acronyms

M	Moment magnitude
GMPE	Ground motion prediction equation
PGA	Peak ground acceleration
PGV	Peak ground velocity
M _{pga}	Magnitude estimation using PGA values
M _{pgv}	Magnitude estimation using PGV values
V _{S30}	Time averaged shear-wave velocity over top 30 m
OT	The time of origin of an earthquake
EEW	Earthquake early warning system
K-net	Kyoshin network which consists of 1034 strong-motion seismographs settled on ground surface.
KiK-net	Kiban Kyoshin network which consists of 660 strong-motion observation stations installed both on the ground surface and at the bottom of boreholes.
NIED	National Research Institute for Earth Science and Disaster Prevention (Japan).
NEHRP	National Earthquake Hazards Reduction Program

M_0	Seismic moment (N.m)
MP	Predicted magnitude using P-phase
MS	Predicted magnitude using S-phase
MPS	Mean value of MP and MS
$\Omega(f)$	Fourier amplitude of the P- or S-wave displacement
Ω_0	Plateau at low frequency
f	Frequency
f_c	Corner frequency
Q	Independent quality factor
t	Travel time of the considered wave
ρ	Density (kg/m^3)
$U_{\theta\theta}$	Mean radiation pattern
σ	Standard deviation
P-waves	P waves are pressure waves generated by an earthquake; P-waves travel with the fastest velocity through Earth
S-waves	Shear waves generated by an earthquake; S-waves do not propagate through liquids

Chapter 1

1 General Introduction

1.1 Objective

The purpose of the research presented in this thesis is to investigate new methods of magnitude estimation for earthquake early warning (EEW) and tsunami early warning systems. The result is the improved performance of EEW and tsunami early warning systems for vulnerable countries exposed to future great earthquakes and/or tsunamis. Alternative methods for magnitude estimation were investigated using a rich, high quality strong ground motion database from Japan with the goals of both improving EEW systems and to effectively translate the outcome of this research to those regions with sparse databases. Furthermore, the results of this study can complement the existing EEW systems in order to provide another constraint for magnitude estimation in those systems.

1.2 Introduction

Earthquakes are one of the most disastrous natural hazards on Earth, and can cause tremendous loss of life and economic losses. For example, over 140,000 people perished in the 1923 Tokyo earthquake (Imamura, 1924) and, more recently, the M9.0 2011 Tohoku-Oki earthquake in Japan killed an estimated 15,000 people and caused an economic cost of US\$235 billion (Mori et al., 2011; Hayes, 2011). There have been many ongoing efforts to prevent and reduce the effects of earthquakes in both the medium- and

long- term. For instance, there are procedures to study the potential seismic sources in each specific area, seismic hazard assessment and risk evaluation, development of seismic building codes to design earthquake-resistant structures, and informing and educating the public about seismic hazard and risk reduction management. Unlike other types of natural hazards such as hurricanes or volcanic eruptions, there is not enough time to take rapid emergency actions such as the evacuation of local residents. The ability to predict earthquakes obviously would be effective, but the nucleation and rupture propagation of earthquakes are complex processes which are controlled by many factors. Because of this complexity, reliable short-term earthquake prediction currently is not possible (Kanamori, 2005; Jordan and Jones, 2010; Jordan and Jones, 2011).

A more practical way to reduce the impact of hazardous earthquakes is through the use of real-time seismic monitoring systems. Recent progress in seismology, including the technology of seismic instrumentation and telecommunication, computers, and data storage facilities, permits the development and implementation of real-time earthquake information systems. These systems are designed to collect and analyze the seismic records during and shortly after a significant seismic event (Kanamori, 2005.) These achievements lead to a new type of short-term earthquake hazard mitigation, EEW systems. The goal of an EEW system is to reduce the damaging effects of earthquakes by providing a few seconds to a few tens of seconds warning before the arrival of damaging ground motion. The physical basis for EEW systems is that destructive S-waves and surface waves travel at about half of the speed of the P-waves and the velocity of seismic waves are much slower than signals transmitted by telephones or radios (Lee and Espinosa-Aranda, 2003). In other words, these systems use the capability of modern real-

time seismic, communications and computing seismic systems to process and transmit information faster than the slower seismic waves propagate (3-6 km/s), once the initial P-wave triggers at the receiver station. The system then provides information that an earthquake is occurring and that potentially damaging ground motion is approaching the user site. Possible warning times vary, depending on the distance between seismic source, sensor and user sites. This timely information can be used to minimize property and structural damage and the loss of lives in urban areas. It also can be used for real-time loss estimation for emergency response and recovery plans (Wu et al., 2002). Operation of the above activity depends on the amount of available warning time, but there is always a trade-off between the amount of available warning time and the reliability of the predictions provided by the EEW system. Reliability of the predictions become more accurate as more seismic sensor data is collected. On the other hand, valuable time is lost for early warning.

The two most important tasks in EEW systems are the rapid estimation of the location of the earthquake (epicentre/hypocenter) and its magnitude (M). From these two parameters, other strong motion parameters (such as intensity and peak ground motion values) are estimated. To provide these parameters, different types of EEW systems currently are implemented or being tested. The classification of EEW systems can vary depending on the type of tectonic environment in which the system is implemented, the technologies that are used to detect hazardous earthquakes and the reliability of those technologies, the length of time needed to produce accurate forecasts, and the types of devices and signals which are used to issue warnings. To make the overall system as robust as possible, it is beneficial to combine as many different methods as possible.

The goal of this research is to improve the robustness of the magnitude estimation for EEW systems, assuming that information about the location of an earthquake is provided by existing EEW networks. Generally, either information from a single seismic station (on-site approach) or information from a seismic network (regional or network-based approach) is used to estimate the earthquake source parameters. Different algorithms to calculate the magnitude of a large earthquake can be implemented in either of these approaches. Most techniques are based on the empirical relationship between magnitude and P-wave parameters such as predominant period (Nakamura, 1998; Kanamori, 2005; Allen et al., 2009), the peak amplitude of the early P-wave (Wu and Zhao, 2006), or a combination of these parameters. However, these methods have some limitations, including the lack of reliability of the magnitude estimates or saturation of the empirical relationships for larger earthquakes (i.e. $M \geq 7.0$) (Rydelek et al., 2007; Yamada and Ide, 2008; Yamada and Mori, 2009).

In this study, I investigated alternative methods to provide real-time early estimations for the magnitude of earthquakes for EEW and tsunami early warning purposes. The large number of accelerometer time series recorded by dense Japanese seismic networks provides an invaluable opportunity to test the ability of these new algorithms to estimate the magnitude of large earthquakes. I applied both regional and single station approaches to estimate the magnitude of events. First, empirical ground motion prediction equations (GMPEs) were employed to calculate the regional magnitude estimation for large earthquakes in Japan (Chapters 2 and 3). The results show that the use of GMPEs for magnitude estimation does not have the saturation problem for large events that exists in empirical relationships such as period parameters-magnitude or peak

amplitude-magnitude relationships (Rydelek et al., 2007; Yamada and Ide, 2008; Yamada and Mori, 2009; Hoshiya et al. 2011). However, because GMPEs are a key component in this method, a high quality and rich database of ground motion recordings that adequately covers the magnitude distance range of interest is needed to develop reliable empirical relationships. Moreover, a dense seismic network is necessary to provide more observations to be used in real-time magnitude estimation, which is not the case for all regions exposed to seismic hazards.

Accordingly, in Chapter 4, a method that is based on the inversion of the displacement spectra is employed in a single station approach to provide real-time magnitude estimation for an ongoing event. The results demonstrate the efficiency of this method for providing faster magnitude measurements for large earthquakes that can be implemented in all types of regions. This method is especially useful for areas exposed to seismic hazard with sparse seismic networks and vulnerable regions that lack adequate empirical data to develop the necessary empirical relationships.

In the following sections, the various early warning methodologies are described along with some details about different magnitude scales (Section 1.3), the basic characteristics of earthquake ground motions (Section 1.4) and a brief description of the Japanese strong ground motion data.

1.2.1 Front Detection

The basic idea behind all EEW systems is first the detection of hazardous earthquakes at one location and then the transmission of a useful warning before the seismic energy arrives at the user site. This concept is called front detection (Allen et al.,

2009). In regions with a predefined active seismic zone, an EEW system can be implemented through the installation of seismic devices that are located as close as possible to this zone in order to ensure the maximum possible warning times. This method is more applicable in subduction areas or other regions with well-defined seismic sources, such as Mexico, Japan, and Taiwan (Alcik et al. 2009). In these regions, seismometers near the earthquake source zone give early warnings to more distant urban areas. All warning systems which use a network also employ the front detection scheme by detecting a hazardous event in one location and providing early warning to another location. In the case in which seismic sources are located at a large distance from a populated area, this method can provide useful warning times, on the order of tens of seconds. The Taiwanese (Wu et al., 1999; Wu and Teng, 2002) and Mexican systems (Espinosa-Aranda et al., 1995; Espinosa-Aranda et al., 2009) are examples of this type of EEW system.

1.2.2 P-Wave parameters

In the front-detection method, S-waves are used to estimate the earthquake magnitude; therefore the determination of earthquake parameters must wait until the arrival of the S-waves. This results in a large "blind-zone" around the epicenter where no warning can be provided because S-waves have already reached the site and there is no time for warning. In order to overcome this problem, several researchers have tried to use the P-wave to determine whether or not an earthquake will cause hazardous ground shaking. Using the P-wave provides additional warning time and also reduces the radius of the blind zone, potentially providing warning at or near the epicenter. Several observational parameters have been developed that employ the P-wave to assess

earthquake hazard. Many are used to estimate the magnitude of an earthquake, which then is used to determine the likely ground shaking caused by subsequent S-waves and surface waves. The predominant period of the first few seconds of the P-wave was one of the first P-wave parameters to be employed in EEW magnitude estimation (Nakamura, 1988). This method was developed because the magnitude of the event scales with this parameter, and it shows no dependency on the epicentral distance within a few hundred kilometers of the event (Allen and Kanamori, 2003; Olson and Allen, 2005). Kanamori (2005) extended the method of Nakamura (1988) and Allen and Kanamori (2003) and derived a period parameter, τ_C , from the initial few seconds of the P-wave. The τ_C method calculates the effective period of the P-wave signal over a fixed time window, typically three seconds. Previous studies show that strong earthquakes of $M > 6$ generally have $\tau_C > 1$ s (Wu et al., 2007) although the scatter on the resulting values is very high (standard deviation between 0.3-0.6).

The other useful parameter for estimating earthquake hazard is the amplitude of the P-wave, if a correction for the epicentral distance can be made. The peak displacement, velocity, or acceleration of the first few seconds of the P-wave have been shown to be related to the earthquake magnitude (Wu and Kanamori 2005 b; Zollo et al., 2006; Wu and Kanamori, 2008a) and ground motion (Wu and Kanamori, 2005a; Böse et al., 2007). The quantity Pd is the peak ground motion displacement during the first three seconds after the P arrival. Wu and Kanamori (2005b) showed that the peak initial displacement amplitude, Pd , correlates well with the peak ground-motion velocity, PGV, at the same site. This approach was successfully tested by Wu and Kanamori (2005b) in Taiwan and by Wu et al. (2007) in southern California. One of the primary concerns with

using the first few seconds of the P-wave to estimate the magnitude of an earthquake is the saturation of these estimates for large magnitude events. There is some evidence for saturation of the empirical relationship between early P-wave parameters and magnitude for $M > 7$ events (Rydelek and Horiuchi 2006; Rydelek et al., 2007; Yamada, and Ide, 2008; Yamada and Mori, 2009). To overcome the problem of magnitude estimation for large events, several techniques have been designed to use longer time windows for the P-wave or the S-wave (Zollo et al., 2006; Kamigaichi et al., 2009). On the other hand, some believe that it is sufficient to know that an event is of $M \geq 6.5$ and issue a warning. However, one way to enhance system performance is to map the finite ruptures of the large magnitude ($M > 7$) earthquakes in a region and incorporate that into the magnitude estimation procedure (Yamada et al., 2007; Yamada and Heaton, 2008).

1.2.3 Onsite Approach (Single station)

In this approach the information recorded by a single station is used to estimate the EEW parameters. In most cases, the beginning part of the ground motion (primarily the P-wave) observed at a site is used to predict the incoming ground motion (mainly S and surface waves) at the same site. This is achieved by using a combination of the P-wave parameters described above. One approach is to look for a relation between the P-wave amplitude and the peak ground motion or magnitude (e.g., Wu and Kanamori 2005b). However, small magnitude earthquakes may have very large amplitudes. As a result, a combination of amplitude with frequency content is a more reliable approach. If large amplitudes also are associated with low frequencies, i.e., larger magnitudes, then a warning would be issued (Kanamori, 2005; Allen et al., 2009)

1.2.4 Regional Approach (Network-based)

The regional warning approach is a traditional seismological method in which data from a seismic network is used to locate an earthquake, determine the magnitude, and estimate the ground motion in the region involved. It may combine many or all of the components described above. Networks also allow data from multiple stations to be combined, which generally leads to more accurate predictions of the earthquake location and magnitude estimations and reduced uncertainties in the associated parameters.

While a regional approach often is more reliable and accurate, it usually takes longer to estimate and cannot provide early warnings close to the epicentral area. In the case where a network is used both to collect the seismic data and to give warning to users, the front detection approach can provide better warning times. Seismometers close to the epicenter are used to detect the event and assess the hazard, and the communication network provides warning to users at greater distances. In the case of large magnitude earthquakes ($M > 6.5$), this approach can provide tens of seconds of warning to areas that can expect damage. But a blind zone still will exist around the epicenter where no warning is available. This is due to the time lost transmitting data to a processing center, processing the data, and sending out a warning. In this situation, an onsite approach (Section 1.2.3) could remove these telemetry delays, but with increased probability of false or missed alarms.

1.3 Earthquake Magnitude

Earthquake magnitude scales were created because of the need for an objective measure of the size of an earthquake. The concept of earthquake magnitude, a

quantitative method for the comparison of earthquakes, was introduced by Richter in the early 1930's (Richter, 1935). Nowadays, the two commonly used magnitude scales are surface-wave magnitude, M_S , and body-wave magnitude, m_b . The variation of source spectra for different earthquakes shows that above a certain size M_S and m_b will have a constant value, which is called saturation. For EEW purposes, a magnitude measure that does not show saturation is desirable as large magnitude events ($M \geq 6$) are the main focus of EEW, tsunami early-warning and rapid-response systems.

The total size of an earthquake is best determined by the seismic moment, M_0 , and the shape of the overall source spectrum. M_0 is an alternative measure of energy, which is a function of the fault rupture area, the average amount of slip, and the required force to overcome the strength of the rocks that were offset by faulting (Aki, 1966; Hanks and Kanamori, 1979). The seismic moment generally is calculated from the amplitude spectra of the seismic waves (Brune, 1970, 1971; Aki and Richards, 1980; Abercrombie, 1995). Details are provided in the next section. To overcome the saturation problem, moment magnitude M was introduced (Aki, 1972; Kanamori, 1977, 1978; Hanks and Kanamori, 1979). It is calculated using the Hanks and Kanamori's (1979) relationship:

$$M = 2/3 \log_{10} (M_0) - 6.03 \quad (1.1)$$

where the scalar moment, M_0 , is the seismic moment in N.m. Hence, in this study, I used the moment magnitude of earthquakes in Japan for EEW purposes.

1.4 Earthquake Ground Motions

During an earthquake, seismic waves propagate from the hypocenter to the receiver site through a heterogeneous medium in a highly complicated manner. A

ground-motion signal recorded at a receiver includes three main parts: source, transmission path, and site effects. Source factors may include size, focal depth, stress drop, and fault geometry. Travel path factors include geometric spreading and inelastic attenuation. Local site effects include the properties of the uppermost several hundred meters of rock and soil and the effect of the surface topography near the recording site. When a site effect is considered, the general form of the amplitude spectrum is (Atkinson and Boore, 1995; Boore, 2003):

$$Y(M_0, R, f) = E(M_0, f) P(R, f) G(f) I(f) \quad (1.2)$$

where M_0 is seismic moment, R is a measure of distance from source to receiver site, and f is the frequency. $E(M_0, f)$ represents the source effect which is dependent on the size of the event, $P(R, f)$ describes the path effect, $G(f)$ is a function related to site effect or the effect of structure, and $I(f)$ is related to the instrument that records the signal. In the following sections, the basics of source, path and site components are discussed.

1.4.1 Source Model

The Fourier amplitude spectrum of the displacements generated at the source is defined as the source spectrum. Most of the source models have a functional form as follows (Boore, 1986; Boore, 2003):

$$E(M_0, f) = C \times M_0 \times S \quad (1.3)$$

where S is the displacement source function. C is a constant given by

$$C = \frac{U_{\theta\theta} F}{4\pi\rho c^3 R_0} \quad (1.4)$$

where $U_{\theta\theta}$ is the mean radiation pattern (0.52 and 0.63 for P- and S-waves, respectively), F denotes the free surface effect (1 and 2 for borehole and surface recording,

respectively), and R_0 is a reference distance (usually $R_0 = 1$ km). ρ and c are the density of the medium and the average velocity of the considered wave, respectively.

A commonly used model used to establish $E(M_0, f)$ is known as the Brune model (1970). The Brune model is a single-corner point-source model that was developed based on a point-source located at the center of a circular fault plane that generates the seismic waves (Brune, 1970):

$$S_{\text{Brun}} = \frac{1}{1 + \left(\frac{f}{f_c}\right)^2} \quad (1.5)$$

Where f is frequency and f_c is the corner frequency that is inversely proportional to the duration of the fault rupture and is given by

$$f_c = 4.9 \times 10^6 c (\Delta\sigma/M_0)^{1/3} \quad (1.6)$$

where c is velocity (km/sec), $\Delta\sigma$ is stress drop in bars and M_0 is in dyne-cm.

Abercrombie (1995) proposed a modified version of source spectral shape given by the following form:

$$\Omega(f) = \frac{\Omega_0 e^{\frac{-\pi ft}{Q}}}{\left[1 + \left(\frac{f}{f_c}\right)^n\right]^{\frac{1}{\gamma}}} \quad (1.7)$$

where $\Omega(f)$ is the Fourier amplitude of the P- or S-wave displacement, Ω_0 is the plateau at low frequencies, f is the frequency, f_c is the corner frequency, n is the high-frequency fall off rate (on a log-log plot), t is travel time, Q is quality factor, and γ is a constant. Note that, when $t = 0$, $n = 2$ and $\gamma = 1$, Equation 1.7 is the same as the Brune (1970) spectral shape model (Equation 1.5). If we obtain the long period amplitude (Ω_0) for all

three components of strong motion data [horizontal (H1 and H2) and vertical (Z) components], then the seismic moment (M_0) can be estimated using the following equation (Abercrombie, 1995):

$$M_0 = \frac{4\pi\rho c^3 \sqrt{\Omega_0(Z)^2 + \Omega_0(H1)^2 + \Omega_0(H2)^2}}{Z(R)U_{\theta\theta} F} \quad (1.8)$$

where ρ is the density of the medium, c is the average velocity of the considered wave, and Ω_0 is the low frequency plateau of the displacement spectra (m/Hz). $U_{\theta\theta}$ is the mean radiation pattern and $Z(R)$ represents the geometrical spreading function that accounts for the decay of ground-motion amplitudes due to geometrical attenuation. We calculate the geometrical spreading using following equation (Boor 2003; Ghofrani and Atkinson, 2011):

$$Z(R) = \begin{cases} \frac{1}{R} & , \quad R < 50km \\ \left(\frac{1}{50}\right) \left(\frac{50}{R}\right)^{0.5} & , \quad R \geq 50km \end{cases} \quad (1.9)$$

where R is the hypocentral distance.

Given the seismic moment from Equation 1.8, the moment magnitude can be calculated from Equation 1.1. In Chapter 4, the Abercrombie (1995) source model (Equation 1.7) is used to estimate the source parameters. Then Equations 1.8 and 1.1 are used to calculate the seismic moment and moment magnitude of the Japanese events, respectively.

1.4.2 Path

The path that seismic waves travel through the crust to reach the receiver site has a strong influence on the characteristic of the resulting ground motion. The amplitude of the ground motion decays with increasing source-to-site distance due to geometrical (elastic)

and intrinsic (anelastic) attenuation. The geometrical spreading attenuation refers to the decay of the ground-motion amplitudes due to spreading of seismic wave energy over a continuously increasing area as a result of expansion of the wave fronts (Stein and Wysession, 2003). Anelastic attenuation expresses the energy lost due to conversion of the seismic wave's energy to heat (through friction and viscosity) (Sheriff and Geldart, 1995; Stein and Wysession, 2003). Usually anelastic attenuation is presented by the Q , the quality factor, which is the inverse of the anelastic attenuation. This means that a lower quality factor corresponds to higher attenuation and vice versa.

1.4.3 Site

The local site conditions can significantly influence the amplitude and frequency content of the recorded ground motions (Singh et al., 1988a, Campillo et al., 1989). The near surface materials can attenuate or amplify the energy of the seismic waves. The difference in physical properties of the bedrock and soil column leads to the amplification or attenuation of the ground motions at the receiver site (Scherbaum, 1987; Williams et al., 1993; Field and Jacob, 1995).

1.4.4 Ground Motion Prediction Equations (GMPEs)

The attenuation of ground-motion amplitudes for a given magnitude, distance and site condition is described by ground motion prediction equations (GMPEs). These relations estimate the mean ground motion parameters, such as peak ground motions or response spectra, as a function of the magnitude, distance, and general site condition parameters (Joyner and Boore, 1981; Street and Turcotte, 1977). Different models of GMPEs have been employed in different regions (Atkinson and Mereu, 1992; Atkinson, 2004; Atkinson and Chen, 1997). In general, ground motion amplitudes decrease or

attenuate with increasing distance between the source and site. In Chapters 2 and 3, simple GMPEs are derived for Japan using both borehole and surface databases recorded by Kiban Kyoshin network. Subsequently, these estimated GMPEs are used as a basis to invert for the magnitude of the events that have 20 or more records available in the database. Very simple forms of attenuation were considered, to focus on the main factors that control ground motion and also to facilitate robust and rapid implementation.

First, in Chapter 2 the following simple form of attenuation model was chosen:

$$\log_{10}(Y) = a \log_{10}(r) + bM + c \quad (1.10)$$

where Y is either PGA (cm/s^2) or PGV (cm/s), r is the epicentral distance in km and M is moment magnitude, and a , b , and c are coefficients to be determined empirically. Note that Equation 1.10 ignores site terms and assumes all of the attenuation is a function of geometrical spreading and magnitude-scaling functions. In Chapter 3, in order to account for site terms, the following equation was considered (Boore et al., 2009):

$$\log_{10}(Y) = a_1 \log_{10}(r) + b_1 M + d_1 \log_{10}(V_{S30}/V_{\text{ref}}) + c_1 \quad (1.11)$$

where V_{S30} is the average shear-wave velocity at an observation station that represents site conditions and defined as (Borcherdt 1994):

$$V_{S30} = 30 / \sum_{i=1}^n (h_i / V_i) \quad (1.12)$$

In Equation 1.12, n is the number of layers in the uppermost 30 m depth and h_i and V_i are the thickness (m) of the layers and the shear-wave velocity (m/sec) of the i th layer, respectively. In Equation 1.11 site amplification is assumed to be linearly dependent on V_{S30} and is determined with respect to the definition for a National Earthquake Hazards

Reduction Program (NEHRP) B–C site condition ($V_{ref} = 760$ m/s). The standard deviation of the resulting GMPEs is calculated via:

$$\sigma = \sqrt{\frac{\sum (\log_{10}(Y_{observed}) - \log_{10}(Y_{predicted}))^2}{m - 2}} \quad (1.13)$$

where m is the number of records in our regression. After determining the unknown coefficients in Equations 1.10 and 1.11, the GMPEs obtained earlier are used to estimate the event magnitude for each PGA and PGV reading in the order that they became available. The results show that the use of V_{S30} results in a reduction in the standard deviation (σ) of ground motion prediction equations. It also improves the accuracy of the magnitude estimations.

1.5 Japanese Data

For all the research found in this thesis, I used strong ground motion time series recorded by Japanese strong-motion seismograph networks. After the 1995 Hyogoken-Nanbu earthquake, the National Research Institute for Earth Science and Disaster Prevention (NIED) established two strong motion seismograph networks, Kiban Kyoshin network (KiK-net) (Aoi et al., 2000) and Kyoshin network (K-net) (Kinoshita, 1998). The stations are distributed throughout Japan with average spacing of about 20 km, and most of the stations have the same type of instrumentation. The sensor type is a tri-axial force-balance accelerometer with a natural frequency of 450 Hz and a damping factor of 0.707. Waveforms are recorded with a sampling rate of 100 or 200 Hz with a 24-bit A/D converter and a maximum measurable acceleration of 2000 cm/s^2 . The instrument's response is approximately flat up to 15 HZ (Aoi et al., 2004).

K-net consists of more than 1000 stations installed at the free surface, primarily on the grounds of public buildings such as fire stations, parks or schools. As a result, K-net stations are located close to regions with more human activity. KiK-net is made up of approximately 700 dual borehole and surface stations. They are primarily situated on sedimentary sites, with some on weathered rock or thinner sediment. Each KiK-net station has six channels of a strong-motion seismograph, where three sensors are installed at the bottom of a borehole between 100 and 3000 m deep and three channels on the surface (Aoi et al., 2004). This network provides us with an excellent opportunity to use both borehole and surface data and to investigate which data provides more reliable results for earthquake and tsunami early warning systems. Both KiK-net and K-net networks are open sourced for users and shortly after the occurrence of an earthquake (within a few hours to one day) strong motion data become available via Internet.

1.6 Organization of thesis

This thesis is comprised of five chapters. Chapter 1 provides an introduction to the work and a literature review of EEW systems, including a brief history and the potential benefits of EEW systems, a review of existing EEW techniques and those characteristics of earthquake ground motions that are important to implementation and interpretation of EEW systems.

Chapter 2 presents a new application of GMPEs for magnitude determination. These GMPEs were developed for peak ground acceleration (PGA) and peak ground velocity (PGV) from both KiK-net borehole and surface databases (1998-2010). These GMPEs then were used as the basis for EEW magnitude determination and an assessment

was made of the relative importance of the various parameters and their impact on the accuracy of that magnitude estimates.

Chapter 3 presents a case study of the method proposed in Chapter 2 for the 11th March 2011 Tohoku earthquake (moment magnitude (**M**) 9.0) along with a modification of the GMPEs, based on a database that is more complete (1998-2011) in terms of magnitude and distance ranges. To account for site effects in the GMPEs, a simple model was developed based on the common site variable shear wave velocity (V_{S30}).

Chapter 4 presents a second method to evaluate the moment magnitude of an event using the displacement spectra of strong ground motion recordings. The results of this moment magnitude determination for both borehole and surface recordings from Japanese earthquakes (2000-2011) are presented in Chapter 4, which shows that this approach is suitable for regions where strong motion data is limited.

Chapter 5 presents overall conclusions and suggestions for future work. The thesis also includes three appendices. Appendix A includes two tables that show information on the events selected for use in Chapter 3, along with the final magnitude estimates for the borehole and surface recording database respectively. Appendix B contains a table that compares the mean residuals and standard deviations for the predicted magnitude using filtered and unfiltered data from Chapter 4 and a figure which illustrates the predicted magnitude versus moment magnitude for the filtered databases. Appendix C contains the computer code. It is noted that Chapters 2 and 3 have been published in *Bull. Seism. Soc. Am. and Pure and Applied Geophysics* respectively; Chapter 4 has been submitted for publication in *Bull. Seism. Soc. Am.* (2014).

1.7 References

Abercrombie, R. (1995). Earthquake source scaling relationships from -1 to 5 ML using seismograms recorded at 2.5-km depth, *J. Geophys. Res.*, 100, B12, 24,015–24,036.

Aki, K. (1966). "Generation and propagation of G waves from the Niigata earthquake of June 14, 1964. Part 2. Estimation of earthquake moment, released energy and stress-strain drop from G wave spectrum". *Bulletin of the Earthquake Research Institute* 44: 73–88.

Alcik, H., O. Ozel, N. Apaydin, and M. Erdik (2009). A study on warning algorithms for Istanbul earthquake early warning system. *Geophys. Res. Lett.* 36, L00B05; doi:10.1029/2008GL036659.

Allen, R.M., and H. Kanamori (2003). The potential for earthquake early warning in southern California. *Science* 300:786–89.

Allen, M., P. Gasparini, O. Kamigaichi, and M. Bose (2009). The status of earthquake early warning around the world: An introductory overview, *Seismol. Res. Lett.* 80, no. 5, doi: 10.1785/gssrl.80.5.682.

Aoi, S., K. Obara, S. Hori, K. Kasahara, and Y. Okada (2000). New strong-motion observation network: KiK-net. *EOS. Trans. Am. Geophys. Union*, 81, F863.

Aoi, S., T. Kungugi, and H. Fujiwara (2004). Strong-motion seismograph network operated by NIED: K-NET and KiK-net, special issue, *J. Japan Assoc. Earthq. Eng.* 4, 3 (special issue), 65–74.

Atkinson, G. M., and R. Mereu (1992). The shape of Ground Motion Attenuation curves in Southeastern Canada, *Bull. Seismol. Soc. Am.* 82, 2014–2031.

Atkinson G.M. and D. M. Boore (1995). Ground-Motion Relations for Eastern North America, *Bull. Seismol. Soc. Am.* 85, 17-30,

Atkinson, G. M. (2004). Empirical Attenuation of Ground-Motion Spectral Amplitudes in Southeastern Canada and the Northeastern United States, *Bull. Seismol. Soc. Am.* 94, 1079- 1095.

Boore, D. M. (1986). Short-period P- and S-wave Radiation from Large Earthquakes: Implications for Spectral Scaling Relations, *Bull. Seismol. Soc. Am.* 76, 43–64.

Boore, D. (2003). Simulation of ground motion using the stochastic method, *Puer Appl. Geophys.* 160, 636–676.

Böse, M., C. Ionescu, and F. Wenzel (2007). Earthquake early warning for Bucharest, Romania: Novel and revisited scaling relations. *Geophys. Res. Lett.* 34, L07302.

Borcherdt, R.D. (1994). Estimates of site-dependent response spectra for design (methodology and justification), *Earthquake Spectra*, EERI 10, 617–653.

Brune, J. N. (1970). Tectonic stress and spectra of seismic shear waves of earthquakes, *J. Geophys. Res.*, 75, 26, 4997-5009.

Brune, J. N. (1971). Corrcction, *J. Geophys. Res.* 76, 20, 5002.

Campillo, M., J. C. Gariel, K. Aki, and F. J. Sanchez-Sesma (1989). Destructive Strong Ground Motion in Mexico City: Source, Path, and Site Effects During Great 1985 Michoacan Earthquake, *Bull. Seismol. Soc. Am.* 79, 1718-1735.

Espinosa-Aranda, J., A. Jiménez, G. Ibarrola, F. Alcantar, A. Aguilar, M. Inostroza, and S. Maldonado (1995). Mexico City seismic alert system. *Seismol. Res. Lett.*, 66, 42-53.

Espinosa-Aranda, J., A., A. Cuellar, A. Garcia, G. Ibarrola, R. Islas, S. Maldonado, and F. Rodriguez (2009). Evolution of the Mexican Seismic Alert System (SASMEX), *Seismol. Res. Lett.* 80, 5, 694–706.

Field, E. H., and K. H. Jacob (1995). A comparison and test of various site-response estimation techniques, including three that are not reference-site dependent, *Bull. Seismol. Soc. Am.* 85, 1127-1143.

Ghofrani, H., and G. M. Atkinson (2011). Forearc versus backarc attenuation of earthquake ground motion, *Bull. Seismol. Soc. Am.* 101, 3032–3045.

Hanks, T. C. and H. Kanamori (1979). A moment magnitude scale. *J. Geophys. Res.* 84, 02348.

Hayes, G. P. (2011). Rapid source characterization of the 2011 Mw 9.0 off the Pacific coast of Tohoku Earthquake, *Earth Planets Space*, 63, 529–534.

Hoshiya, Y., K. Iwakiri, N. Hayashimoto, T. Shimoyama, K. Hirano, Y. Yamada, Y. Ishigaki, and H. Kikuta (2011). Outline of the 2011 off the Pacific coast of Tohoku Earthquake (M9.0) Earthquake Early Warning and observed seismic intensity, *Earth Planets Space*, 63, 547–551.

Imamura, A. (1924). Preliminary note on the great earthquake of southeastern Japan on September 1, 1923, *Bull. Seismol. Soc. Am.* 14, 136–149.

Jordan, T. H., and L. M. Jones (2010). Operational earthquake forecasting: Some thoughts on why and how. *Seismol. Res. Lett.* 81, 4, 571–574.

Jordan, T. H., and L. M. Jones (2011). Reply to ‘A Second Opinion on “Operational Earthquake Forecasting: Some Thoughts on Why and How,” by Thomas H. Jordan and Lucile M. Jones,’ by Stuart Crampin Thomas H. Jordan and Lucile M. Jones, *Seismol. Res. Lett.* 82 (2), 231-232, doi: 10.1785/gssrl.82.2.231.

Kamigaichi, O., M. Saito, K. Doi, T. Matsumori, S. Tsukada, K. Takeda, T. Himoyama, K. Nakamura, M. Kiyomoto, and Y. WAatanabe (2009). Earthquake early warning in Japan: Warning the general public and future prospects, *Seismol. Res. Lett.* 80, 717–726.

Kanamori, H. (2005). Real-time seismology and earthquake damage mitigation, *Annual Review of Earth and Planetary Sciences* 33, 195–214.

Kinoshita, S. (1998). Kyoshin Net (K-NET), *Seism. Res. Lett.* 69, 309-332.

Lee, W. H. K., and J. M. Espinosa-Aranda (2003). Earthquake early warning systems: Current status and perspectives, in *Early Warning Systems for Natural Disaster Reduction*, J. Zschau and A. N. Koppers (Editors), Springer, Berlin, 409–423.

Mori, N., T. Takahashi, T. Yasuda, and H. Yanagisawa (2011). Survey of 2011 Tohoku earthquake tsunami inundation and runup, *Geophys. Res. Lett.* 38, L00G14.
doi:10.1029/2011GL049210.

Nakamura, Y. 1988. On the urgent earthquake detection and alarm system (UrEDAS). In *Proceedings of the 9th World Conference on Earthquake Engineering VII*, 673–678.

Olson, E., and R. M. Allen (2005). The deterministic nature of earthquake rupture, *Nature* 438, 212–215.

Rydelek, P., and S. Horiuchi (2006). Is earthquake rupture deterministic? *Nature* 442, E5–E6.

Rydelek, P., C. Wu, and S. Horiuchi (2007). Comment on “Earthquake magnitude estimation from peak amplitudes of very early seismic signals on strong motion records” by Aldo Zollo, Maria Lancieri, and Stefan Nielsen, *Geophys. Res. Lett.*, 34, L20302, doi: 10.1029/2007GL029387.

Richter C.F. (1935). An instrumental earthquake magnitude scale *Bull. Seismol. Soc. Am.* 25, 1.

Scherbaum, F. (1987). Seismic imaging of the site response using microearthquake recordings. Part I. method, *Bull. Seismol. Soc. Am.* 77, 1905-1923.

Sheriff, R. E., Geldart, L. P., (1995), 2nd Edition. *Exploration seismology*. Cambridge University Press.

Singh, S. K., E. Mena, and R. Castro (1988). Some aspects of source characteristics of the 19 september 1985 Michoacan earthquake and ground motion amplification in and near Mexico city from strong motion data, *Bull. Seismol. Soc. Am.* 78, 451-477.

Stein, S., and M. Wysession (2003). *An introduction to seismology, earthquakes, and Earth structure*, Blackwell Publishing Ltd, UK, 498 pages.

Williams, R. R., K. W. King, J. C. Tinsley (1993). Site Response Estimates in Salt Lake Valley, Utah, from Borehole Seismic Velocities, *Bull. Seismol. Soc. Am.* 83, 862-889.

Wu, Y. M., N. C. Hsiao, T. L. Teng, and T. C. Shin (2002). Near real-time seismic damage assessment of the rapid reporting system, *Terr. Atmos. Ocean. Sci.*, 13, 313-324

Wu, Y. M., J. K. Chung, T. C. Shin, N. C. Hsiao, Y. B. Tsai, W. H. K. Lee, T. L. Teng (1999). Development of an integrated seismic early warning system in Taiwan- case for Hualien earthquakes. *Terrestrial, Atmospheric and Oceanic Sciences*, 10, 719-736.

Wu, Y.M., and T.L. Teng (2002). A virtual subnetwork approach to earthquake early warning. *Bull. Seismol. Soc. Am.* 92:2008–18.

Wu, Y.M., and H. Kanamori (2005a). Experiment on an onsite early warning method for the Taiwan early warning system. *Bull. Seismol. Soc. Am.* 95, 347– 353.

Wu, Y.M., and H. Kanamori (2005b). Rapid assessment of damage potential of earthquakes in Taiwan from the beginning of P waves. *Bull. Seismol. Soc. Am.* 95, 1,181–1,185.

Wu, Y. M., and L. Zhao (2006), Magnitude estimation using the first three seconds P-wave amplitude in earthquake early warning, *Geophys. Res. Lett.*, 33, L16312, doi:10.1029/2006GL026871

Wu, Y.M., H. Kanamori, R. M. Allen, and E. Hauksson (2007). Determination of earthquake early warning parameters, τ_c and P_d , for southern California. *Geophysical Journal International*, doi: 10.1111/j.1365-246X.2007.03430.

Wu, Y.M., and H. Kanamori (2008a). Development of an earthquake early warning system using real-time strong motion signals. *Sensors*, 8, 1–9.

Wu, Y.M., and H. Kanamori (2008b). Exploring the feasibility of onsite earthquake early warning using close-in records of the 2007 Noto Hanto earthquake. *Earth, Planets, and Space* 60, 155–160.

Yamada, M., T. Heaton, and J. Beck (2007). Real-time estimation of fault rupture extent using near-source versus far-source classification. *Bull. Seismol. Soc. Am.* 97, 1,890–1,910.

Yamada, T., and S. Ide (2008). Limitation of the predominant-period estimator for earthquake early warning and the initial rupture of earthquakes, *Bull. Seismol. Soc. Am.*, 98, 6, 2739– 2745

Yamada, M., and T. Heaton (2008). Real-time estimation of fault rupture extent using envelopes of acceleration. *Bull. Seismol. Soc. Am.* 98, 607–619.

Yamada, M., and J. Mori (2009). Using τ_c to estimate magnitude for earthquake early warning and effects of near-field terms, *J. Of Geophys. Res.* 114, B05301, doi:10.1029/2008JB006080, 2009

Zollo, A., M. Lancieri, and S. Nielsen (2006). Earthquake magnitude estimation from peak amplitudes of very early seismic signals on strong motion records. *Geophys. Res. Lett.* 33, L23312.

Chapter 2

2 Using Borehole Records to Estimate Magnitude for Earthquake and Tsunami Early-Warning Systems¹

¹ A version of this chapter has been published. Eshaghi, A., K. F. Tiampo, H. Ghofrani, and G. M. Atkinson (2013). Using Borehole Records to Estimate Magnitude for Earthquake and Tsunami Early-Warning Systems, *Bull. Seism. Soc. Am.* **103**. doi:10.1785/0120120319.

This chapter presents a new application of ground-motion prediction equations (GMPEs) to estimate the event magnitude for earthquake and tsunami early warning systems. Here both borehole and surface strong-motion records from Japanese earthquakes (1998-2009) with moment magnitude (M) ranging from 5.0 to 8.1 were analyzed. In total, 2160 borehole strong ground motion accelerograms with peak ground acceleration (PGA) larger than 10 cm/s^2 and 890 surface waveforms with PGA larger than 80 cm/s^2 were used to derive GMPEs for PGA and peak ground velocity (PGV) in Japan. These empirical GMPEs were used as the basis for regional magnitude determination. Predicted magnitudes from PGA values (MPGA) and predicted magnitudes from PGV values (MPGV) were defined separately for borehole and surface recordings. MPGA and MPGV show strong correlation with the moment magnitude of the event, provided that at least 20 records for each event are available. Among the estimated magnitudes, MPGV from borehole data has the smallest standard deviation and provides an accurate early assessment of earthquake magnitude. The results of this study show that incorporation of borehole strong ground motion records immediately available after the occurrence of large earthquakes significantly increases the accuracy of earthquake magnitude estimation and improves the performance of the EEW system.

2.1 Introduction

An earthquake early-warning (EEW) system is a practical and promising tool to reduce losses caused by a damaging earthquake (Espinosa-Aranda et al., 1995; Kanamori et al., 1997; Teng et al., 1997; Wu et al., 1998, 2007; Allen and Kanamori, 2003; Lee and Espinosa-Aranda, 2003; Allen et al., 2009). It also can be used for real-time tasks such as loss estimation for emergency response and recovery plans (Wu and Teng, 2002). Kanamori (2005) classified EEW approaches into two categories: regional and site-specific (onsite). In the regional seismological approach, magnitude and location are estimated from the earliest available data and then used to predict ground motions at other sites. This approach is employed in Japan, Taiwan, and Mexico. In the site-specific approach, the beginning portion of the ground motion observed at a given site, specifically the P wave, is used to predict the amplitude of the following incoming seismic waves at the same site, primarily S waves and surface waves that have larger amplitudes and carry more destructive energy than the P wave (Wu et al., 2007). Lin and Wu (2010) have proposed a regional method that employs a strong ground motion attenuation relationship for peak ground acceleration (PGA) for large crustal earthquakes in Taiwan to estimate the magnitude using the observed PGA (M_{pga}). Their results showed that, with sufficient PGA readings, the M_{pga} estimate is similar to the actual moment magnitude (M) of an event. This method was tested for the 2010 JiaSian, Taiwan, earthquake and implementation in real time of this method was proposed for future EEW practice (Lin et al., 2011). In Japan, the EEW system determines the magnitude (M_{JMA}), the hypocenter location of the earthquake, the expected maximum seismic intensity, and an estimation of arrival time of the strong ground motion for each

specific area (Kamigaichi, 2004; Kamigaichi et al., 2009). To determine the location of an ongoing event, a method using the first two seconds of waveform data to estimate epicentral distance and azimuthal direction of epicenter at each station has been proposed by the Japan Meteorological Agency (JMA) and Railway Technical Research Institute (Odaka et al., 2003; Tsukada et al., 2004). These estimations are updated every one second as more data become available (Kamigaichi, 2004). Note that all the above methods use data from surface seismograph stations.

In this paper we propose a regional method to estimate the magnitude of an earthquake employing strong ground motion data from both borehole and surface data, immediately after the current EEW system provides the location of the event. Note that the current EEW system starts to estimate the location of event by employing a method that uses the first two seconds of the waveform after the initial seismic-wave detection and updates the estimated location as more data become available. We obtained borehole and surface ground-motion prediction equations (GMPEs) by inverting for the parameters of the PGA and peak ground velocity (PGV) attenuation equations using data for large earthquakes ($M \geq 5.0$) recorded by both Kiban Kyoshin network (KiK-net) borehole and surface stations over the interval of 1998 to 2010 (see Data and Resources section). These GMPEs are used as the basis for magnitude determination. In this study, predicted magnitude using PGA readings (M_{pga}) and predicted magnitude using PGV readings (M_{pgv}) were defined for both KiK-net's borehole and surface data separately. Our calculated magnitudes show strong correlation with the reported magnitude of the large events, provided enough PGA and PGV readings are available. This is the first time that borehole records have been used for magnitude determination for EEW and tsunami early

warning purposes in Japan. The results for the borehole database show better precision than surface record database (Table 2.1), which suggests that the use of these data should be incorporated into real-time EEW practice. The results of this study can be integrated with current and future EEW and tsunami early-warning systems to improve the reliability and robustness of EEW magnitude estimations. This method also provides another constraint to the EEW system by taking into account the time that is required to accurately estimate the moment magnitude. Furthermore, this method can be added to the existing EEW systems of other countries that already have dense seismic network stations.

Table 2.1 Standard deviation for predicted magnitude.

	Surface data	Borehole data
Number of earthquakes with 20 and more records	13	25
Standard deviation of M_{pga} (M)	0.30	0.24
Standard deviation of M_{pgv} (M)	0.25	0.18

2.2 Strong Ground Motion Database

Japan is located in one of the most active seismic and volcanic zones, where the Pacific and Philippine Sea plates subduct beneath the Eurasian plate. The accumulation of crustal stress and strain results in large earthquakes and tsunamis in this region (Lee and Espinosa-Aranda, 2003). Over 140,000 people perished in the 1923 Tokyo earthquake (Imamura, 1924) and, more recently, the 2011 **M9.0** Tohoku earthquake triggered a large tsunami that caused over 15,000 deaths and an economic cost of

US\$235 billion (Hayes, 2011; Mori et al., 2011). Efforts to prevent and mitigate such disasters are considered among the most important nationwide programs in Japan. The JMA is responsible for providing tsunami forecasts and issuing EEW for upcoming strong motion. The JMA started its nationwide EEW service for advanced users in August 2006 and for the public in October 2007 (Doi, 2011). When a JMA seismic scale intensity degree “5-lower” (which is equivalent to an acceleration of 0.80–1.40 m/s²) or more is expected, an EEW is issued to the general public. More than 1000 stations, including ~200 and ~800 operated by the JMA and the National Research Institute for Earth Science and Disaster Prevention (NIED) respectively, are monitored continuously as part of the JMA EEW system (Doi, 2011). These stations are distributed throughout Japan with an average spacing of about 20 km. In this study we used the KiK-net strong ground motion data from stations provided by NIED (see Data and Resources section). Each of the KiK-net stations has six channels of strong-motion seismographs, with three channels installed at the bottom of the borehole and three channels on the surface (Aoi et al., 2004). The borehole depth varies between 100 and 3000 m. The sensor is a triaxial force-balanced accelerometer with a natural frequency of 450 Hz and a damping factor of 0.707. Acceleration waveforms are recorded with a sampling rate of 200 Hz. The maximum measurable acceleration is 2000 cm/s² and the instrument’s response is approximately flat up to 15 Hz (Aoi et al., 2004).

We adopted moment magnitude M and epicentral distance r as the parameters for the initial model in our regression analysis. We use epicentral distance because it is available immediately after an event. The value of M for each event is that reported (in order of preference) by NIED and the Global Centroid Moment Tensor catalog. For this

study, we collected large magnitude earthquake ($5.0 \leq \mathbf{M} \leq 8.1$) records with focal depth ≤ 50 km and epicentral distance up to 400 km over the interval of 1998 to 2010. We used the epicentral distance cutoffs (R_c) for each event to ensure signal quality (see Table 2.2).

Table 2.2. Epicentral Distance Cutoffs (R_c) for Each Event

Magnitude (\mathbf{M})	Epicentral Distance Cutoffs (R_c)
$5 \leq \mathbf{M} < 6$	$R_c = 150$ km;
$6 \leq \mathbf{M} < 6.5$	$R_c = 200$ km;
$6.5 \leq \mathbf{M} < 7.5$	$R_c = 250$ km;
$7.5 \leq \mathbf{M} < 8$	$R_c = 300$ km;
$\mathbf{M} \geq 8$	$R_c = 400$ km;

For the borehole data, we analyzed those records with $PGA \geq 10$ cm/s² and for the surface data we collected records with $PGA \geq 80$ cm/s². The threshold of 80 cm/s² was chosen because it represents the degree “5-lower” of the JMA’s seismic-intensity scale, which corresponds to the minimum strong motion that is capable of causing damage to buildings (Kamigaichi et al., 2009). To choose the threshold for the borehole recordings, we tested a number of different threshold levels (8–30 cm/s²). We found that, in general, 10 cm/s² for borehole data is the optimal threshold to provide stable and accurate estimations. Table 2.3 shows the number of records used in this study. The earthquake epicenters are shown in Figure 2.1, along with the borehole stations that recorded these events. The distribution of \mathbf{M} with epicentral distance and focal depth for the borehole records database used here is shown in Figure 2.2. The majority of events have $\mathbf{M} \leq 7.4$

and the magnitude with depth is randomly distributed, ranging from 0 to 50 km (Figure 2.2).

Table 2.3 Data Employed in Regression Analysis

	Borehole	Surface
Records	2160	890
Earthquakes	67	62
PGA	$\geq 10 \text{ cm/s}^2$	$\geq 80 \text{ cm/s}^2$
Epicentral distance	$\leq 390 \text{ km}$	$\leq 270 \text{ km}$
Magnitudes	5.1 - 8.1	5 - 8.1

The earthquake epicenters of the selected events and the surface stations that recorded those events are shown in Figure 2.1. The distribution of M with epicentral distance and focal depth for the surface record database are shown in Figure 2.2. Note that we plotted the stations that recorded $\text{PGA} \geq 10 \text{ cm/s}^2$ for borehole recordings and those stations that recorded $\text{PGA} \geq 80 \text{ cm/s}^2$ for surface recordings. All records were corrected for baseline trend and a noncausal, band-pass Butterworth filter of order 4 and corner frequencies of 0.1–15 Hz was applied (Ghofrani and Atkinson, 2011). The upper limit of 15 Hz was implemented because the instruments' amplitude-transfer function decreases significantly for frequencies above 15 Hz. In order to calculate the PGA and PGV values for each record, we considered the entire signal.

2.3 Strong Ground Motion Prediction Equation

The following simple form of attenuation model was chosen:

$$\log_{10}(Y) = a \log_{10}(r) + bM + c; \quad (2.1)$$

in which Y is either PGA (cm/s^2) or PGV (cm/s), M is the moment magnitude of the event, r is epicenter distance in km, and a , b , and c are coefficients to be determined empirically. a represents attenuation of ground motion, b is the coefficient for the source parameter (magnitude), and c is a constant. Moment magnitude is chosen to prevent magnitude saturation for large events (Kanno et al., 2006), as large magnitude events ($M \geq 6$) are the main focus of EEW, tsunami early-warning, and rapid-response systems. Note that this is a very simplistic form that ignores site terms and assumes all of the attenuation is a function of geometrical spreading and magnitude-scaling functions. We choose this simple form to focus on the main factors that control ground motion. For surface record database, the site-term correction is considered, as discussed in the Site Effects Term section. The EEW procedure is one form of a calibration method, or reverse regression (Miller, 1966; Garden et al., 1980), the practice of obtaining a desired parameter x from an instrumental response y (Brownlee, 1960). This is, effectively, a data-assimilation problem. The strong ground motion records are used to determine the best fit to the governing equations, in order to accurately predict the magnitude for future events based on the parameters from the historic database. Here we employed a linear least-squares inversion to determine the unknown coefficients (a , b , c) in Equation 2.1.

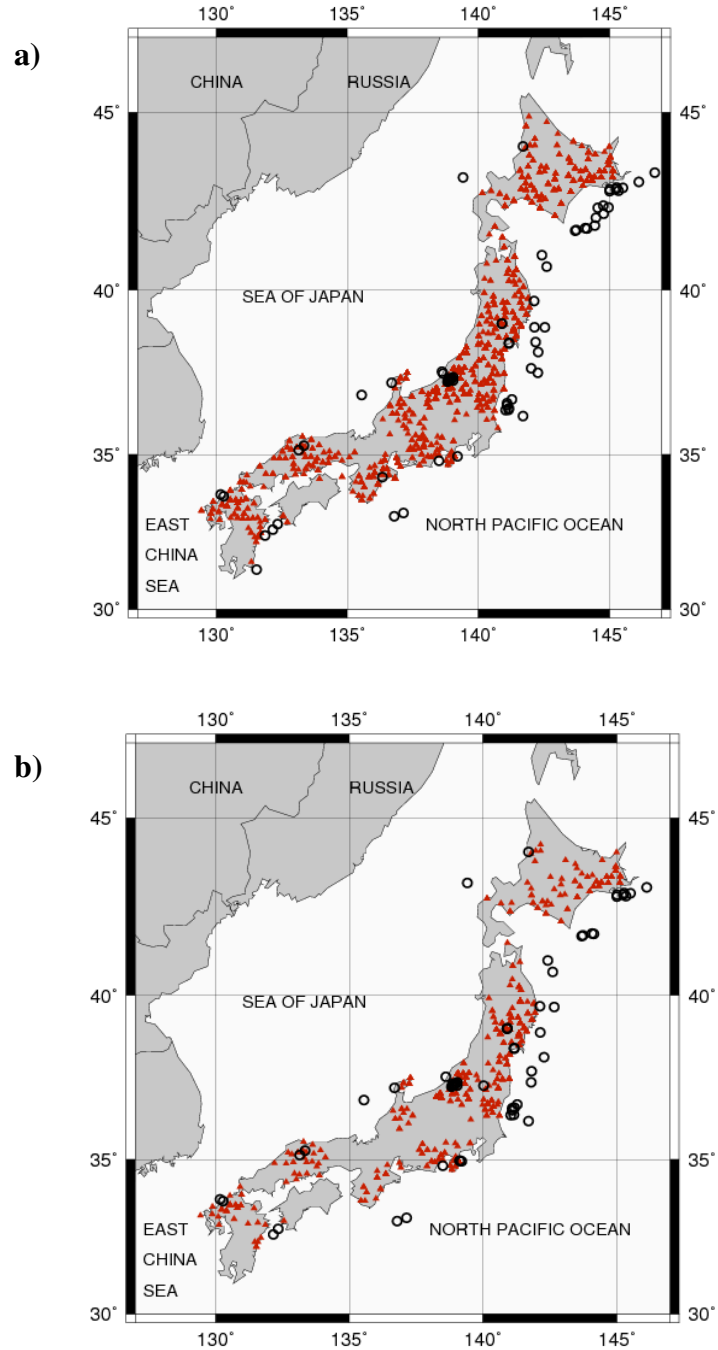


Figure 2.1 Distribution of the KiK-net stations (solid triangles) that recorded the selected events. (a) The distribution of borehole stations. (b) The surface stations that recorded the selected events. Open circles are the epicenters of the earthquakes used in this study for each database.

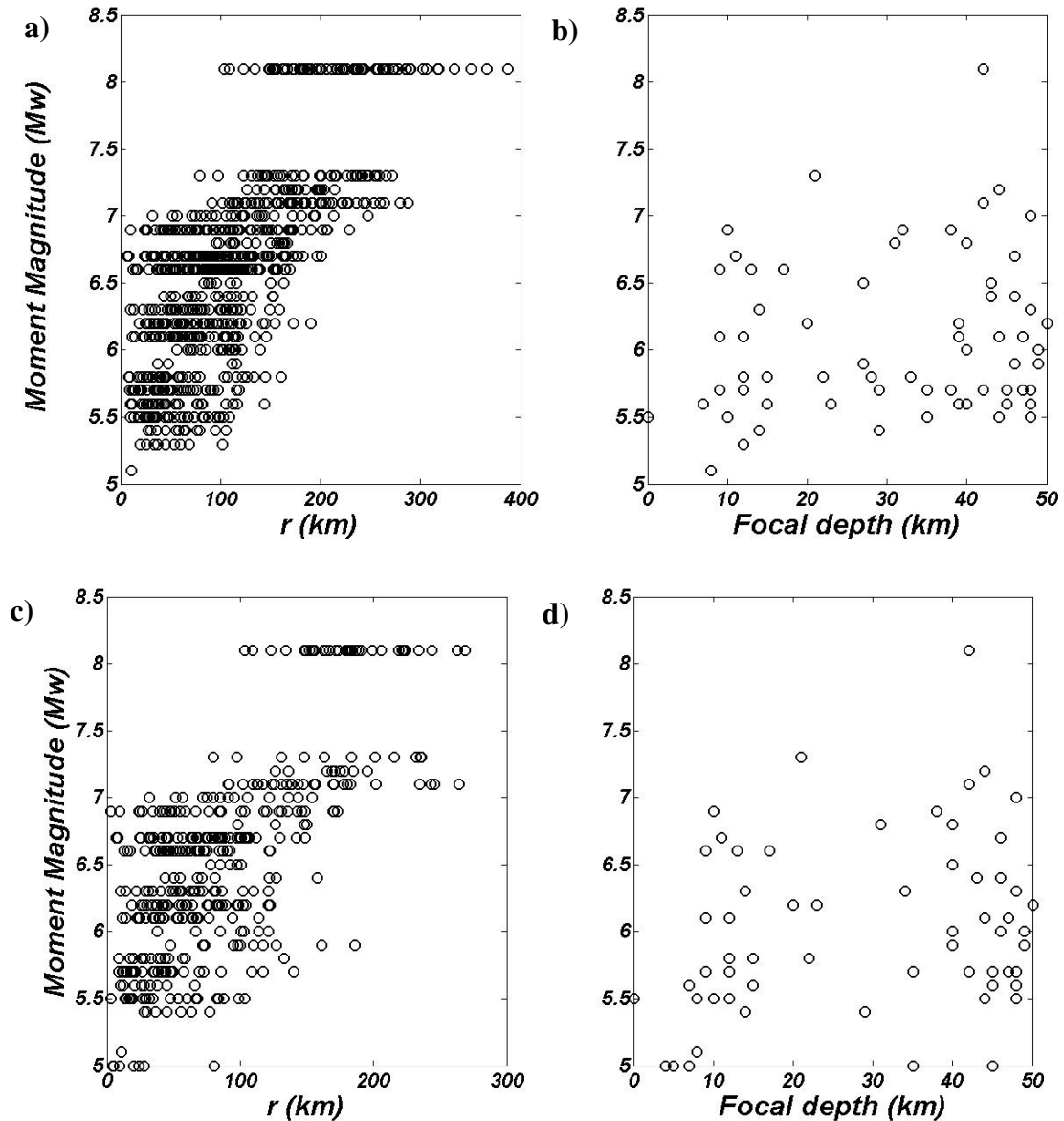


Figure 2.2 Magnitude-epicentral distance distributions for (a) borehole database and (c) surface database. Magnitude-focal depth for the (b) borehole database and (d) surface database.

Note that we did not consider an elastic attenuation (a linear r term) in our attenuation model, in order to ensure a reasonable function for all events, as the use of a linear r term results in upward curvature at large distances for some events.

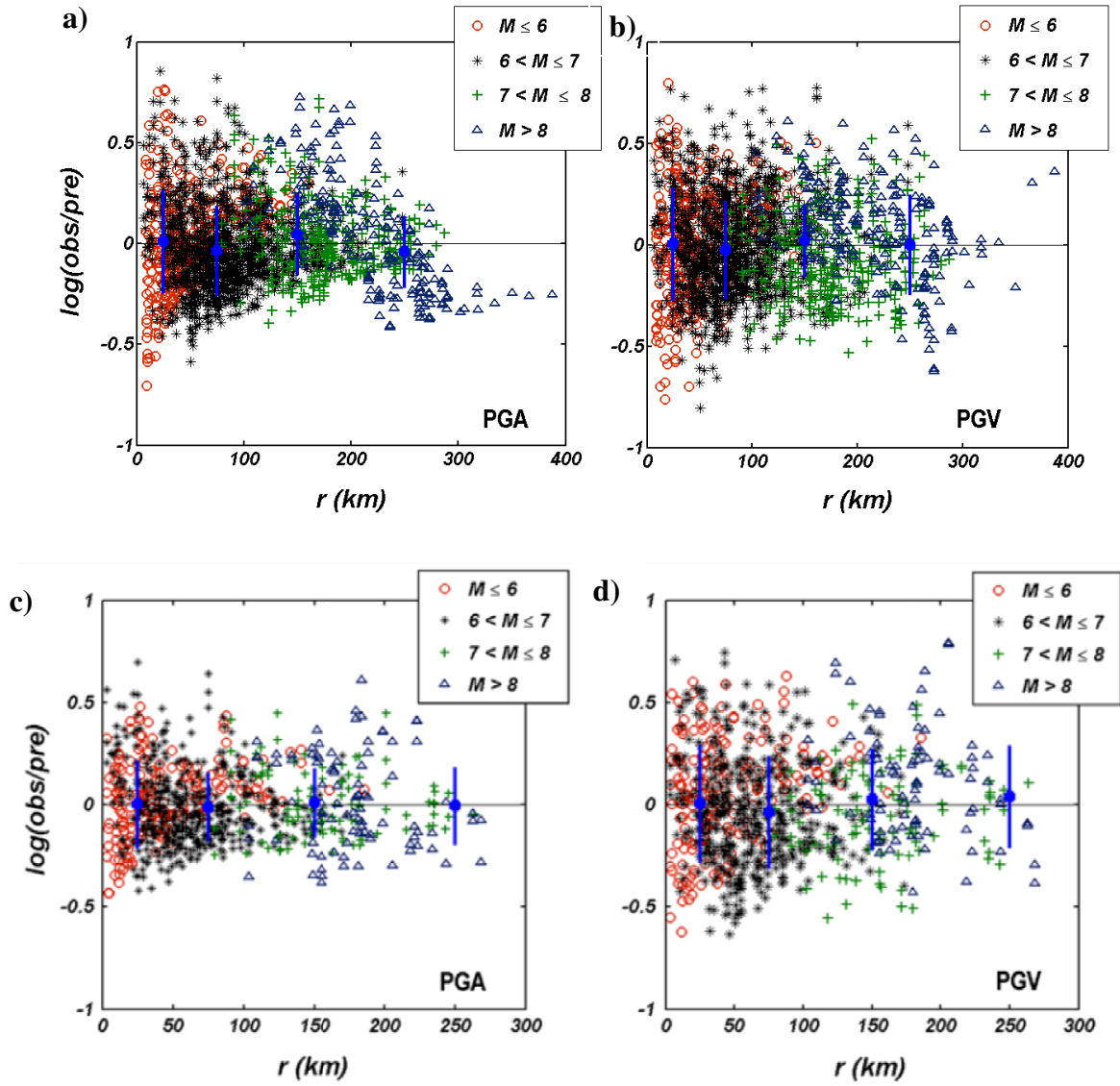


Figure 2.3 Distribution of residuals versus epicentral distance for PGA and PGV for the (a and b) borehole record database and (c and d) surface record database. Different symbols show the range of magnitudes. Large square symbols show the mean value of the residuals contained in a specific distance bin, whereas bars represent ± 1 standard deviation.

2.4 Ground-Motion Prediction Equation for Borehole Record

Database

To derive the GMPEs for this study, we analyzed 2160 PGA readings of greater than 10 cm/s², recorded by KiK-net borehole stations from 67 large magnitude earthquakes (Figure 2.1a). The accelerograms were integrated in time to obtain the velocity records and both datasets were incorporated into separate regression analyses. Using the current borehole database, the following GMPEs for PGA and PGV were obtained:

$$\log_{10} \text{PGA} = [-0.813 \log_{10}(r) + 0.327M + 0.719] \pm 0.22 \quad (2.2)$$

$$\log_{10} \text{PGV} = [-0.772 \log_{10}(r) + 0.598M - 2.119] \pm 0.25 \quad (2.3)$$

The standard deviation for the resulting GMPEs is given by:

$$\sigma = \sqrt{\frac{\sum (\log_{10}(Y_{observed}) - \log_{10}(Y_{predicted}))^2}{n-2}} \quad (2.4)$$

in which n is the number of records in our regression. The GMPEs from Equations 2.2 and 2.3 are used to estimate the event magnitude for each PGA and PGV reading in the order that they became available in the borehole and surface record datasets. Figure 2.3 shows the distribution of residuals between observed and predicted PGAs and PGVs [$\log_{10}(\text{observed/predicted})$] as a function of epicentral distance for the borehole database. Different symbols show the range of magnitudes. No trend is observed between the residuals and epicentral distance or the reported magnitude of the events in Figure 2.3. Histograms of the residuals for PGA and PGV, shown in Figure 2.4a,b, suggest that the residuals of the borehole database follow a normal distribution with zero mean.

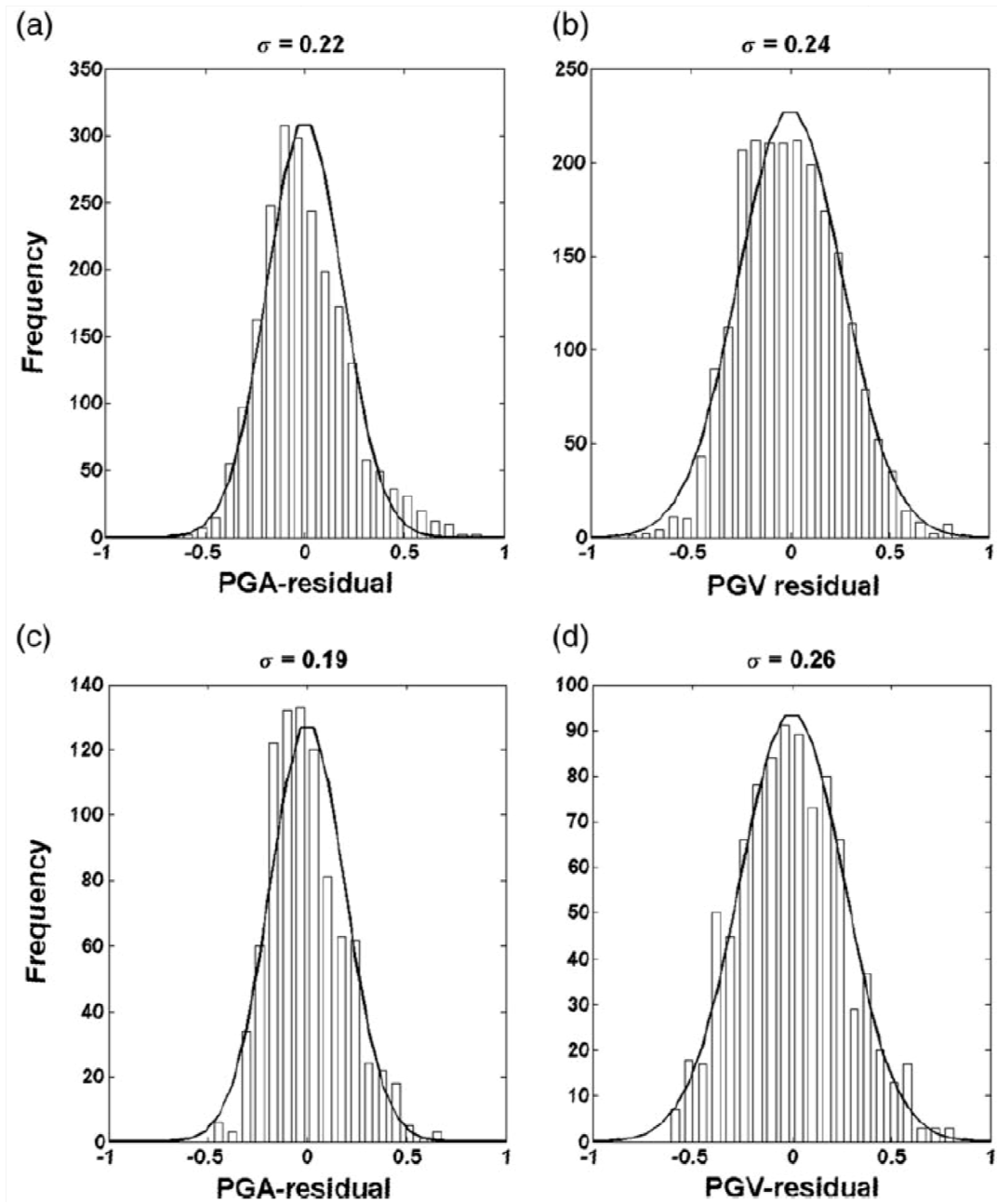


Figure 2.4 The histogram of the residuals for PGA and PGV for the (a and b) borehole record database and (c and d) surface record database. σ represents the standard deviation of the residuals. Solid curves represent normal distributions with zero mean and given standard deviation.

2.5 Ground-Motion Prediction Equation for Surface Record

Database

This database included 62 events of M 5.0–8.1 with focal depths ≤ 50 km (Figure 2.1b), resulting in 890 free-field (surface) records with $PGA \geq 80$ cm/s². These events were used to develop GMPEs for PGA and PGV, respectively. The following GMPEs for PGA and PGV were obtained:

$$\log_{10} PGA = [-0.435 \log_{10}(r) + 0.205M + 1.611] \pm 0.19 \quad (2.5)$$

$$\log_{10} PGV = [-0.621 \log_{10}(r) + 0.422M - 0.781] \pm 0.26 \quad (2.6)$$

Figure 2.3 shows the distribution of residuals versus epicentral distance for PGA and PGV for surface database. Different symbols show the range of magnitudes. Figure 2.3 indicates that there is no trend for the residuals with epicentral distance or magnitude of the events. Histograms of the residuals for PGA and PGV are shown in Figure 2.4c,d. The residuals for PGA and PGV follow a normal distribution with zero mean. Following the same procedure as employed for the borehole record database, we used the GMPEs (Equations 2.5 and 2.6) to estimate the magnitude of events for each PGA and PGV reading in the order that became available.

2.6 Magnitude Estimation

The current EEW system in Japan provides an accurate estimation of epicenter location shortly after the occurrence of a large earthquake (Kamigaichi, 2004). Substituting the initial epicentral location estimate into the obtained GMPEs, we solve Equations 2.2, 2.3, 2.5, and (2.6) for magnitude and estimate M_{pga} and M_{pgv} for each PGA and PGV reading immediately as it becomes available. By adding a new record, the

new magnitude is calculated as the weighted average of the previous magnitude estimation and the new magnitude observation. Therefore, the magnitude is updated as more stations contribute data. The time for each PGA or PGV is the true occurrence time of the corresponding observation (PGA or PGV) with reference to the origin time of the earthquake. For example, for an **M**6.6 event it took approximately 40 s to acquire enough records to provide a stable magnitude estimate (Figure 2.5). We have calculated the M_{pga} and the M_{pgv} using borehole (25 earthquakes) and surface (13 earthquakes) data for those events that had 20 or more records available in our databases. As more readings become available for a large event, the average of the estimated magnitudes converges on the reported **M** (Figures 2.5 and 2.6). Figure 2.5 shows an example of M_{pga} and M_{pgv} estimation history as a function of time after earthquake onset for both borehole and surface datasets, along with the reported **M** for the 23 October 2004 **M**6.6 event. Figure 2.6 shows an additional example for the 16 August 2005 **M**7.1 event. Generally, PGV readings provide more stable magnitude predictions using a smaller number of recordings than PGA readings (e.g., Borehole: $\sigma[PGV] = 0.18 < \sigma[PGA] = 0.24$). The magnitude prediction using borehole record database also provides better magnitude estimates with smaller error in most cases compared to those of the surface record database (e.g., PGV: $\sigma[Borehole] = 0.18 < \sigma[surface] = 0.25$). Detailed analysis (Table 2.1) shows that borehole data predicts magnitude better than surface data and the smallest standard deviation in our analysis corresponds to M_{pgv} using the borehole record database. The predicted magnitudes from inversion of the GMPEs for PGA and PGV (Equations 2.2, 2.3, 2.5, and 2.6) are generally in good agreement with the reported **M**, with the best results (Table 2.1) for PGV records from the borehole record dataset (Equation 2.3).

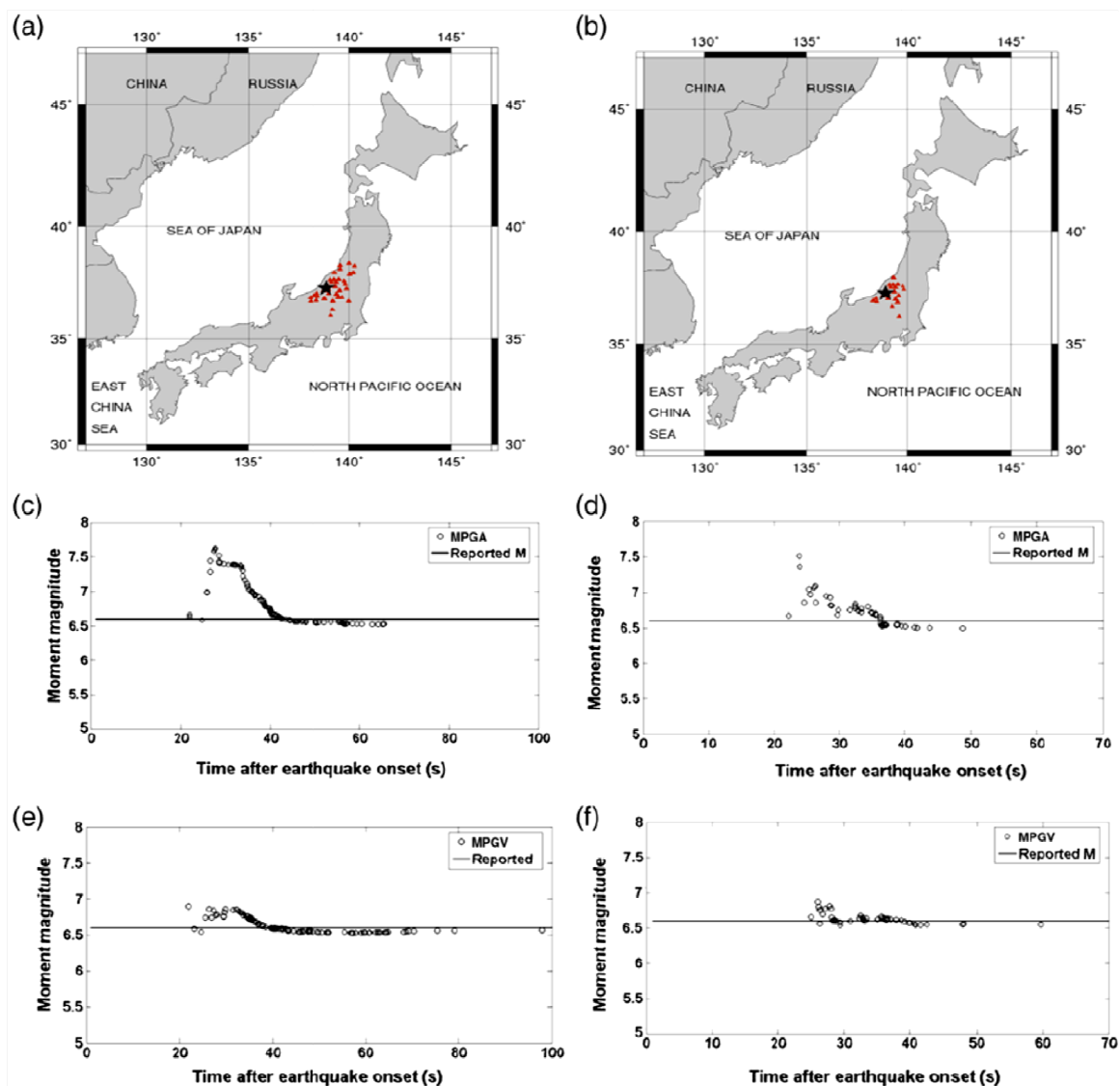


Figure 2.5 Map of KiK-net stations that recorded PGA and PGV for the 23 October 2004 M6.6 event (a) for borehole records with $\text{PGA} \geq 10 \text{ cm/s}^2$ and (b) for surface records with $\text{PGA} \geq 80 \text{ cm/s}^2$. Mpga versus time (seconds) after origin time for current (c) borehole dataset, and (d) surface dataset. Mpgv versus time (seconds) after origin time for current (e) borehole dataset, and (f) surface dataset.

2.7 Site Effects Term

In our attenuation model (Equation 2.1) we tried to choose a simple form with a minimum number of source and path parameters. The borehole recordings are not contaminated by the effects of wave travel through the surface layers and thus site effects are negligible (Abercrombie, 1997). However, this is not the case for surface recordings for which the local site condition affects the recorded strong motion. Local site effects include the properties of the uppermost several hundred meters of rock and soil and the effect of the surface topography near the recording site. The importance of recording site effects on seismic ground motion has been well studied by many researchers (see Abercrombie, 1997; Macias et al., 2008; Oth et al., 2011). In order to account for these effects in our surface strong-motion records, we determined the site effects term for each site in that database. We calculated the residual between the predicted magnitude and the final magnitude estimate (M_{pga} and M_{pgv}) for each site and each event. We then determined the site-effects term as the average residual for each site over multiple events (Figure 2.7). We corrected the final magnitude estimate by subtracting these site-effects terms from the estimated magnitude at each site for the surface record database. After applying this correction, we were able to compare the magnitude estimates from borehole and surface record databases to determine which database can provide us with better magnitude estimates (i.e., lower standard deviations).

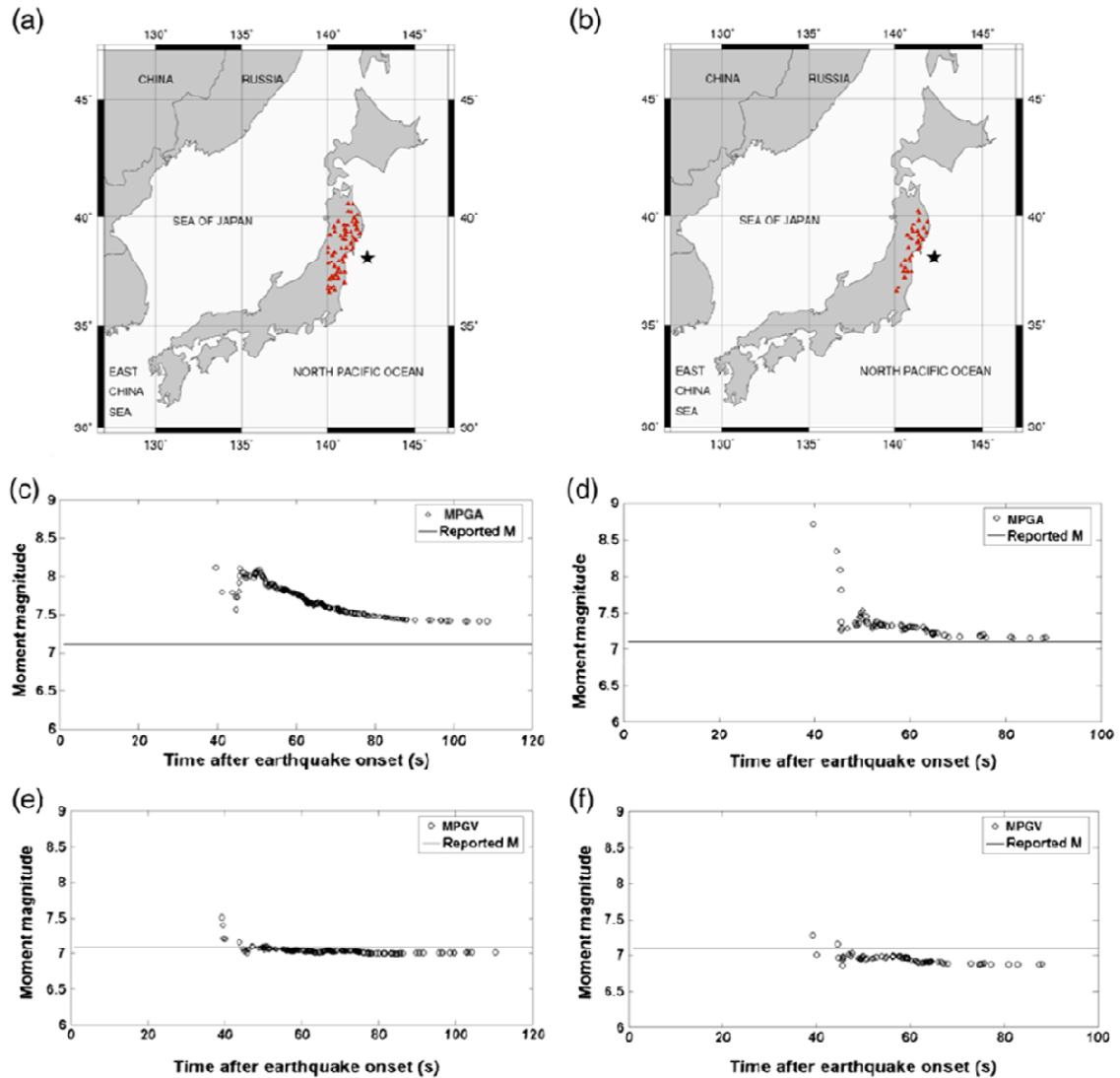


Figure 2.6. Map of KiK-net stations that recorded PGA and PGV for the 16 August 2005 M7.1 event for (a) borehole records with $PGA \geq 10 \text{ cm/s}^2$ and (b) surface records with $PGA \geq 80 \text{ cm/s}^2$. Mpga versus time (seconds) after origin time for current (c) borehole dataset and (d) surface dataset. Mpgv versus time (seconds) after origin time for current (e) borehole dataset, and (f) surface dataset.

The comparison confirms that borehole data provide us with more accurate estimates of magnitude, even if site terms are used to improve the estimates based on the surface data

(Table 2.1). We used the above mentioned technique for the borehole records database as well, but there was no significant difference in the results.

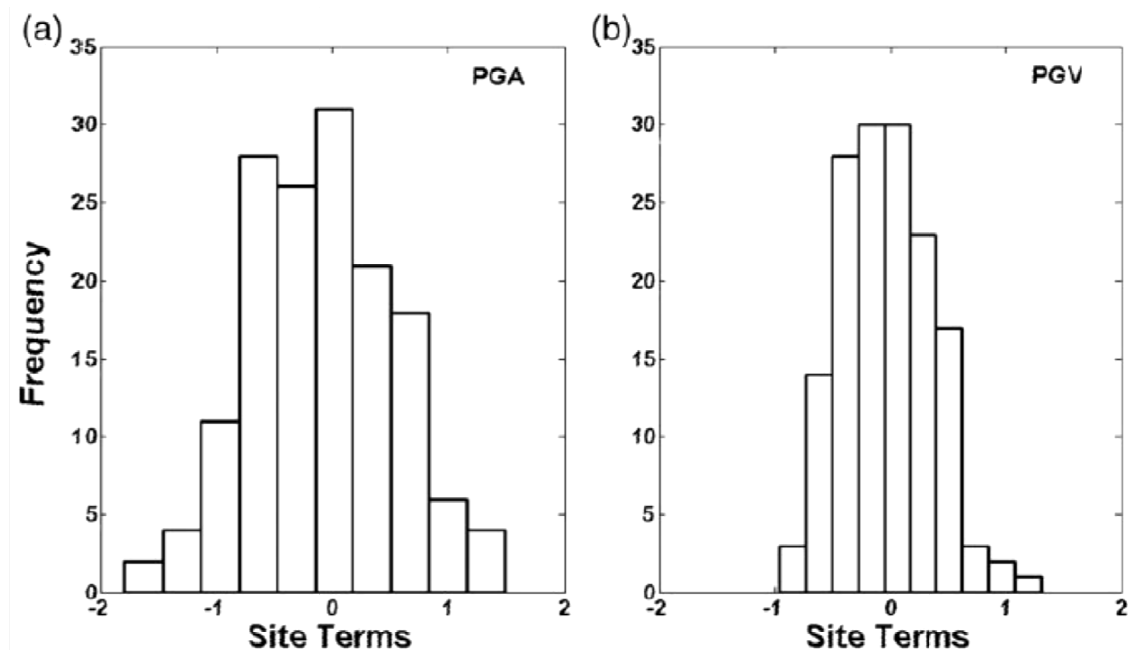


Figure 2.7 (a) Histograms of the site terms for magnitude estimates from PGA values. (b) Histograms of the site terms for magnitude estimates from PGV values.

2.8 Conclusions

The goal of EEW and rapid reporting systems is to provide warning and early information about upcoming large earthquakes capable of disastrous damage. One of the most important parameters is the accurate estimation of magnitude as quickly as possible for large events (e.g., $M \geq 6$). In this study we demonstrate that we can obtain a good approximation of M for a large event using GMPEs after about 40 seconds after the onset of a major earthquake. As shown in Table 2.1, M_{pgv} can provide more accurate and stable magnitude estimates than M_{pga} for both borehole and surface databases (Figures 2.5 and 2.6). Magnitude estimates from borehole data have significantly smaller standard

deviations than those derived from surface data, even if the surface data are corrected for site terms (Figure 2.8). Because a dense seismic network can provide many PGA and PGV observations within a very short time (<1 min) following earthquake occurrence, we can improve the accuracy of magnitude estimation for EEW using PGA and PGV observations. In addition, the use of borehole seismic records can significantly increase the accuracy of magnitude estimation for both M_{pga} and M_{pgv} relative to surface recordings. Accurate magnitude estimates are critical during strong earthquakes, particularly for those that are capable of causing tsunamis, such as the Tohoku earthquake. Faster earthquake and tsunami early-warning systems in seismogenic areas can provide more time to evacuate people from hazardous areas and improve emergency response efficiency. Based on our study results, we conclude that the use of PGV GMPEs based on borehole data as a tool to estimate magnitude would improve the performance of EEW and tsunami early-warning systems.

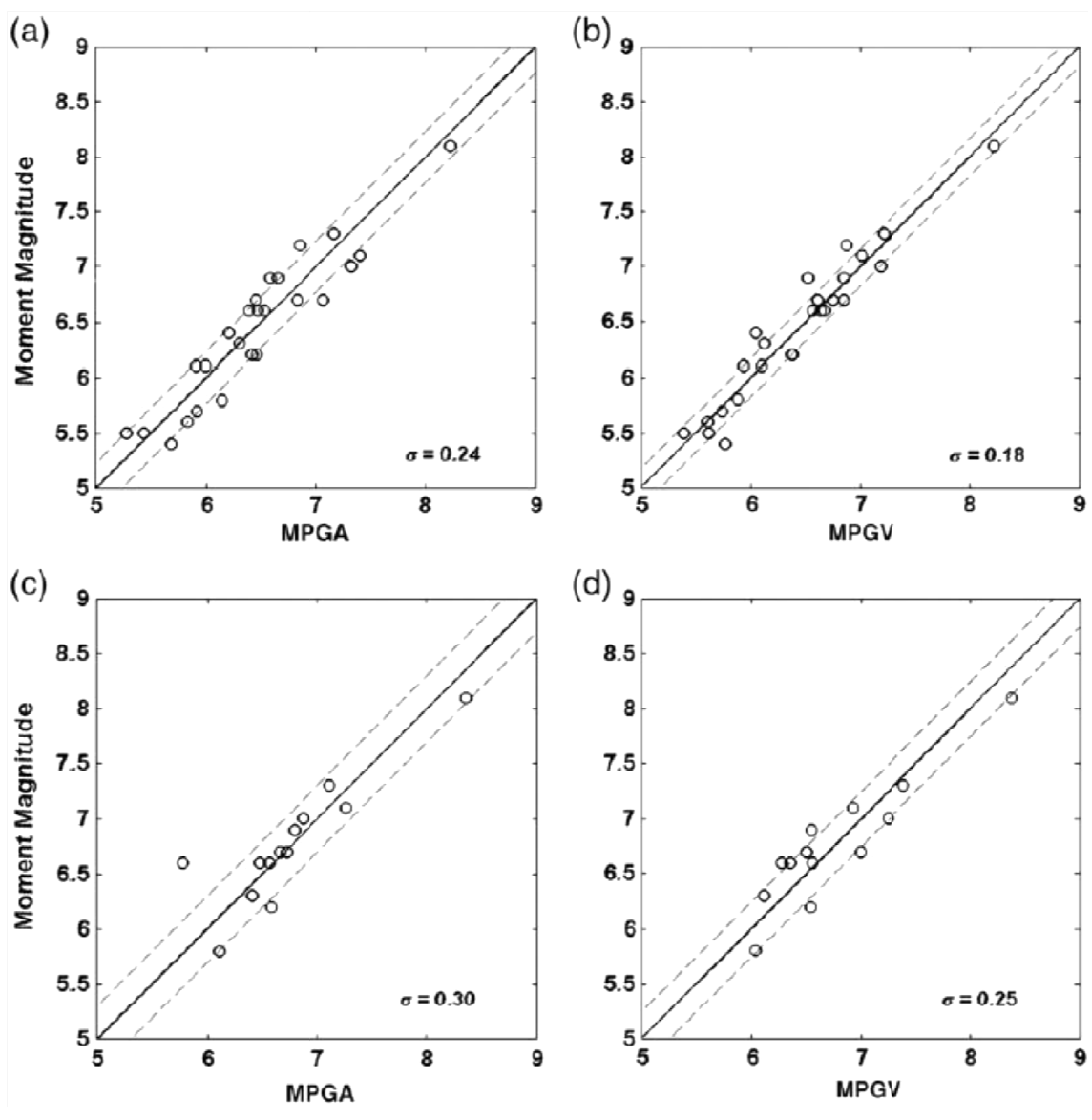


Figure 2.8 M versus predicted magnitude (Mpga and Mpgv) for the (a, b) borehole database and (c, d) surface dataset.

2.9 References

Abercrombie, R. E. (1997). Near-surface attenuation and site effects from comparison of surface and deep borehole recordings, *Bull. Seismol. Soc. Am.* 87, 731–744. Allen, M.,

and H. Kanamori (2003). The potential for earthquake early warning in southern California, *Science* 300, 786–789.

Allen, M., P. Gasparini, O. Kamigaichi, and M. Bose (2009). The status of earthquake early warning around the world: An introductory overview, *Seismol. Res. Lett.* 80, no. 5, doi: 10.1785/gssrl.80.5.682.

Aoi, S., T. Kungugi, and H. Fujiwara (2004). Strong-motion seismograph network operated by NIED: K-NET and KiK-net, special issue, *J. Japan Assoc. Earthq. Eng.* 4, no. 3 (special issue), 65–74.

Brownlee, K. A. (1960). *Statistical Theory and Methodology in Science and Engineering*, Second Ed., John Wiley and Sons, New York, 346 pp.

Doi, K (2011). The operation and performance of earthquake early warnings by the Japan Meteorological Agency, *Soil Dynam. Earthq. Eng.* 31, doi: 10.1016/j.soildyn.2010.06.009.

Espinosa-Aranda, J. M., A. Jimenez, G. Ibarrola, F. Alcantar, A. Aguilar, M. Inostroza, and S. Maldonado (1995). Mexico City seismic alert system, *Seismol. Res. Lett.* 66, 42–52.

Garden, J. S., D. G. Mitchell, and W. N. Mills (1980). Non-constant variance regression techniques for calibration-curve-based analysis, *Anal. Chem.* 52, 2310–2315.

Ghofrani, H., and G. M. Atkinson (2011). Forearc versus backarc attenuation of earthquake ground motion, *Bull. Seismol. Soc. Am.* 101, 3032–3045.

Hayes, G. P. (2011). Rapid source characterization of the 2011 Mw off the Pacific coast of Tohoku Earthquake, *Earth Planets Space* 63, 529–534.

Imamura, A. (1924). Preliminary note on the great earthquake of southeastern Japan on September 1, 1923, *Bull. Seismol. Soc. Am.* 14, 136–149.

Kamigaichi, O. (2004). JMA earthquake early warning, *J. Japan Assoc. Earthq. Eng.* 4, no. 3.

Kamigaichi, O., M. Saito, K. Doi, T. Matsumori, S. Tsukada, K. Takeda, T. Shimoyama, K. Nakamura, M. Kiyomoto, and Y. Watanabe (2009). Earthquake early warning in Japan: Warning the general public and future prospects, *Seismol. Res. Lett.* 80, no. 5, 717–726.

Kanamori, H. (2005). Real-time seismology and earthquake damage mitigation, *Annu. Rev. Earth Planet Sci.* 33, 195–214.

Kanamori, H., E. Hauksson, and T. Heaton (1997). Real-time seismology and earthquake hazard mitigation, *Nature* 390, 461–464.

Kanno, T., A. Narita, N. Morikawa, H. Fujiwara, and H. Fukushima (2006). A new attenuation relation for strong ground motion in Japan based on recorded data, *Bull. Seismol. Soc. Am.* 96, 879–897.

Lee, W. H. K., and J. M. Espinosa-Aranda (2003). Earthquake early warning systems: Current status and perspectives, in *Early Warning Systems for Natural Disaster Reduction*, J. Zschau and A. N. Koppers (Editors), Springer, Berlin, 409–423.

- Lin, T., and Y. M. Wu (2010). Magnitude determination using strong ground motion attenuation in earthquake early warning, *Geophys. Res. Lett.* 37, no. 7, L07304, doi: 10.1029/2010GL042502.
- Lin, T., Y. M. Wu, D. Chen, N. Hsiao, and C. Chang (2011). Magnitude estimation in earthquake early warning for the 2010 JiaSian, Taiwan earthquake, *Seismol. Res. Lett.* 82, no. 2, 201–206.
- Macias, M., G. M. Atkinson, and D. Motazedian (2008). Ground-motion attenuation, source, and site effects for the 26 September 2003 M 8.1 Tokachi-Oki earthquake sequence, *Bull. Seismol. Soc. Am.* 98, no. 4, 1947–1963, doi: 10.1785/0120070130.
- Miller, R. P. (1966). *Simultaneous Statistical Inference*, McGraw-Hill, New York, 272.
- Mori, N., T. Takahashi, T. Yasuda, and H. Yanagisawa (2011). Survey of 2011 Tohoku earthquake tsunami inundation and run-up, *Geophys. Res. Lett.* 38, L00G14, doi: 10.1029/2011GL049210.
- Odaka, T., K. Ashiya, S. Tsukada, S. Sato, K. Ohtake, and D. Nozaka (2003). A new method of quickly estimating epicentral distance and magnitude from a single seismic record, *Bull. Seismol. Soc. Am.* 93, 526–532.
- Oth, A., D. Bindi, S. Parolai, and D. Di Giacomo (2011). Spectral analysis of K-NET and KiK-net data in Japan, part II: On attenuation characteristics, source spectra, and site response of borehole and surface stations, *Bull. Seismol. Soc. Am.* 101, 667–687.

Teng, T. L., L. Wu, T. C. Shin, Y. B. Tsai, and W. H. K. Lee (1997). One minute after: Strong motion map, effective epicenter, and effective magnitude, *Bull. Seismol. Soc. Am.* 87, 1209–1219.

Tsukada, S., S. Odaka, K. Ashiya, K. Ohtake, and D. Nozaka (2004). Analysis of the envelope waveform of the initial part of P waves and its application to quickly estimating the epicentral distance and magnitude, *Jisin 2*, 56, 351–361 (in Japanese).

Wu, Y. M., and T. L. Teng (2002). A virtual subnetwork approach to earthquake early warning, *Bull. Seismol. Soc. Am.* 92, 2008–2018.

Wu, Y. M., H. Kanamori, R. M. Allen, and E. Hauksson (2007). Determination of earthquake early warning parameters, τ_c and P_d , for southern California, *Geophys. J. Int.* 170, 711–717, doi: 10.1111/j.1365-246X.2007.03430.x.

Wu, Y. M., T. C. Shin, and Y. B. Tsai (1998). Quick and reliable determination of magnitude for seismic early warning, *Bull. Seismol. Soc. Am.* 88, 1254–1259.

Chapter 3

3 Magnitude Estimation for the 2011 Tohoku-Oki Earthquake Based on Ground Motion Prediction Equations²

² A version of this chapter has been published. **Eshaghi, A.**, K. F. Tiampo, H. Ghofrani, and G. M. Atkinson (2013). Magnitude Estimation for the 2011 Tohoku-Oki Earthquake Based on Ground Motion Prediction Equations, *Pure Appl. Geophys.* doi: 10.1007/s00024-013-0746-y

This chapter presents results for the application of the GMPEs estimated in the previous chapter to estimate the magnitude of the 2011 Tohoku-Oki earthquake in Japan. Ultimately, such an estimate could be used as input data for both an earthquake and a tsunami forecast, leading to more robust earthquake and tsunami early warnings. Furthermore, this study extends the findings from the previous chapter for the simple GMPEs by using a more complete database (1998 – 2011), which increased by only one year but included approximately twice as much data as the initial catalog. New GMPEs were developed using this new catalog in order to improve the estimation of attenuation parameters and magnitude scaling. The magnitude of the Tohoku-Oki event was estimated from these new GMPEs, in addition to that of all earthquakes in the new catalog with at least 20 records. The estimates obtained for the Tohoku event were compared with real time magnitude estimates provided by the existing EEW system in Japan. This comparison demonstrated that, unlike the estimation provided by the Japanese EEW system, the GMPE estimation does not show saturation. Instead, robust estimates of moment magnitude for both catalogs were determined within 100 s of the earthquake onset. It also was found that correcting for average shear-wave velocity in the uppermost 30 m improved the accuracy of magnitude estimates from surface recordings, particularly for magnitude estimates of PGV. Results show that the magnitude estimate from PGV values using borehole recordings had the smallest standard deviation among the estimated magnitudes and produced more stable and robust magnitude estimates. This confirms that incorporating borehole strong ground-motion records immediately available after the occurrence of large earthquakes can provide more robust and accurate magnitude estimation.

3.1 Introduction

On 11 March 2011, a megathrust earthquake occurred at Tohoku-Oki, Japan. This event is the largest recorded earthquake in the modern history of Japan (Hayes, 2011). This earthquake occurred in the western Pacific Ocean where the Pacific plate subducts beneath northern Honshu at a rate of ~ 9 cm/yr (DeMets et al., 2010). The hypocenter was located 130 km east of Oshika peninsula at a focal depth of 24 km. The earthquake generated strong, widespread shaking that registered a seismic intensity of 7 on the Japan Meteorological Agency (JMA) scale at Kurihara city, Miyagi Prefecture and an intensity of 6+ along the Pacific region (Hoshiba et al., 2011). There were foreshock sequences two days prior to the main event, and numerous aftershock sequences (Peng et al., 2012). Thousands of accelerograms, seismograms and geodetic instruments recorded these foreshock-mainshock-aftershock sequences across Japan, which made this event the best recorded mega-thrust earthquake in history. The event rupture spread over an area of about 450 km (NS direction) and 200 km (EW direction) (Mori et al., 2011), resulting in a devastating tsunami that propagated to the Pacific coast. The tsunami caused the greatest loss of life and damage in coastal areas, and also led to the Fukushima-Daiichi nuclear crisis (Mori et al., 2011). This event provided a real time test for the Earthquake Early Warning (EEW) system in Japan, providing evidence for both the performance benefits and flaws in the current EEW system operated by JMA. This earthquake provides us with an opportunity to test a new proposed magnitude determination method for the EEW system, detailed in Eshaghi et al. (2013) and the previous chapter.

EEW systems based on seismic methods operate in different countries, such as Japan and Taiwan (Allen et al., 2009). Most of the methods use the earliest P-arrivals to

provide longer warning times. Usually these methods are based on the empirical relationship between magnitude and either predominant period (Nakamura, 1998; Kanamori, 2005; Allen et al., 2009), the peak amplitudes of the early P-wave (Wu and Zhao, 2006), or a combination of these parameters. There is some limitation to these methods, including the lack of reliability of the magnitude estimations or the problem of saturation in the empirical relationships for large magnitudes (Yamada and Mori, 2009). Lin and Wu (2010) proposed a regional method that employs a strong ground motion prediction equation (GMPE) for large crustal earthquakes in Taiwan to estimate the magnitude using the observed PGA (M_{pga}). Their results showed that, with sufficient PGA readings, the M_{pga} estimate is similar to the actual moment magnitude of an event. This method was tested for the 2010 JiaSian, Taiwan earthquake and implementation in real time of this method was proposed for future EEW practice (Lin et al., 2011).

The JMA has operated an EEW system for advanced users since August 2006 and for the general public since October 2007 (Doi, 2011). This system is based on front detection, a regional method in which seismometers near the earthquake source zone will give early warnings to more distant urban areas. The operating EEW system in Japan is divided into three steps: earthquake detection, forecast and, finally, warning dissemination (Hoshihara et al., 2008; Kamigaichi et al., 2009; Doi, 2011). There are approximately 1100 seismic stations run by JMA and Japan's National Research Institute for Earth Science and Disaster Prevention (NIED), which provide information for earthquake detection, magnitude and source location determination. A combination of several methods is used to locate the earthquake (hypocenter/epicenter) and the magnitude (M_{JMA}) is estimated from the maximum displacement amplitude (Horiuchi et

al., 2005, Kamigaichiet al., 2009; Hoshiha et al., 2011). When a magnitude of 3.5 or greater is estimated, or if the expected JMA intensity scale is 3 or larger, an EEW forecast is issued to advance users. When the expected JMA intensity is 5-lower or larger, in an area where an intensity of 4 or greater is expected, an EEW warning is issued to the general public. The warning is updated as more data become available which improves the accuracy of the warning (Hoshiha et al., 2011).

When a tsunamigenic earthquake occurs in coastal regions of Japan, the immediate provision of tsunami information is essential in order to mitigate the catastrophic losses caused by tsunamis. After the occurrence of a large earthquake ($M \geq 8.0$), the possibility of tsunami generation is estimated from the first seismic observation data. Immediately after an earthquake occurs, JMA uses the estimated location and magnitude to calculate the related tsunami risk. The magnitude and focal mechanism of the event are the two most important factors in determining the tsunami hazard. The JMA then determines if the event occurs in a subduction zone of the estimated location of the event, and from the estimated magnitude and distance to the coastal area, JMA can calculate the maximum tsunami heights and the first arrival time of the waves to the coastal area (Japan Meteorological Agency, 2013).

Eshaghi et al. (2013) proposed the use of GMPEs for both observed PGA and peak ground velocity (PGV) values from borehole and surface recordings to determine the moment magnitude of large earthquakes in Japan. The GMPEs were found for borehole recordings and surface recordings separately using the attenuation model:

$$\log_{10}(Y) = a \log_{10}(r) + bM + c, \quad (3.1)$$

where Y is either PGA (cm/s^2) or PGV (cm/s), r is the epicentral distance in km and M is moment magnitude. A simple functional form was chosen to facilitate robust and rapid implementation and epicentral distance was used because it is available immediately after occurrence of an event. The authors analyzed strong ground motion data from earthquakes with $5.0 \leq M \leq 8.1$ recorded by KiK-net stations provided by NIED from 1998 to 2010 (hereafter designated Catalog 1, Table 3.1). Catalog 1 included 2160 strong ground motion accelerograms with PGA larger than 10 cm/s^2 recorded by borehole seismographs, and 890 waveforms with PGA larger than 80 cm/s^2 recorded by surface seismographs. The GMPEs derived from Equation 3.1 for PGA and PGV (Table 3.2) were used to estimate the event magnitude for each PGA (M_{pga}) and PGV (M_{pgv}) reading in the order that they became available in the borehole and surface record datasets. The mean value of these estimates showed strong correlation with the reported moment magnitude of the large events, provided at least 20 records were available (Eshaghi et al., 2013).

In this study we calculate and compare the magnitude estimations from the existing EEW system in Japan (EEW M), the GMPE for PGA values, and the GMPE for PGV values for the 2011 Tohoku earthquake. We also collected the data from 2010 – 2011 and we added these recordings to Catalog 1 to improve the database for magnitude ranges, as this data represented a nearly two-fold increase in overall data, and create a more complete database (hereafter designated Catalog 2, Table 3.1). Using Catalog 2 we developed new GMPEs for both PGA and PGV, which will then be used to estimate the M_{pga} and M_{pgv} for the Tohoku event as well as other events in Catalog 2 that have at least 20 records available in the database. Finally, for surface recordings we explore the

use of the common site variable, average shear-wave velocity in the uppermost 30 m (V_{S30}) (Borcherdt, 1994) to improve the estimation of M_{pga} and M_{pgv} .

Table 3.1 Data used in this study

Catalog	1 (1998-2010)		2 (1998-2011)	
	Borehole	Surface	Borehole	Surface
Records	2160	890	3793	1255
Earthquakes	67	62	129	111
PGA	$\geq 10 \text{ cm/s}^2$	$\geq 80 \text{ cm/s}^2$	$\geq 10 \text{ cm/s}^2$	$\geq 80 \text{ cm/s}^2$
Epicentral distance	$\leq 390 \text{ km}$	$\leq 270 \text{ km}$	$\leq 400 \text{ km}$	$\leq 400 \text{ km}$
Magnitudes	5.1 - 8.1	5 - 8.1	5.0 - 9.0	5.0- 9.0

3.2 Performance of the Existing EEW System for the M9.0

Tohoku Earthquake

The origin time (OT) of the M9.0 event was 14:46:23 JST, March 11, 2011. The first station detected the initial P-wave arrival and recorded the seismic movement at 14:46:40.2 JST at the Ouri station, in Isonomaki city (Okada, 2011; Hoshiya et al., 2011). The first forecast was issued 5.4 s later with an estimated magnitude of 4.3. An EEW was issued to the general public with an estimated magnitude of 7.2 and seismic intensity of 5 – lower to the Sendai area in central Miyagi Prefecture 3.2 seconds after the first forecast (Japan Meteorological Agency, 2011). Because of the small amplitude of the initial part of the waveform, which was comparable to the noise level for displacement, the forecast magnitude was underestimated (Hoshiya et al., 2011). Within

two minutes after the first seismic detection, a total of 15 announcements were issued (Japan Meteorological Agency, 2011). The first warning was 15 s earlier than the time that shaking occurred at the station closest to the epicenter. After this warning, the magnitude estimates declined between the fifth and seventh forecasts, due to the small amplitude of the first portion of the waveform at one of the stations close to the epicenter (Hoshiya et al., 2011). Finally, 116.8 s after the first detection, the fifteenth forecast updated the magnitude to 8.1. JMA revised the magnitude at 16:00 JST to **M8.4** and at 17:30 JST the magnitude was announced as **M8.8**. The final magnitude of **M9.0** was determined two days later (Okada, 2011).

3.3 Strong Ground Motion Databases

The wealth of accelerometer recordings acquired by the KiK-net stations in 2011 provides an invaluable opportunity to develop a more complete strong motion database for an unprecedented range of magnitudes and distances. Since the largest magnitude in Catalog 1 was 8.1, we used these additional recordings to improve the range of magnitudes in order to estimate new GMPEs. To do this, we collected all the recordings from earthquakes with $5.0 \leq M$ from 2010 to 2011 records with focal depth ≤ 50 km with the same criteria for PGA threshold and epicenter distance cut-offs, as discussed in detail in Eshaghi et al. (2013). The value of **M** for each event is that reported by NIED (see Data and Resources Section). We add this new dataset to the Catalog 1 (i.e. 1998 – 2010) to prepare the new more complete catalog (i.e. 1998 - 2011, Catalog 2). Catalog 2 includes 3793 borehole recordings with $PGA \geq 10 \text{ cm/s}^2$ from 129 events and 2155 surface recordings with $PGA \geq 80 \text{ cm/s}^2$ from 111 earthquakes in total (Table 3.1, Figures 3.1 and 3.2). Table 3.1 shows the number of records used in this study for both catalogs.

The earthquake epicenters are shown in Figure 3.1, along with the stations that recorded these selected events for Catalog 2. The distribution of M with epicentral distance and focal depth for both the borehole and surface records database in Catalog 2 is shown in Figure 3.2, which implies that the majority of events have $M \leq 7.4$ and the magnitude with depth is randomly distributed ranging from 0 to 50 km.

Table 3.2 Equation 1 parameters for each database.

Coefficients		a	B	c	σ	
1998-2010	Borehole	PGA	-0.8129	0.3270	0.7194	0.2183
		PGV	-0.7720	0.5981	2.1191	0.2444
	Surface	PGA	-0.4350	0.2050	1.6115	0.1872
		PGV	-0.6210	0.4216	0.7808	0.2590
1998-2011	Borehole	PGA	-0.6555	0.2609	0.8415	0.2263
		PGV	-0.6235	0.4730	-1.6137	0.2415
	Surface	PGA	-0.3937	0.1758	1.7322	0.1850
		PGV	-0.5117	0.3263	-0.3931	0.2497

All records were corrected for baseline trend and a noncausal, band-pass Butterworth filter of order 4 and corner frequencies of 0.1-15 Hz was applied (Ghofrani et al., 2013).

The accelerograms were integrated in time to obtain the velocity records.

3.4 New Strong Ground Motion Prediction Equation

Following the same procedures of Eshaghi et al. 2013, in this study we use Equation 3.1 to develop new GMPEs for Catalog 2 (as summarized in Table 3.2). We employ the newly derived GMPEs to invert the magnitude for each PGA and PGV reading (Table 3.4 and Table 3.5). Note that we do not consider anelastic attenuation in Equation 3.1, in order to ensure that the function is reasonable for all events, as the use of a linear r term results in upward curvature at large distances for some events (Eshaghi et al., 2013).

The influence of site effects on ground motion amplitudes is well known (e.g., Abercrombie, 1997; Macias et al., 2008; Ghofrani et al., 2013). The commonly used site parameter is the V_{S30} (Borcherdt, 1994). We developed an empirical model to account for site effects for KiK-net surface stations and applied that correction to the surface record data. The average shear-wave velocity at an observation station was adopted as the parameter representing site conditions. It is defined as:

$$V_{S30} = 30 / \sum_{i=1}^n (h_i / V_i), \quad (3.2)$$

(Borcherdt, 1994) where n is the number of layers in the uppermost 30 m depth and h_i and V_i denote the thickness (m) of the layers and the shear-wave velocity (m/sec) of the i th layer respectively. A general form of attenuation considering the source, path and site effects can be written as (Boore and Atkinson, 2008):

$$\log_{10}(Y) = a_1 \mathbf{M} + b_1 \log_{10}(r) + d_1 \log_{10}(V_{S30}/V_{ref}) + c_1 \quad (3.3)$$

where we assumed that site amplification is linearly dependent on V_{S30} and is determined with respect to the motions that would be recorded in a National Earthquake Hazards

Reduction Program (NEHRP) B-C site condition ($V_{\text{ref}} = 760 \text{ m/s}$). We used those stations with available shear-wave velocity profiles in this study. We employed a linear least-squares inversion to determine the unknown coefficients (a_1 , b_1 , c_1 and d_1) in Equation 3.3. We considered the borehole recordings to be uncontaminated by the effects of wave travel through the surface layers, so that site effects could be considered negligible (Abercrombie, 1997). The GMPEs using the model obtained from Equation 3.3 (for both catalogs) then were used to estimate the magnitude of events for the surface recordings databases.

The resulting coefficients for Equation 3.3 for both catalogs are shown in Table 3.3. Correction for site amplification using V_{S30} results in reduction in the standard deviation (σ) of ground motion predictions, particularly for GMPEs for PGV (Table 3.2 and Table 3.3). The distributions of residuals [$\log_{10}(\text{observed/predicted})$] versus epicentral distance for PGA and PGV for Catalog 2 are shown in Figure 3.3, where different symbols show the range of magnitudes. Note that we used Equation 3.1 for borehole recordings and Equation 3.3 for surface recordings. Figure 3.3 indicates that there is no trend for the residuals with epicentral distance or magnitude of the events for both equations. Histograms of the residuals for PGA and PGV are shown in Figure 3.4 and illustrate that residuals for PGA and PGV follow a normal distribution with zero mean.

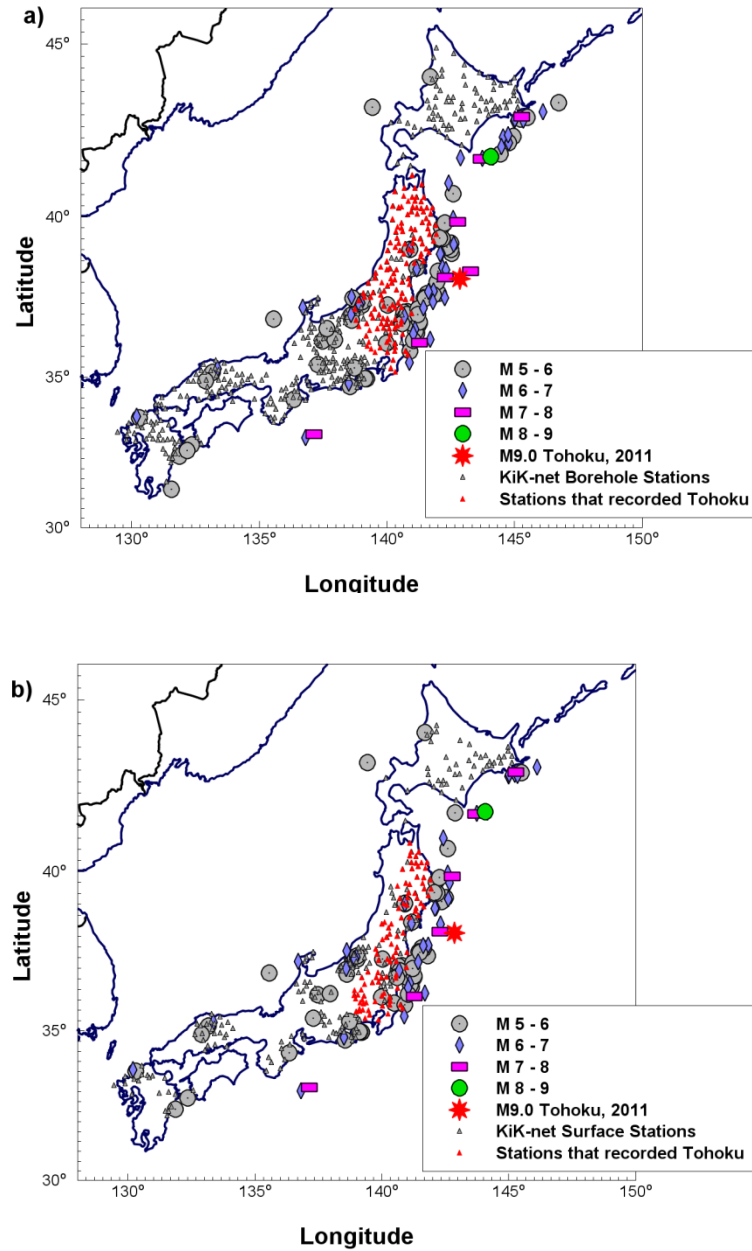


Figure 3.1 Spatial distribution of the epicenter of selected events (Catalog 2) used in this study (open circles). KiK-net stations (grey triangles) that registered the (a) borehole recordings with $\text{PGA} \geq 10 \text{ cm/s}^2$ and (b) surface recordings with $\text{PGA} \geq 80 \text{ cm/s}^2$. KiK-net stations that recorded the Tohoku event are identified as red triangles. The star represents the epicenter of 2011 Tohoku event.

Tables 3.2 and 3.3 show that the parameters between catalogs 1 and 2 are different, which can be interpreted as a result of the dependency of these parameters on the magnitude. The functional form used is very simple and does not include complexities such as distance saturation effects for large magnitude events. As a consequence, when we improve the dataset to include larger magnitudes, the absolute value of the geometric spreading coefficient (which is an average attenuation effect that smoothes over various complexities) will decrease. For example, geometrical spreading for the borehole database in Table 3.2 is -0.8129 for Catalog 1 and -0.6555 for Catalog 2. The extrapolation of simple GMPEs may cause unknown biases if the magnitude scaling for very large events is not empirically constrained (Ghofrani et al., 2013). Therefore, it is important to use a catalogue that adequately covers the magnitude-distance range of interest for this application. We note that this is why ground motions are often simulated in regions where recordings of motion from potentially damaging earthquakes are not available (e.g. Boore, 2003), to allow extension of the database to larger magnitudes.

Table 3.3 Equation 3.3 parameters for surface recordings.

Catalog		a_1	b_1	c_1	d_1	σ
1998-2010	PGA	0.2001	-0.4242	-0.0825	1.5988	0.1849
	PGV	0.4092	-0.6249	-0.5873	-0.8660	0.2363
1998-2011	PGA	0.1752	-0.3928	-0.0358	1.7251	0.1850
	PGV	0.3282	-0.5480	-0.5875	-0.5033	0.2257

3.5 Magnitude Estimation for M9.0 Tohoku Event

The Tohoku earthquake was well recorded in the near field by numerous KiK-net stations at the surface and boreholes. We collected all available acceleration time histories recorded by both borehole and surface KiK-net stations. The epicentral distance in our database is up to 400 km. In total, 409 borehole records with $PGA \geq 10 \text{ cm/s}^2$ from 143 stations and 219 records with $PGA \geq 80 \text{ cm/s}^2$ from 86 stations were collected. To calculate the magnitude, we substitute the initial epicentral location estimate and PGA or PGV values into the obtained GMPEs and we solve the equation to estimate the magnitude of the event for each recording. By adding a new record, the new magnitude is calculated as the weighted average of the previous magnitude estimation and the new magnitude observation. Therefore, the magnitude is updated as more stations contribute data (Eshaghi et al., 2013).

We calculate the magnitude of the Tohoku earthquake using observed PGA and PGV values and we compare these magnitude estimations to predicted magnitudes provided by the EEW system in Japan (Figure 3.5 and 3.6). Table 3.4 shows the obtained M_{pga} and M_{pgv} values using GMPEs from both catalogs. The M_{pga} , M_{pgv} and EEW magnitude estimation histories as a function of time after earthquake onset, along with the reported M for this event, are shown in Figure 3.5 (based on GMPEs from Catalog 1), and Figure 3.6 (based on GMPEs from Catalog 2) respectively. Figure 3.5a shows the M_{pga} for borehole recordings from Catalog 1, where between 50 and 90 s after the origin time (OT) the estimated magnitude is above $M9.0$. After 90–160 s the M_{pga} fluctuates around $M8.9$ (it varies between $M8.7$ and $M8.9$). About 165s after OT, the M_{pga} becomes

stable around $M8.7$ and it remains stable at this value until the end of the event ($M8.70 - M8.85$).

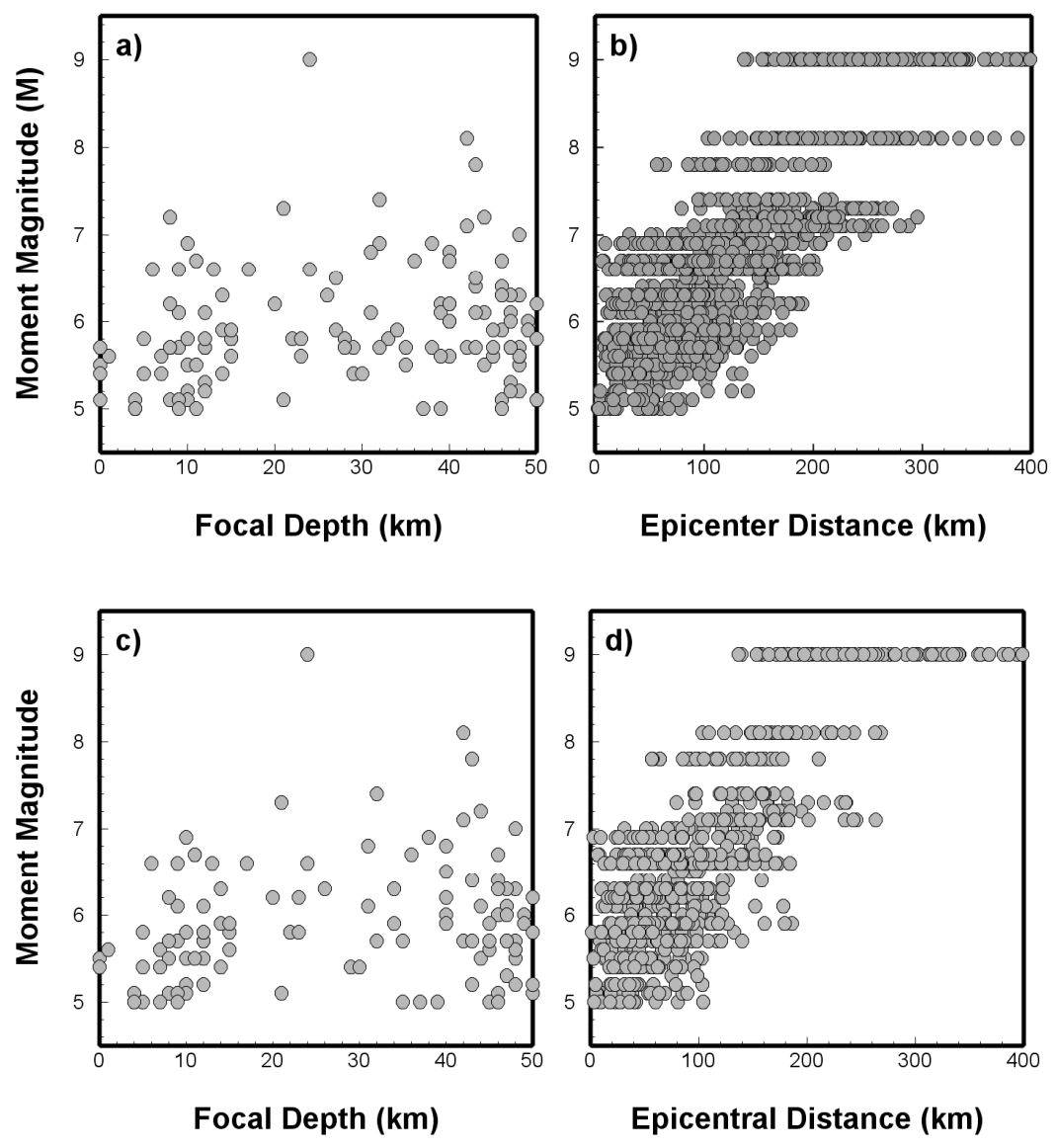


Figure 3.2 Magnitude-focal depth for borehole database (a) and surface database (c). Magnitude-epicentral distance distributions for the borehole database (b) and surface database (d).

As can be seen in Figure 3.5b, the M_{pgv} became stable after receiving the first five records from the borehole stations, about 100 s after the earthquake onset (with fluctuations between 8.4 and 8.5). The surface database in Catalog 1 produced approximately the same values for final M_{pga} and M_{pgv} (Table 3.4; Figures. 3.5c, d). The M_{pga} from the surface recordings dropped to $M9.0$ around 120 s after OT, and it fluctuated between $M8.9$ and $M9.0$ subsequently (Figure 3.5c). Figure 3.5d shows the variation of M_{pgv} for the surface database from Catalog 1, where it starts at $M9.2$ (67 s after OT) and then drops to $\sim M8.6$ about 90 s after OT and remains stable until the end of the event. Note that these estimations are based on GMPEs obtained from Catalog 1 where the highest magnitude was $M8.1$. Therefore, despite the fact that the range of magnitude in Catalog 1 did not contain magnitudes larger than $M8.1$, this method still provides reasonable magnitude estimates for the Tohoku event and, unlike the existing EEW system, it did not saturate. Figure 3.6a–d shows the magnitude estimation using the GMPEs from Catalog 2 and the EEW magnitude estimation histories as a function of time after earthquake onset. Although the Tohoku event was complex, the estimated magnitudes are within a reasonable range. Figure 3.6a shows that the M_{pga} from borehole recordings overestimates the magnitude from 50 s to about 100 s after OT. Approximately 100 s after earthquake onset, the magnitude became stable around $M9.0$, although there were some fluctuations.

The M_{pgv} evolution with time (from borehole recordings) is shown in Figure 3.6b. The magnitude is overestimated for the first ten records, but it becomes stable at $M9.0$ approximately 100 s after OT. M_{pga} for surface recordings (Figure 3.6c) fluctuates more than other estimations. It overestimates the magnitude from beginning to end but it

gradually drops to around **M9.1**. Finally, the M_{pgv} from surface recordings is shown in Figure 3.6d. It has the same trend as Figure 3.6b, where the magnitude is overestimated from the first ten records, but after receiving more recordings the magnitude converges to **M9.0** (about 100 s after OT) and it remains stable around this value until the end of the event. Figures 3.6b and 3.6d show that, as expected, M_{pgv} values are more stable than M_{pga} values. The M_{pgv} is estimated at **M8.9** and **M9.0** for the borehole and surface databases (from Catalog 2), respectively, at 100 s after OT. Our estimation of magnitude from both catalogs ranges from **M8.46** to **M9.17**, which implies that this method would have been capable of predicting the magnitude of the Tohoku earthquake ~100 s after rupture initiation. Our results confirm that M_{pgv} from borehole recordings provided more stable magnitude estimations compared to surface recordings.

Table 3.4 Estimated magnitudes, Tohoku earthquake.

	based on GMPEs obtained from Catalog 1 (1998-2010)		based on GMPEs obtained from Catalog 2 (1998-2011)	
	Borehole data	Surface data	Borehole data	Surface data
M_{pga}	8.74	8.98	9.01	9.17
M_{pgv}	8.46	8.61	8.86	9.05

In order to analyze the sensitivity of our proposed technique, we performed two additional tests for the Tohoku earthquake. In these tests, we calculated the magnitude of Tohoku event incorporating GMPEs from two different databases. For the first test, we used the Catalog 2 database, but excluded the records of the Tohoku event and the earthquakes that occurred after this event. For the second test, we excluded the recordings

from Tohoku event itself from Catalog 2 database but we kept the events that occurred after Tohoku.

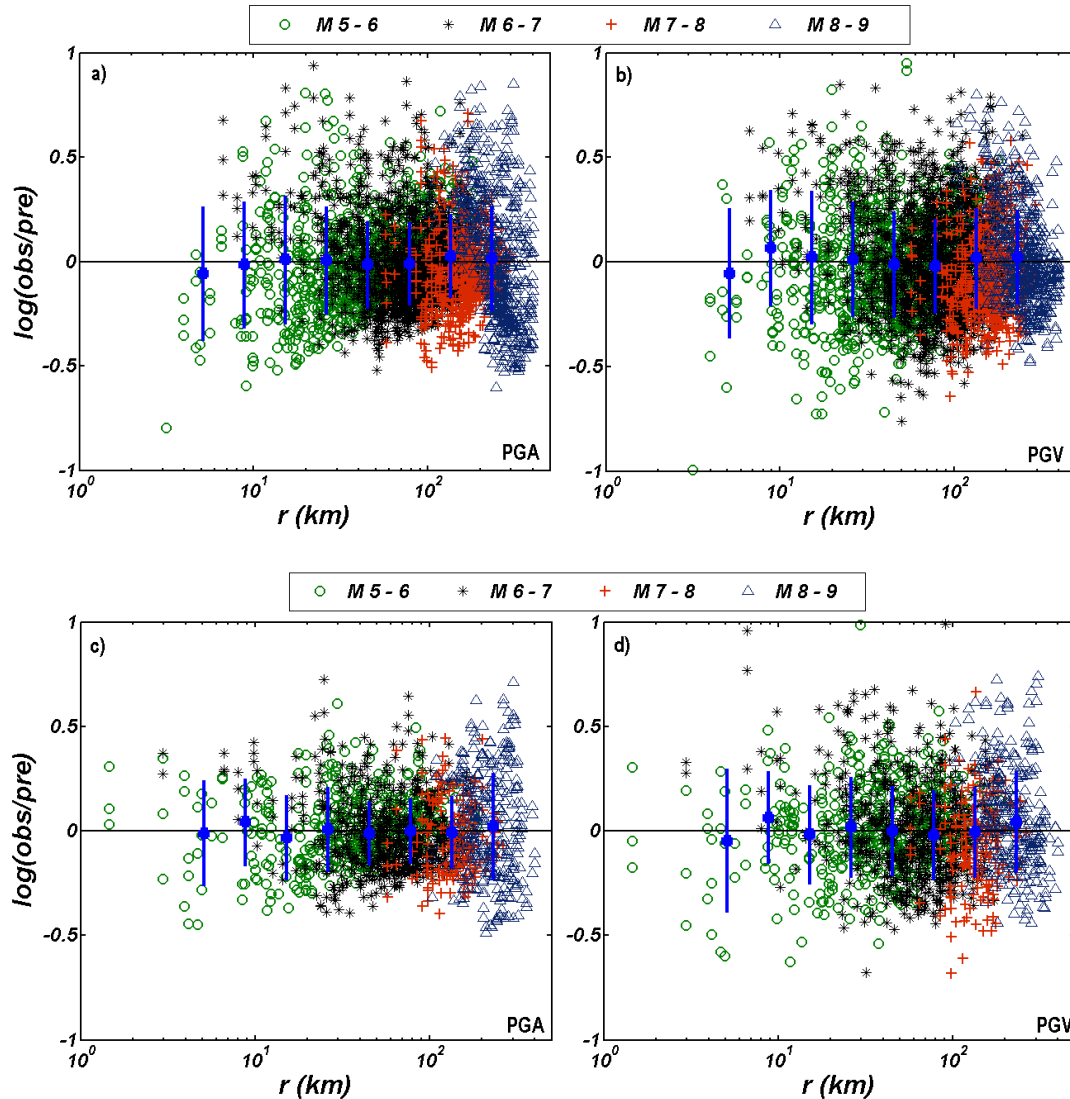


Figure 3.3 Distribution of residuals against epicentral distances for the borehole record database from Equation 3.1 for PGA and PGV (a and b respectively) and for the surface record database from Equation 3.2 for PGA and PGV (c and d respectively). Different symbols show the range of magnitudes. Large square symbols show the mean value of the residuals contained in a specific distance bin, where bars represent ± 1 standard deviation.

We named the databases used for the first and the second test as Catalog 3 and Catalog 4, respectively. Additionally, for each of these catalogues we found the magnitude estimates using borehole and surface GMPEs, separately. The estimated magnitudes are presented in Table 3.6. These results show that in all of the performed tests the estimated magnitudes are reasonably close to the reported magnitude for the Tohoku event.

Table 3.5 Standard deviation for predicted magnitude

	Catalog 1 (1998-2010)			Catalog 2 (1998-2011)		
	Borehole data	Surface data		Borehole data	Surface data	
		No site term	With vs30		No site term	With vs30
Number of earthquakes with 20 and more records	25	13	13	46	31	31
Standard deviation of Mpga (M)	0.24	0.30	0.28	0.31	0.28	0.27
Standard deviation of Mpgv (M)	0.18	0.25	0.15	0.23	0.33	0.25

The magnitude estimates using Catalog 3 and Catalog 4 range from **M8.46** to **M9.48**, which confirms that our method is able to estimate the magnitude of Tohoku

earthquake even when the database does not contain **M9.0**. Table 3.6 shows that the results from surface recordings have higher values in comparison to borehole recordings for both Catalog 3 and Catalog 4. Moreover the estimates obtained from Catalog 4 indicate greater values compare to results from Catalog 3. Although the magnitude estimates from Catalog 2, which includes **M9.0**, show more precise estimations for Tohoku earthquake, still the values obtained from these two tests are in reasonable ranges. We conclude that this method is able to provide robust magnitude estimation even for very large and complex events such as the Tohoku earthquake.

Table 3.6 Estimated magnitudes for Tohoku earthquake based on Catalogs 3 and 4.

	based on GMPEs obtained from Catalog 3		based on GMPEs obtained from Catalog 4	
	Borehole data	Surface data	Borehole data	Surface data
M _{pga}	8.73	8.98	9.07	9.48
M _{pgv}	8.46	8.62	8.67	9.14

3.6 Results Using New GMPEs

We used the new GMPEs to calculate the M_{pga} and M_{pgv} for the Tohoku event as discussed in the previous section as well as all other events that had at least 20 records available in Catalog 2. Figure 3.7 gives three examples of the M_{pga} and M_{pgv} magnitude estimation in real time from the new GMPEs along with the reported **M** for the borehole database (left) and the surface database (right). Table 3.5 shows the standard deviations of M_{pga} and M_{pgv} values for each database for both catalogs.

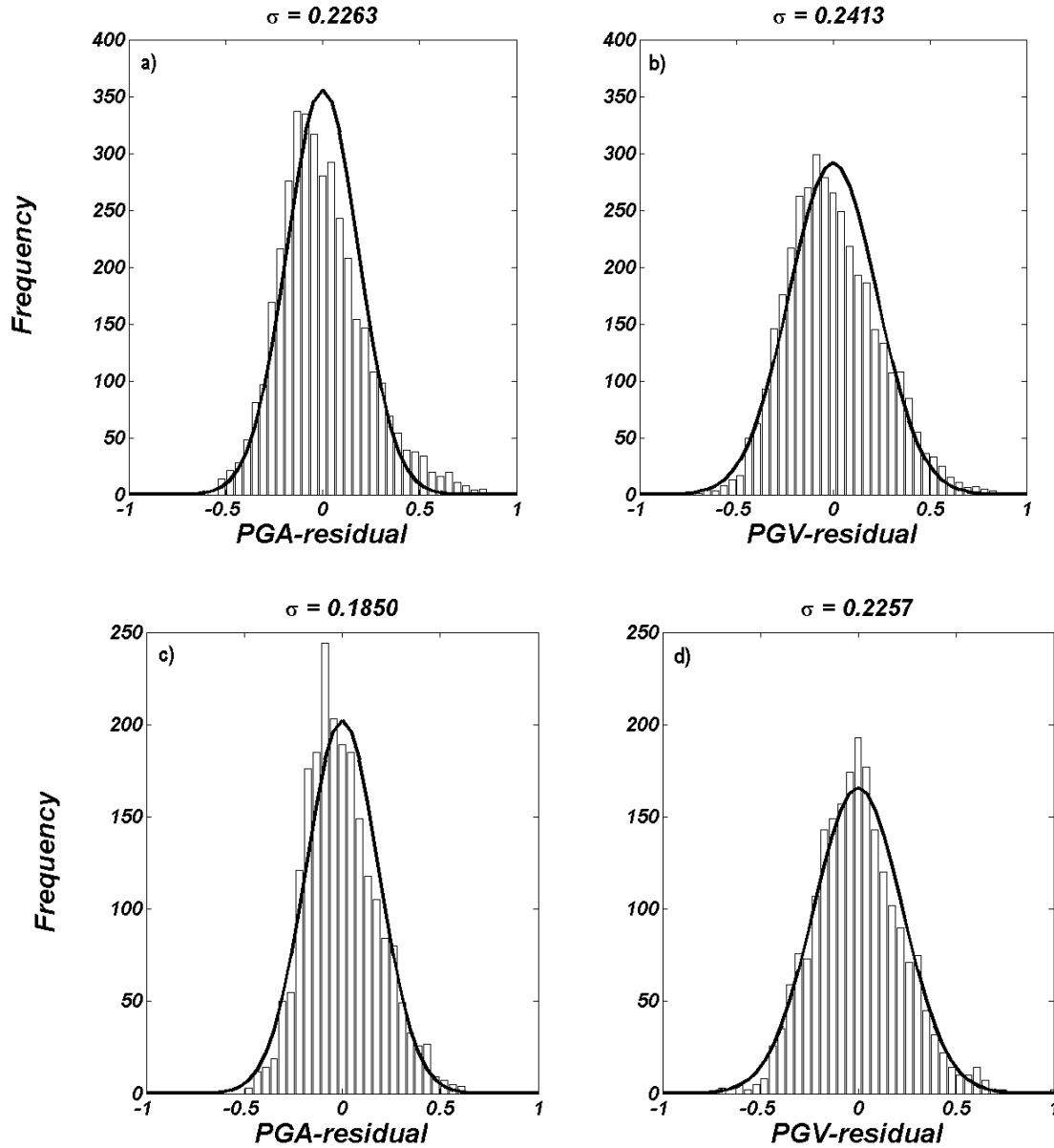


Figure 3.4 The histogram of the residuals for PGA and PGV for the borehole record database (a, b) and surface record database (c, d). σ represents the standard deviation of the residuals. Solid curves represent normal distributions with zero mean and given standard deviation.

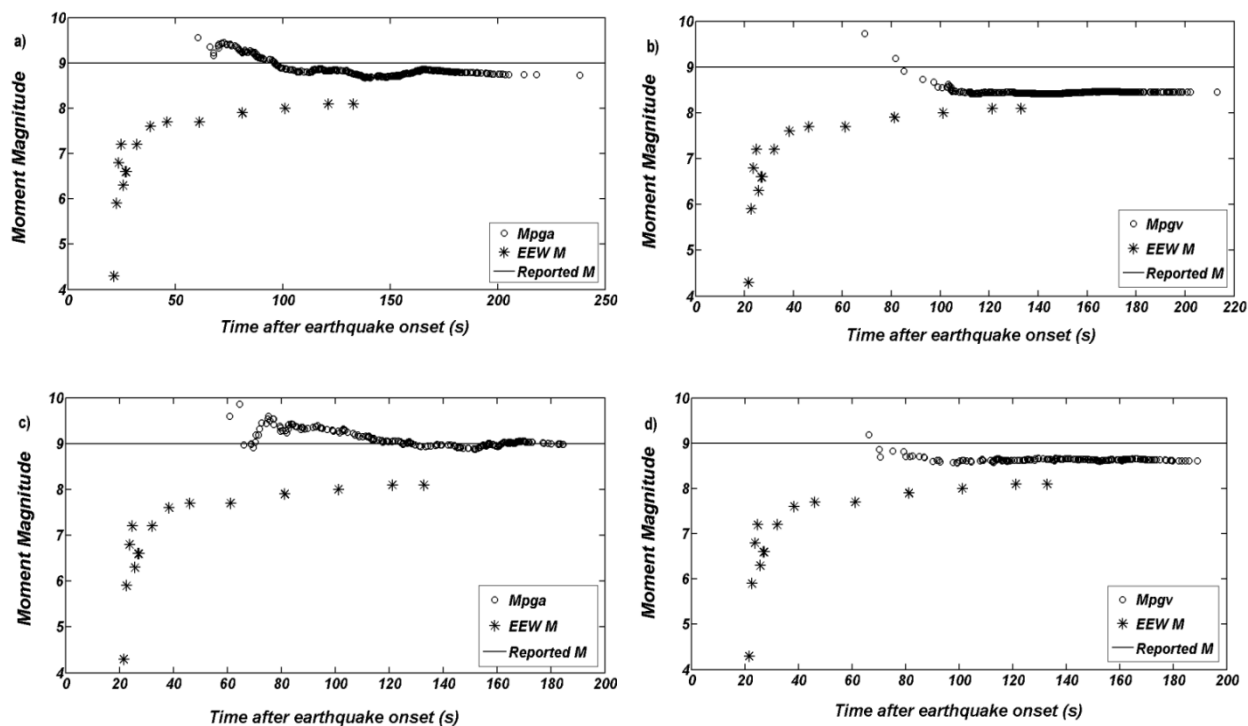


Figure 3.5 Mpga and Mpgv versus time (seconds) after OT for M9.0 Tohoku event based on GMPEs obtained from Catalog 1. Mpga versus time for current (a) borehole dataset and (c) surface dataset. Mpgv versus time for current (b) borehole dataset and (d) surface dataset. EEW M is the magnitude estimated by the existing EEW system in Japan. Solid line shows the moment magnitude ($M = 9.0$)

Figure 3.8a–d compares the obtained Mpga and Mpgv for borehole and surface recordings in Catalog 2 using new GMPEs. Figure 3.8 indicates that the estimated magnitudes are in good agreement with the reported moment magnitude of the events. To investigate the effect of V_{S30} , we used both Equations 3.1 and 3.2 to estimate the magnitudes from surface recordings and we compare the associated standard deviations of the obtained Mpga and Mpgv in Table 3.5. The use of V_{S30} significantly decreases the standard deviation of Mpgv for surface recording in both catalogs (Table 3.5) but it has

no significant effect on M_{pga} for surface recordings. This result suggests that the use of V_{S30} accounts for site effects for PGV GMPEs.

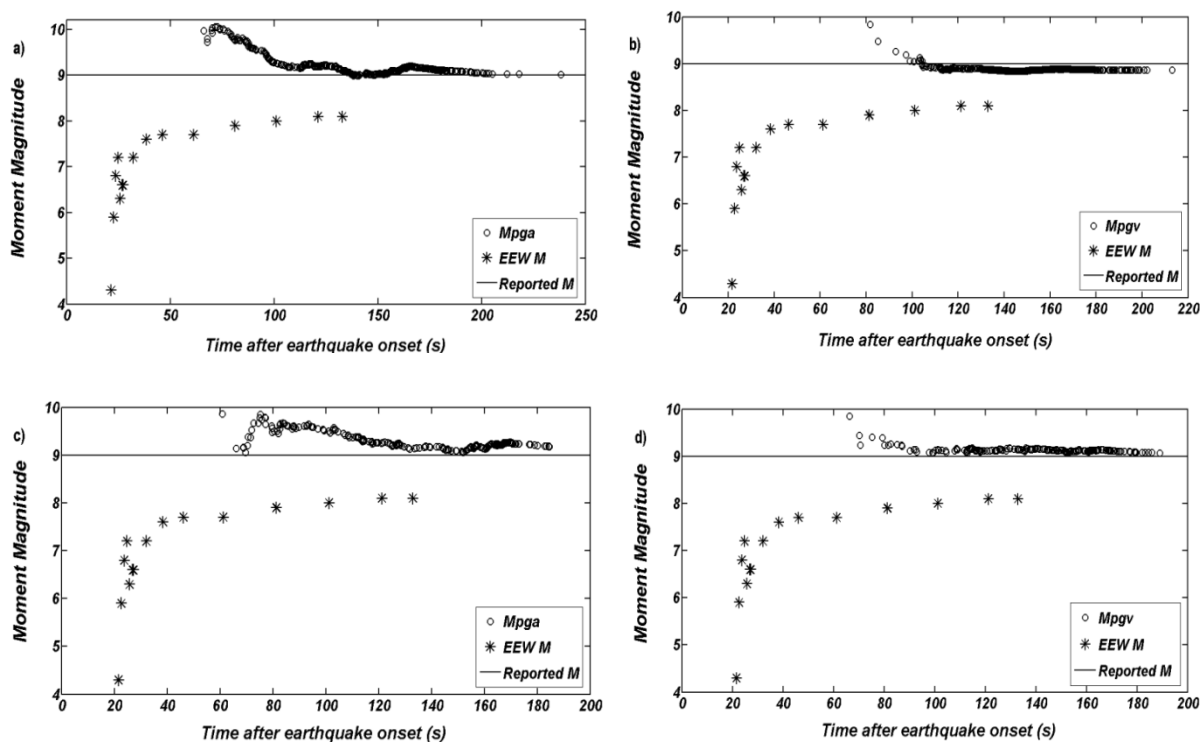


Figure 3.6 M_{pga} and M_{pgv} versus time (seconds) after OT for M9.0 Tohoku event based on GMPEs obtained from Catalog 2. M_{pga} versus time for current (a) borehole dataset and (c) surface dataset. M_{pgv} versus time for current (b) borehole dataset and (d) surface dataset. EEW M is the magnitude estimated by the existing EEW system in Japan. Solid line shows the moment magnitude ($M = 9.0$)

3.7 Discussion and Conclusions

We have compared the real-time magnitude determination for the 2011 Tohoku event by the current EEW system in Japan and the offline test for the new regional magnitude determination method (Eshaghi et al., 2013) using the strong motion data recorded by KiK-net stations (Figures 3.5 and 3.6). We also calculated the magnitude of

all events with at least 20 records available in our catalog using the new GMPEs obtained in this study. In order to compare with another EEW performance, we compare the existing EEW system's history of magnitude estimation (after the first seismic wave detection) and our magnitude estimates for the **M**6.9 ($M_{jma} = 7.2$) for the 14 June 2008 event (Tables 3.7 and 3.8).

Table 3.7 The history of magnitude estimation in each issuance of EEW for $M_{JMA} = 7.2$ (**M** = 6.9) earthquake on 14/06/2008 (from Kamigachi et al., 2009)

Issuance #	Lapse time after first seismic wave detection (sec)	Estimated M_{jma}
1	3.5	5.7
2	4.5	6.1
3	5.4	6.2
4	6.1	6.3
5	8.4	6.7
6	11.4	6.7
7	22.4	6.9
8	30.4	7
9	51.4	7
10	62.9	7

It should be noted that in this study we estimate the moment magnitude, while the EEW system estimated the M_{JMA} , which makes a direct comparison difficult. Our results demonstrate the utility of real-time PGA and PGV data for EEW and tsunami warning systems for large subduction zone earthquakes. We note that the new method provides us

with better estimation of the moment magnitude of the Tohoku event than the operating EEW system in Japan.

Table 3.8 The history of moment magnitude estimation using the proposed method in this study for M6.9 earthquake on 14/06/2008 (Borehole database, Catalog 2).

Issuance #	Time after origin time (sec)	Mpga	Time after origin time (sec)	Mpgv
1	17.76	8.16	17.64	7.64
2	25.01	8.12	23.66	7.73
3	29.98	8.01	26.13	7.5
4	32.26	7.76	32.72	7.33
5	36.63	7.20	34.67	7.23
6	45.63	6.71	39.46	7.05
7	51.26	6.67	45.19	7.01
8	59.98	6.67	51.17	7.01
9	63.99	6.67	65.32	7.01
Final estimation	79.01	6.67	118.51	7.01

However, there are some aspects about this earthquake that should be considered. This event had a complex rupture process and various studies have explored the different aspects of this earthquake in order to model the propagation of that rupture (e.g. Wang and Mori, 2011; Yoshida et al., 2011; Aochi and Ide, 2011; Meng et al., 2011; Hideo and Ide, 2009). Overall, these studies suggest that the earthquake was complex and comprised of at least two phases. Also, it has demonstrated that the rupture moved in two directions, first northwestward with a rather slow speed and then to the southwest with a faster speed

(Wang and Mori, 2011). Because of the complexity of this event, we consider two hypotheses. The first hypothesis argues that there was one event with a moment magnitude of 9.0. The second hypothesis claims that there were two fault segments that ruptured during the earthquake [Geospatial Information Authority of Japan (GSI), 2011], where the first segment generated a **M8.8** event and the second one generated a **M8.3** event. For the first hypothesis, the M_{pga} provides us the actual moment magnitude and the variation of M_{pga} could be explained by the variation in speed and direction of the rupture.

Under the second hypothesis, there were two events and their total energy added together to produce a total moment magnitude of **M8.9** (GSI). In our analysis, we used the peak value of each record; therefore, the final magnitude estimate should represent the magnitude of the larger earthquake from these two events (**M8.8**). Considering this assumption, the M_{pgv} is a better representative for magnitude of this earthquake. The additional tests for magnitude estimation of Tohoku event from Catalog 3 and Catalog 4 further indicate the robustness of our method to estimate the magnitude of large events. The results of this study confirm that the M_{pgv} from borehole recordings provides a more stable and accurate estimation for EEW and tsunami early warning systems (Figure 3.8).

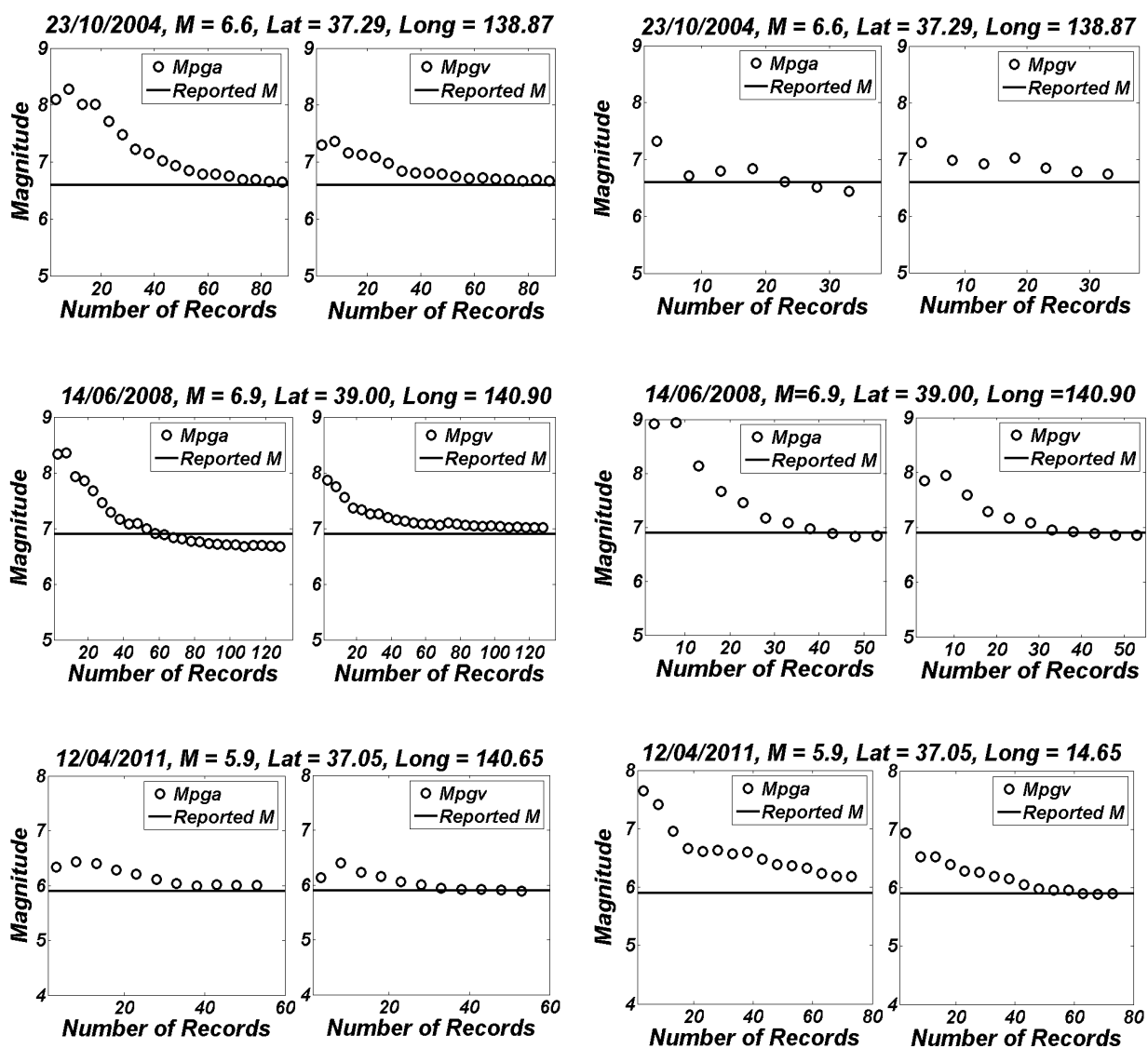


Figure 3.7 Magnitude estimation history in real time given by new GMPEs along with the reported **M** for borehole database (left) and surface database (right) for **M**6.6 (23/10/2004), **M**6.9 (14/06/2008), and **M**5.9 (12/04/2011). Solid line represents the moment magnitude.

Based on analysis of the standard deviations of magnitude estimates, we conclude that the use of PGV GMPEs from borehole data as a tool to estimate magnitude would improve the performance of EEW and tsunami early warning systems. Therefore, we suggest the incorporation of borehole recordings into real-time EEW practice for vulnerable countries exposed to future great earthquakes and tsunamis. We should mention that in this study we performed an offline test for different events, but in real time practice, the behaviour of magnitude convergence varied based on the size of the event, the distances between the source and the sites in vicinity of the source, and network configuration which makes it hard to come up with a fixed number of stations. In addition, we provide the number of records that were used in magnitude estimation for different events in Appendix. Note that this method is not intended to replace very short term warning methods, but can provide important information to better determine the ultimate size of an event rapidly, e.g. within about a minute. The information provided by the method is complementary to the existing EEW system and is critical for tsunami warnings and post-event response. Finally, the off-line test for the Tohoku event shows that either M_{pga} or M_{pgv} could provide us better estimation than the EEW M . Using this method, we do not need to have any predefined fault geometry or other information about the source of the earthquake; we need only the PGA and PGV values and epicentral distances, which can be provided by the currently operating EEW system in Japan.

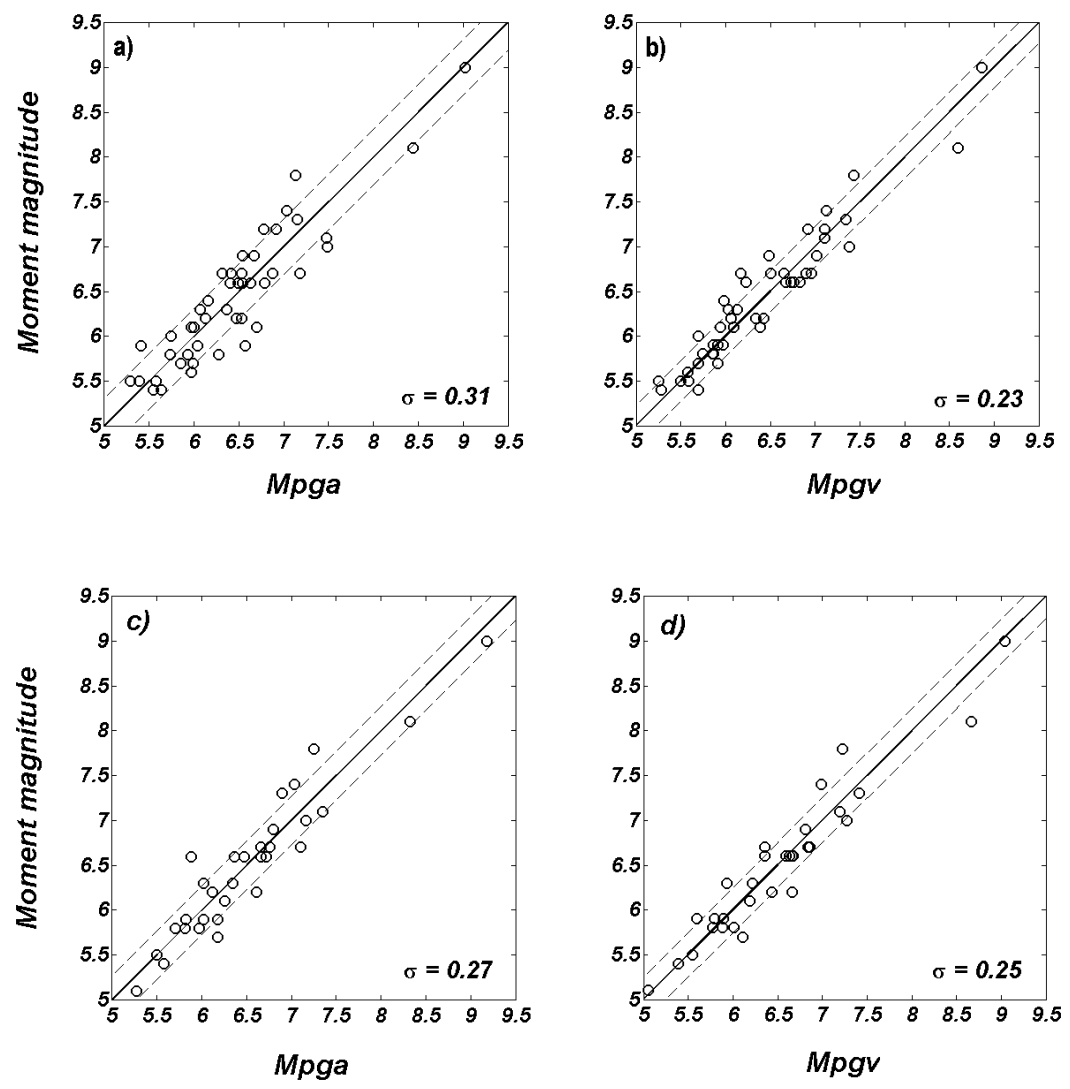


Figure 3.8 M versus predicted magnitude (M_{pga} and M_{pgv}) for Catalog 2 for the borehole database (a and b) and surface dataset (c and d). The solid line shows the 1:1 relation and dashed lines show one standard deviation.

3.8 References:

Abercrombie, R. E. (1997). Near-surface attenuation and site effects from comparison of surface and deep borehole recordings, *Bull. Seismol. Soc. Am.* 87, 731–744.

Allen, M., P. Gasparini, O. Kamigaichi, and M. Bose (2009). The status of earthquake early warning around the world: An introductory overview, *Seismol. Res. Lett.* 80, 682–693, doi: 10.1785/gssrl.80.5.682.

Aochi, H. and S. Ide (2011). Conceptual multi-scale dynamic rupture model for the 2011 off the Pacific coast of Tohoku Earthquake, *Earth Planets Space*, 63, 761–765.

Boore, D. (2003). Simulation of ground motion using the stochastic method. *Puer Appl. Geophys.* 160, 636-676.

Boore, D. M. and G. M. Atkinson (2008). Ground-motion prediction equations for the average horizontal component of PGA, PGV, and 5%-damped PSA at spectral periods between 0.01 s and 10.0 s, *Earthquake Spectra* 24, 99-138.

Borcherdt, R.D. (1994). Estimates of site-dependent response spectra for design (methodology and justification), *Earthquake Spectra*, EERI 10, 617–653

DeMets, C., R. Gordon, and D. F. Argus (2010). Geologically current plate motions, *Geophysical Journal International* 181, 1-80.

Doi, K (2011). The operation and performance of earthquake early warnings by the Japan Meteorological Agency, *Soil Dynam. Earthq. Eng.* 31,119-126, doi: 10.1016/j.soildyn.2010.06.009.

Eshaghi, A., K. F. Tiampo, H. Ghofrani, G. M. Atkinson (2013). Using Borehole Records to Estimate Magnitude for Earthquake and Tsunami Early-Warning Systems, *Bull. Seismol. Soc. Am.* 103, doi: 10.1785/0120120319

- Ghofrani, H., G. M. Atkinson and K. Goda (2013). Implications of the 2011 M9.0 Tohoku Japan earthquake for the treatment of site effects in large earthquakes, *Bull. Earthquake Eng.* 11:171–203, doi: 10.1007/s10518-012-9413-4.
- Hayes, G. P. (2011). Rapid source characterization of the 2011 Mw 9.0 off the Pacific coast of Tohoku Earthquake, *Earth Planets Space*, 63, 529-534.
- Hideo, A. and S. Ide (2011). Conceptual multi-scale dynamic rupture model for the 2011 off the Pacific coast of Tohoku Earthquake, *Earth Planets Space*, 63, 761-765.
- Horiuchi, S., H. Nrgishi, K. Abe, A. Kaminuma, and Y. Fujinawa, (2005). An automatic processing system for broadcasting earthquake alarms, *Bull. Seismol. Soc. Am.*, 95, 708-718.
- Hoshiaba, M., O. Kamigaichi, M. S. Tsukada, and N. Hamada (2008). Earthquake Early Warning starts nationwide in Japan, *EOS Trans. AGU*, 89, 73-74.
- Hoshiaba, Y., K. Iwakiri, N. Hayashimoto, T. Shimoyama, K. Hirano, Y. Yamada, Y. Ishigaki, and H. Kikuta (2011). Outline of the 2011 off the Pacific coast of Tohoku Earthquake (M 9.0) Earthquake Early Warning and observed seismic intensity, *Earth Planets Space*, 63, 547–551.
- Geospatial Information Authority of Japan. (Crustal Deformation and Fault Model obtained from GEONET data analysis). Last accessed <http://www.gsi.go.jp/cais/topic110422-index-e.html>.

Japan Meteorological Agency, (2011). Retrieved from http://www.seisvol.kishou.go.jp/eq/EEW/kaisetsu/joho/20110311144640/content/content_out.html, last accessed July, 2013.

Japan Meteorological Agency, (2013). Retrieved from <http://www.seisvol.kishou.go.jp/eq/eng/fig/tsunamiinfo.html>, last accessed July, 2013.

Kamigaichi, O., M. Saito, K. Doi, T. Matsumori, S. Tsukada, K. Takeda, T. Himoyama, K. Nakamura, M. Kiyomoto, and Y. Watanabe (2009). Earthquake early warning in Japan: Warning the general public and future prospects, *Seismol. Res. Lett.* 80, 717–726.

Kanamori, H. (2005). Real-time seismology and earthquake damage mitigation, *Annual Review of Earth and Planetary Sciences* 33, 195–214.

Lin, T., and Y. M. Wu (2010). Magnitude determination using strong ground motion attenuation in earthquake early warning, *Geophys. Res. Lett.* 7, L07304, doi: 10.1029/2010GL042502.

Lin, T., Y. M. Wu, D. Chen, N. Hsiao and C. Chang (2011). Magnitude Estimation in Earthquake Early Warning for the 2010 JiaSian, Taiwan, Earthquake, *Seismol. Res. Lett.* 82 (2), 201-206.

Macias, M., G. M. Atkinson, and D. Motazedian (2008). Ground-motion attenuation, source, and site effects for the 26 September 2003 M 8.1 Tokachi-Oki earthquake sequence, *Bull. Seismol. Soc. Am.* 98, 4, 1947–1963, doi: 10.1785/0120070130.

Meng, L., I. Asaf and J.P. Ampuero (2011). A window into the complexity of the 2011 M_w 9 Tohoku-Oki earthquake, *Geophys. Res. Lett.* 38 (7), doi: 10.1029/2011GL048118.

Mori, N., T. Takahashi, T. Yasuda, and H. Yanagisawa (2011). Survey of 2011 Tohoku earthquake tsunami inundation and run-up, *Geophys. Res. Lett.* 38, L00G14, doi:10.1029/2011GL049210.

Nakamura, Y. (1998). On the urgent earthquake detection and alarm system (UrEDAS). In *Proceedings of the 9th World Conference on Earthquake Engineering VII*, 673–678.

Okada, Y. (2011). Preliminary report of the 2011 off the pacific coast of Tohoku Earthquake. http://www.bosai.go.jp/e/pdf/Preliminary_report110328.pdf, last accessed May 2013.

Peng Z., C. Aiken, D. Kilb, D. R. Shelly, and B. Enescu (2012). Listening to the 2011 Magnitude 9.0 Tohoku –Oki, Japan, Earthquake, *Seismol. Res. Lett.* 83, 287-293.

Wang, D. and J. Mori (2011). Rupture process of the 2011 off the Pacific coast of Tohoku Earthquake (M_w 9.0) as imaged with back-projection of teleseismic P-Wave, *Earth Planets Space*, 63, 603-607.

Wu, Y. M., and L. Zhao (2006). Magnitude estimation using the first three seconds P-wave amplitude in earthquake early warning, *Geophys. Res. Lett.* 33, L16312, doi:10.1029/2006GL026871.

Yamada, M., and J. Mori (2009). Using T_c to estimate magnitude for earthquake early warning and effects of near-field terms, *J. Geophys. Res.* 114, B05301, doi:10.1029/2008JB006080.

Yoshida, K., K. Miyakoshi and K. Irikura (2011). Source process of the 2011 off the pacific coast of Tohoku Earthquake inferred from waveform inversion with long-period strong-motion records. *Earth Planets Space*, 63, 577-582.

Chapter 4

4 Real-Time Moment Magnitude Estimation from Displacement Spectral Inversion³

³ A version of this chapter has been submitted for publication. **Eshaghi, A.**, K. F. Tiampo, H. Ghofrani, G. M. Atkinson and P. J. González (2014). Real-Time Moment Magnitude Estimation from Displacement Spectral Inversion, *Bull. Seism. Soc. Am.*

In this chapter, real-time inversion of displacement spectra is incorporated into a single station EEW system approach. The magnitude of $M \geq 4.5$ earthquakes is estimated using both borehole and surface recordings from the Japanese networks (KiK-net and K-net). This is first time that the inversion of displacement spectra has been used to estimate the magnitude of $M \geq 7.0$ events in an EEW framework. The source parameters were determined using the inversion of displacement spectra for available P- and S-waves windows. Magnitude is estimated based on the information obtained from recordings at the closest station to the epicenter, one second after the first P-wave detection, and that estimation is updated as the time series progresses. Results show that the estimated real-time magnitudes agree well with the moment magnitudes as reported by the National Research Institute for Earth Science and Disaster Prevention. The results also show that the magnitude predicted from the P-wave window (**MP**) provides a longer warning time, but with a larger uncertainty, in comparison with the estimation based on the S-wave window (**MS**). Magnitude predictions from an offline test of the 2011 Tohoku earthquake were compared with the magnitude estimates provided by the EEW system in Japan. The results support the hypothesis that the Tohoku event was comprised of two events, where the energy of both added together produced an **M9.0** event [Geospatial Information Authority of Japan (GSI), 2011]. One important conclusion is that the magnitude estimate based on inversion of the displacement spectra is independent of magnitude scaling relationships and directly determines the moment magnitude from the estimated source parameters. Therefore, a single-station approach can be applied for EEW in regions with a sparse seismic network in order to provide a low-cost tool to mitigate seismic hazards, by placing a single station close to the seismic source.

4.1 Introduction

The goal of an earthquake early warning (EEW) system is to reduce the damaging effects of earthquakes by providing a short warning, from a few seconds to a few tens of seconds, before the arrival of damaging ground motion. The first EEW system that issued public warnings was implemented only twenty years ago. Today, Japan has a nationwide EEW system, Mexico has expanded its system, and Turkey, Taiwan and Romania have active systems which provide early warning to one or more users (Alcik et al., 2009; Allen et al., 2009). Ongoing EEW projects in Italy, Switzerland, China, Hawaii, and California test the feasibility of EEW in their seismic networks (Allen and Kanamori, 2003; Allen et al., 2009). Improvement and updating of these systems continues today.

One of the most important requirements for EEW systems is to provide an accurate early estimation of the earthquake magnitude. There are several methods to estimate the magnitude of a large earthquake in an EEW system that are based on either the information from a single station (on-site approach) or on recordings from a seismic network (network-based or regional approach). For example, P-wave parameters such as the predominant period of the first few seconds of the P-wave, τ_p (Nakamura, 1988), or the effective period of the P-wave signal over a fixed time window, τ_c (Kanamori, 2005), are used to estimate the magnitude of an ongoing event based on the early portion of the P-wave. These methods were developed because the magnitude of the event scales with these parameters and there is no dependency on the epicentral distance within a few hundred kilometers of the event (Allen and Kanamori, 2003; Allen et al. 2009). If a correction for epicentral distance is available, the amplitude of the P-wave is another useful method for estimating the magnitude of an event. The peak displacement, velocity, or acceleration in

the first few seconds of the P-wave has been shown to be correlated with the event magnitude (Wu and Kanamori, 2005a,b; Zollo et al., 2006; Wu and Kanamori, 2008a,b).

A primary concern regarding the use of the first few seconds of the P-wave to estimate earthquake magnitude is that these estimates saturate for large magnitude events. Previous studies discussed saturation of the *P*-wave parameters that were used to estimate magnitude for large earthquakes ($M > 7$) (e.g., Rydelek and Horiuchi 2006; Rydelek et al., 2007; Yamada and Ide 2008; Yamada and Mori, 2009). To overcome the problem of the magnitude estimation for large events, several techniques have been developed that use longer time windows for the P- or the S-wave (Zollo et al., 2006; Kamigaichi et al., 2009). Alternative methods have been proposed that use either the peak ground acceleration (PGA) or peak ground velocity (PGV) of the ground motion recordings to estimate the event magnitude based on ground motion prediction equations (GMPEs) (Lin and Wu, 2010; Lin et al., 2011; Eshaghi et al., 2013a,b). The estimated magnitude converges to the reported moment magnitude (M) with approximately twenty PGA and PGV readings (Eshaghi et al., 2013a,b).

Recently, Caprio et al. (2011) proposed a new, network-based approach that calculates the moment magnitude and its uncertainty based on the real-time inversion of the displacement spectra of the available portion of the seismic record as it arrives at the station. They employed broadband and strong motion waveform data from southern California and Japanese events with a magnitude range of $3.0 \leq M \leq 7.0$. Their results show that the proposed method provided stable estimates of the moment magnitude within 10 seconds after the first P-wave arrival at the closest station to the epicenter.

The operational EEW system implemented by the Japan Meteorological Agency (JMA) combines both an alert-seismograph concept and a network-based approach (Kamigaichi et al., 2009). The system uses more than 1100 seismic instruments across Japan, operated by JMA and Japan's National Research Institute for Earth Science and Disaster Prevention (NIED) (Hoshiya, 2013), and integrates methodologies developed by JMA (Hoshiya et al., 2008) and NIED (Nakamura et al., 2009). When ground shaking above a predefined threshold is observed at a single station, an alert is triggered (the alert-seismograph/single station approach). In addition, the regional approach uses all available data from a seismic network to estimate the earthquake location, magnitude and strong motion parameters (Kamigaichi, 2004; Allen et al., 2009). A combination of several methods is used to estimate earthquake location (Odaka et al., 2003; Kamigaichi, 2004; Tsukada et al., 2004; Kamigaichi et al., 2009). The magnitude (M_{JMA}) is calculated from the peak ground displacement (Kamigaichi et al., 2002; Kamigaichi, 2004; Katsumata, 2004; Horiuchi et al., 2005; Kamigaichi et al., 2009; Hoshiya et al., 2011). In the current operational system, warnings are issued to the public when the maximum intensity is predicted to be 5- or greater on the JMA scale (~VII– VIII on the Modified Mercalli Intensity scale).

In this study, we use real-time strong ground motion displacement spectra to estimate the magnitude of earthquakes of $4.5 \leq M \leq 9.0$, as recorded on both surface and borehole stations of the Kiban Kyoshin network (KiK-net) and Kyoshin network (K-net) stations between 03/06/2000 and 03/12/2011. We extend the study by Caprio et al. (2011) to include events of $M > 7.0$ in order to test the ability of this method to accurately estimate the magnitude of large events. Instead of a network-based approach (regional

approach), a single-station approach is used to estimate the moment magnitude of the selected events. Single-station methods offer great practical utility and economy, as they can be used successfully in sparse networks, as well as in more complete network environments such as Japan. Later the results of the single station approach can be integrated into a network-based approach to further improve performance. Source parameters, including the low frequency plateau (Ω_0), and the corner frequency (f_c), along with the quality factor (Q) are calculated using the three components of strong motion recordings (both P- and S-phases) at a single station, assuming a simple single-corner point-source model.

To find the moment magnitude, first we find the source parameters through inversion of the recorded displacement spectra, and then we calculate the seismic moment from Ω_0 , as detailed in the next section. For EEW purposes, the magnitude estimation begins immediately after the initial P-wave detection and the magnitude is updated as the time series progresses. Final evaluation of the results is based on the accuracy of the magnitude estimation over various time periods.

4.2 Spectral Analysis

We choose the following general model to fit the displacement spectra of both P- and S- waves (Abercrombie, 1995):

$$\Omega(f) = \frac{\Omega_0 e^{\frac{-\pi ft}{Q}}}{\left[1 + \left(\frac{f}{f_c}\right)^{2n}\right]^{\frac{1}{2}}} \quad (4.1)$$

where $\Omega(f)$ is the Fourier amplitude of the P- or S-wave displacement, Ω_0 is the plateau at low frequencies, f is the frequency, f_c is the corner frequency, n is the high-frequency fall off rate (on a log-log plot), and γ is a constant. By changing the γ value, we obtain the modified versions of spectral models proposed by Brune (1970) and Boatwright (1980). Here $n = 2$ and $\gamma = 1$, similar to the Brune (1970) spectral shape model. Note that the anelastic attenuation is represented by the exponential term, where Q is the frequency-independent quality factor and t is the travel time of the considered wave. To determine the best fitting parameters, we employ a bonded Nelder-Mead (1965) simplex algorithm. After obtaining the low frequency plateau (Ω_0) for all three components of strong motion data [horizontal (H1 and H2) and vertical (Z) components], the seismic moment (M_0) is calculated using the following equation (Abercrombie, 1995):

$$M_0 = \frac{4\pi\rho c^3 \sqrt{\Omega_0(Z)^2 + \Omega_0(H1)^2 + \Omega_0(H2)^2}}{Z(R)U_{\theta\theta} F}, \quad (4.2)$$

where M_0 is the seismic moment in (N.m), ρ is the density (2700 kg/m^3), c is the average wave velocity (for P-wave and S-wave, in m/s), and Ω_0 is the value of the spectral amplitude at low frequencies (in m/Hz). $U_{\theta\theta}$ is the mean radiation pattern (0.52 and 0.63 for P- and S-waves, respectively) (Aki and Richards, 1980; Abercrombie, 1995). F is the free surface effect (1 and 2 for borehole and surface recording, respectively). $Z(R)$ represents the geometrical spreading function that accounts for the decay of ground-motion amplitudes due to geometrical attenuation. We calculate the geometrical spreading using the following simple form (Boore 2003; Ghofrani and Atkinson, 2011):

$$Z(R) = \begin{cases} \frac{1}{R} & , \quad R < 50km \\ \left(\frac{1}{50}\right)\left(\frac{50}{R}\right)^{0.5} & , \quad R \geq 50km \end{cases} \quad (4.3)$$

where R is the hypocentral distance (in meters). Other geometric spreading functions could potentially be used, but it should be noted that there is a trade-off between source parameters and geometric attenuation (Boore et al., 2010). There is also a trade-off between geometric spreading and near-distance saturation effects on attenuation, as discussed by Yenier and Atkinson (2014). The selected form represents the simplest model that can adequately accommodate these effects. Given the seismic moment estimated from Equation (4.2), we calculate the moment magnitude (Hanks and Kanamori, 1979, converted to SI units):

$$M = \frac{2}{3} \log_{10}(M_0) - 6.03 \quad (4.4)$$

4.3 Data and processing

The large number of accelerometer recordings in Japan provides an invaluable opportunity to analyze a rich strong-motion database over a very broad range of magnitudes and distances. Here we analyzed recordings from earthquakes with $M_{JMA} \geq 5.0$ ($M \geq 4.5$) from 2000 - 2011 with focal depth ≤ 50 km and epicentral distance of up to 150 km, recorded by KiK-net (borehole and surface) and K-net stations. The value of M for each event is that reported by NIED (F-net Catalogue). Figure 4.1 shows the selected earthquake epicenters recorded by KiK-net and K-net stations. In total 207, 197 and 195 events were used in the KiK-net borehole, Kik-net surface and K-net database respectively.

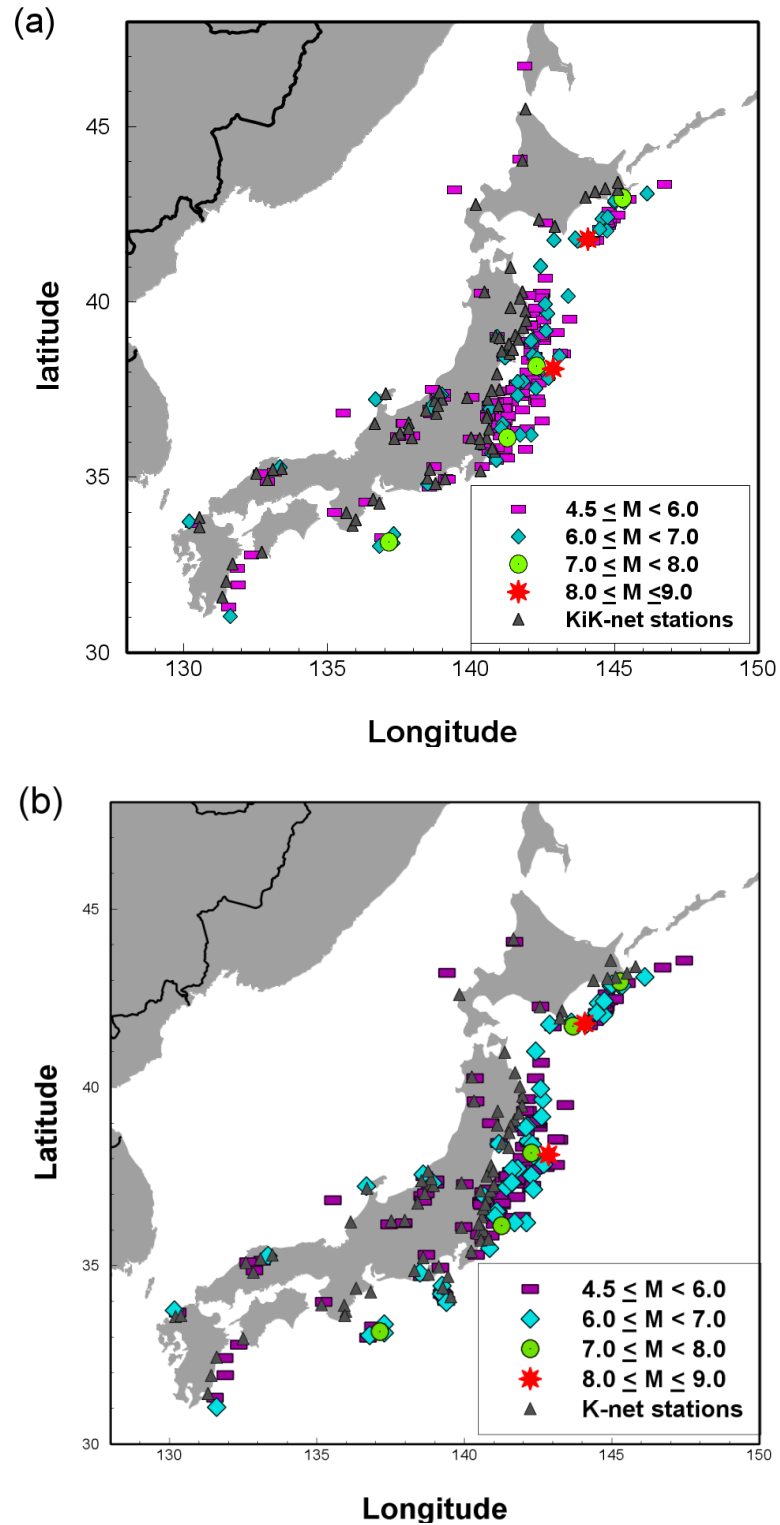


Figure 4.1 Spatial distribution of the events used in this study recorded by (a) KiK-net stations, and (b) K-net stations. Every station did not record all the events.

The distribution of M with focal depth and epicentral distance are shown in Figure 4.2. The magnitude variation with focal depth is randomly distributed. The majority of earthquakes used in this study have $M \leq 7.0$. Baseline correction (removing the mean value of the time-series and the trend) was performed for all recordings (Boore and Akkar, 2003).

Because the magnitude is estimated based on the low-frequency plateau of the spectrum (Ω_0) in this study, it is important that Ω_0 values are estimated reliably. First we applied an acausal, band-pass Butterworth filters with an order of 4 and corner frequencies of 0.1–15 Hz for all earthquakes. The frequency range of the analysis was 0.1 to 15 Hz, where previous studies showed that the lower frequency limit is suitable to produce well-shaped displacement time series, with a flat displacement spectra at low frequencies (Ghofrani and Atkinson, 2011; Ghofrani et al., 2011). The upper band was chosen because the instrument response is approximately flat up to 15 Hz (Aoi et al., 2004). We found that using this fixed low-cut filter resulted in the removal of the actual corner frequency and subsequent underestimation of magnitude for large events (Table 1, e.g. $M9.0$ event where the event corner frequency is ~ 0.01 Hz for a stress drop of 100 bars). It is well-established that larger events are enriched at low-frequencies and for those events the corner frequency moves to the lower part of the spectrum (e.g. Boore, 2003). Therefore, in order to avoid losing the relevant part of the spectrum, especially for larger events, we repeated the analysis without the fixed low-cut filter for all events. Instead, we did not use we constrained the lower frequency bandwidth by requiring that the signal/noise ratio was greater than 3.0, within the range from 0.01 to 15 Hz. The background noise was estimated from a pre-event time window. As a result, the corner

frequency is not removed. In order to ensure a robust inversion of source parameters, we checked many example spectra to ensure that the bandwidth selection criterion based on the signal/noise ratio results in a flat displacement spectrum at low frequencies. Typical Examples for different magnitudes are provided in Figure 3.

Table 4.1 Mean residuals for the predicted magnitude (moment magnitude) using the single station approach.

	KiK-net- Borehole	KiK-net-Surface	K-net	
Number of earthquakes in database	207	197	195	
Filtered data	Mean residuals of MP*	0.17 ± 0.40	-0.04 ± 0.40	-0.15 ± 0.43
	Mean residuals of MS*	-0.02 ± 0.30	-0.28 ± 0.34	-0.27 ± 0.35
	Mean residuals MPS*	0.07 ± 0.31	-0.16 ± 0.32	-0.21 ± 0.33
Unfiltered data	Mean residuals of MP*	0.23 ± 0.38	0.01 ± 0.37	-0.04 ± 0.42
	Mean residuals of MS*	0.08 ± 0.24	-0.20 ± 0.29	-0.18 ± 0.29
	Mean residuals of MPS*	0.15 ± 0.26	-0.09 ± 0.28	-0.11 ± 0.28

* Range represents one standard deviation.

To estimate the P-wave arrival, t_p , at a given station the automatic short-term average/long-term average (STA/LTA) picker (Allen, 1978) was used. We checked the accuracy of the P-wave detection by visual inspection of all of the recordings. We used the hypocenter distance and the average S-wave velocity (3.5 km/s) (Abercrombie, 1995) to determine the S-wave arrival time. The difference between P- and S- wave arrivals is

used as the length of the P-wave window in our calculation. We considered the S-wave window (T_s) in our calculation as:

$$T_s = 2/f_c + \alpha * R, \quad (4.5)$$

where f_c is the estimated corner frequency from the final P-wave window and is inversely proportional to the duration of the fault rupture (Madariaga, 1976; Caprio et al., 2011). The ground motion duration increases with source-to-site distance. $\alpha * R$ term in Equation 4.5 is the distance-dependent duration, where R is the hypocentral distance (in km) and α is a region dependent parameter (Atkinson and Boore, 1995; Atkinson and Silva, 2000) that is assumed to have constant value of 0.1. At any given time, t_n , after the first P-arrival at each station (t_p), the available strong motion time series that is used for the magnitude estimation has a time window with length of $t_n - t_p$. To obtain the displacement time series at t_n we performed double integration of the available strong motion time series in time, after baseline correction. For each record, a 5% cosine taper was applied to both ends and a Fourier transformation was used to obtain the displacement spectra for all three components. The observed spectra were smoothed by binning at frequencies with a spacing of 0.3 log frequency unit and the $\text{Log}_{(10)}$ amplitudes of the spectra were averaged in each bin.

After obtaining the displacement spectra and determining the useable frequency band as described previously, the low-frequency plateau, corner frequency, and Q are inverted for using Equation 4.1 and the bounded Nelder-Mead (1965) simplex algorithm. Equation 4.1 is an overdetermined non-linear problem that does not have a unique solution. In this type of inversion, there generally is a trade-off between the resulting values of the unknown parameters. Here, the low-frequency plateau is likely to be the

parameter that is most easily and accurately determined, while there is more trade-off between the corner frequency and Q . This results in a more reliable moment estimation in comparison to the obtained corner frequency and Q . A simplex algorithm is a nonlinear optimization technique using a derivative-free method (Nelder and Mead 1965; Lagarias et al., 1998). In our analysis, the objective function was defined as the root-mean-square deviation. The termination tolerance on the objective function value was set to $1.0\text{e-}8$ (Lagarias et al., 1998; Nelder and Mead 1965; Abercrombie, 1995; Luersen et al., 2003 and references therein). After obtaining the Ω_0 values for all three components of strong motion data, the seismic moment was derived using Equation 4.2. The moment magnitude is calculated from Equation 4.4. The magnitude at the station is updated with each second of data that becomes available at that station.

In the single-station approach, the magnitude is estimated based on information obtained from the three components of the strong motion recordings from the closest station to the epicenter (the station that has smallest epicentral distance). First, we determine the moment magnitude from the first available portion of the P-phase (**MP**) and the magnitude is updated as more information registered. Then, from the theoretical S-phase arrival, the magnitude is calculated based on the available portion of the S-phase (**MS**) and the estimation is updated each second as more data is recorded. Accordingly, we calculate the mean value of the final **MP** and **MS** as **MPS** as proposed by Abercrombie (1995).

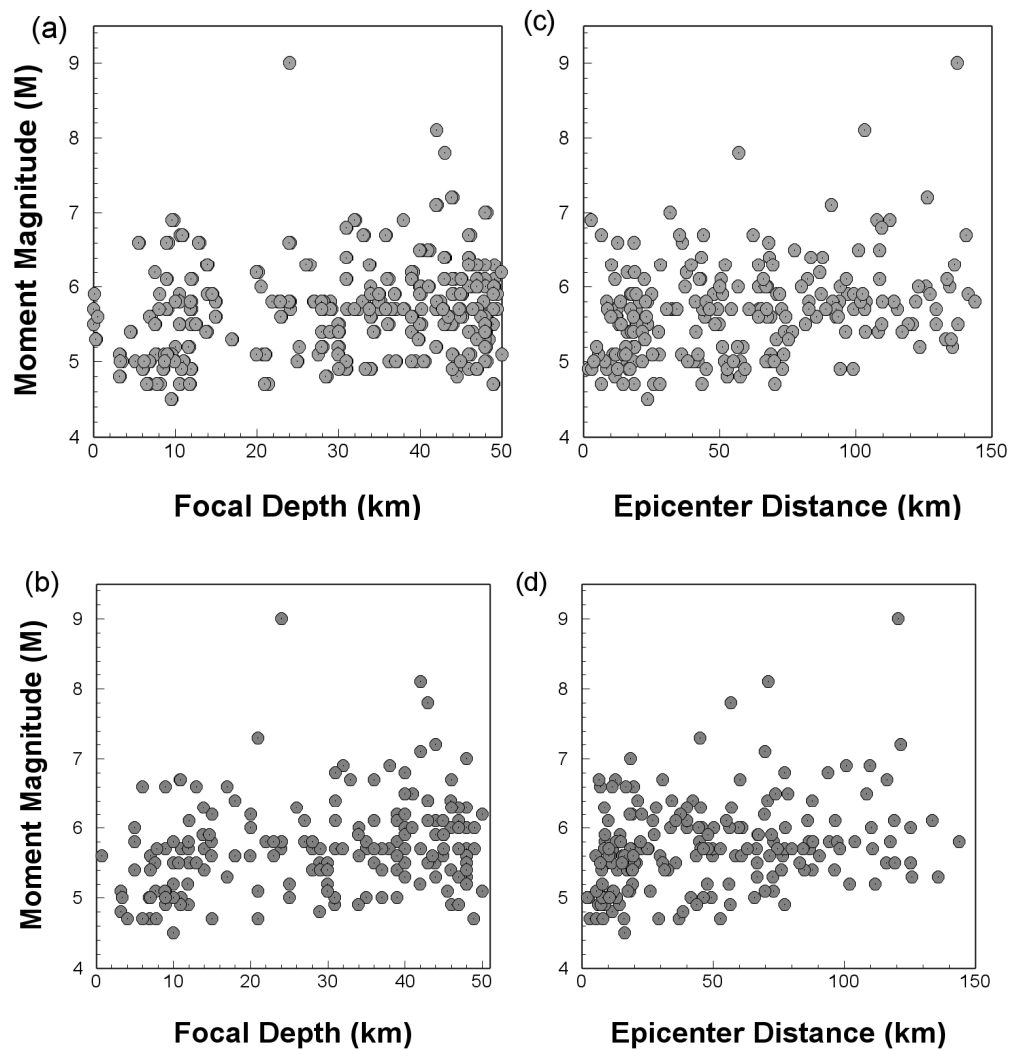


Figure 4.2 Magnitude vs. focal depth distribution used in this study for (a) KiK-net and (b) K-net database. Magnitude vs. epicentral distance distribution for (c) KiK-net and (d) K-net database used in this study.

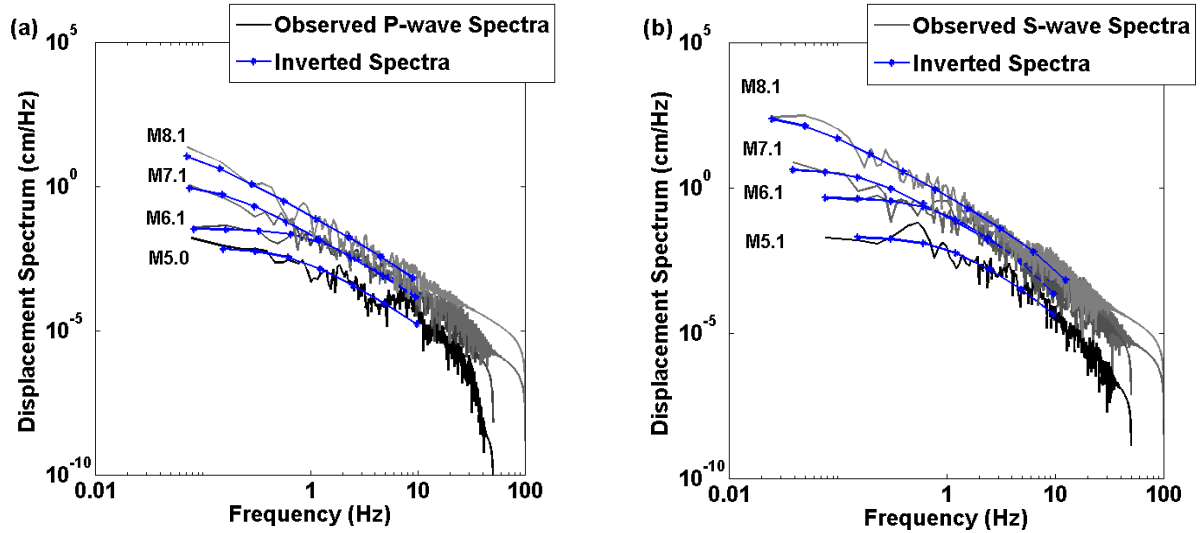


Figure 4.3 Observed and inverted spectra of (a) P-waves and (b) S-waves of the vertical components for the October 23, 2009, **M5.0** event at a hypocentral distance of 108.2 km; the March 23, 2011, **M6.1** event at a hypocentral distance of 101.45 km; the August 16, 2005, **M7.1** event at a hypocentral distance of 110.6 km; and the September 26, 2003, **M8.1** Tokachi-Oki event at a hypocentral distance of 117 km. The inverted spectra shown are computed for the frequency range where the signal/noise ratio is larger than 3.

In real time practice, an apparent decrease in the magnitude as estimated from the S-phase occurs because the S-phase amplitude starts from zero. To avoid this effect, the magnitude estimation from P-wave can be held for an appropriate time until the estimation from the S-phase becomes stable, as is done in existing EEW system in Japan (Kamigaichi, 2004; Kamigaichi et al., 2009). Figures 4.4, 4.5 and 4.6 show examples of the vertical component time series along with the selected P- and S-phase windows that were used in magnitude calculation for the **M4.5** (12/04/2011), **M4.9** (05/08/2011), and **M5.5** (08/09/2004) events respectively. Also shown are the observed and inverted P- and

S-waves spectra along with noise spectra. Note that the inverted spectra are shown in the frequency range where the signal/noise ratio is larger than 3.

4.4 Results

We used the three strong ground motion components recorded at the closest station to the epicenter area from KiK-net and K-net databases to estimate the magnitude of the selected events using the procedure explained in Sections 4.2 and 4.3. Figure 4.7 compares the obtained **MP**, **MS** and **MPS** with the reported moment magnitude for the KiK-net borehole database (a, b and c), KiK-net surface database (d, e and f), and K-net database (g, h and i). Figure 4.7 shows that the estimated magnitudes are in agreement with the reported moment magnitude of the events, despite the fact that the estimate included information from only one station. Mean residuals (residual: $\mathbf{M}_{\text{predicted}} - \mathbf{M}_{\text{reported}}$) and the standard deviations of **MP**, **MS** and **MPS** for each database are presented in Table 4.1. Generally, use of borehole data with our algorithm tends to overestimate the magnitude, especially for smaller events, while it provides better estimation for larger events (Figures 4.7 and 4.8).

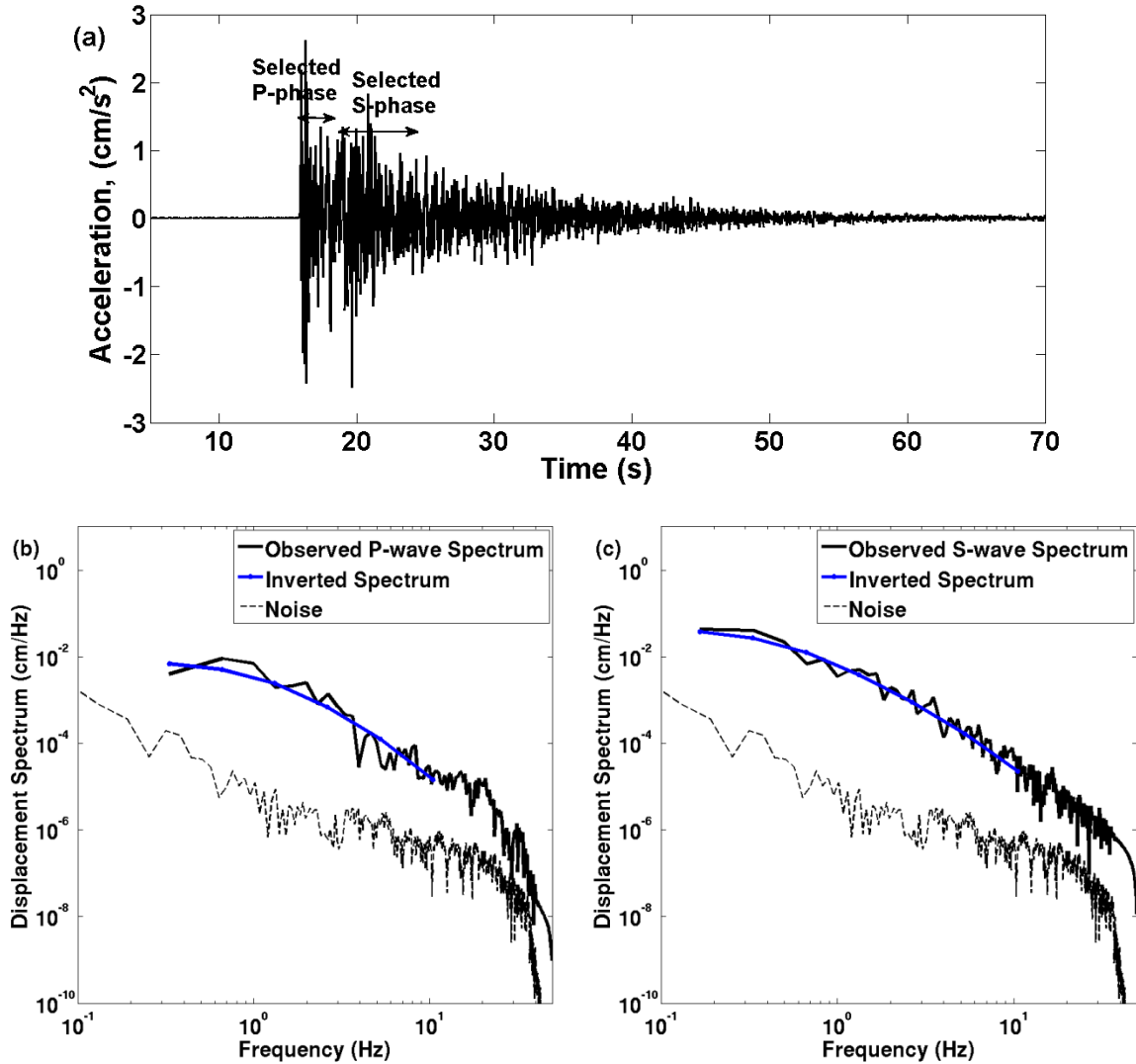


Figure 4.4 Example of observed and inverted spectra of P- and S-waves (vertical component) for the April 12, 2011 **M**4.5 event at 25.44 km hypocentral distance. (a) Vertical component of the acceleration time series from the FKSH12 KiK-net borehole station; black arrows show the selected P- and S- phase windows (3 and 6 sec respectively). (b) Observed and inverted P-wave spectra; **MP** and f_c are **M**5.1 and 0.76 (Hz) respectively (c) observed and inverted S-wave spectra; **MS** and f_c are **M**4.9 and 0.72 (Hz) respectively.

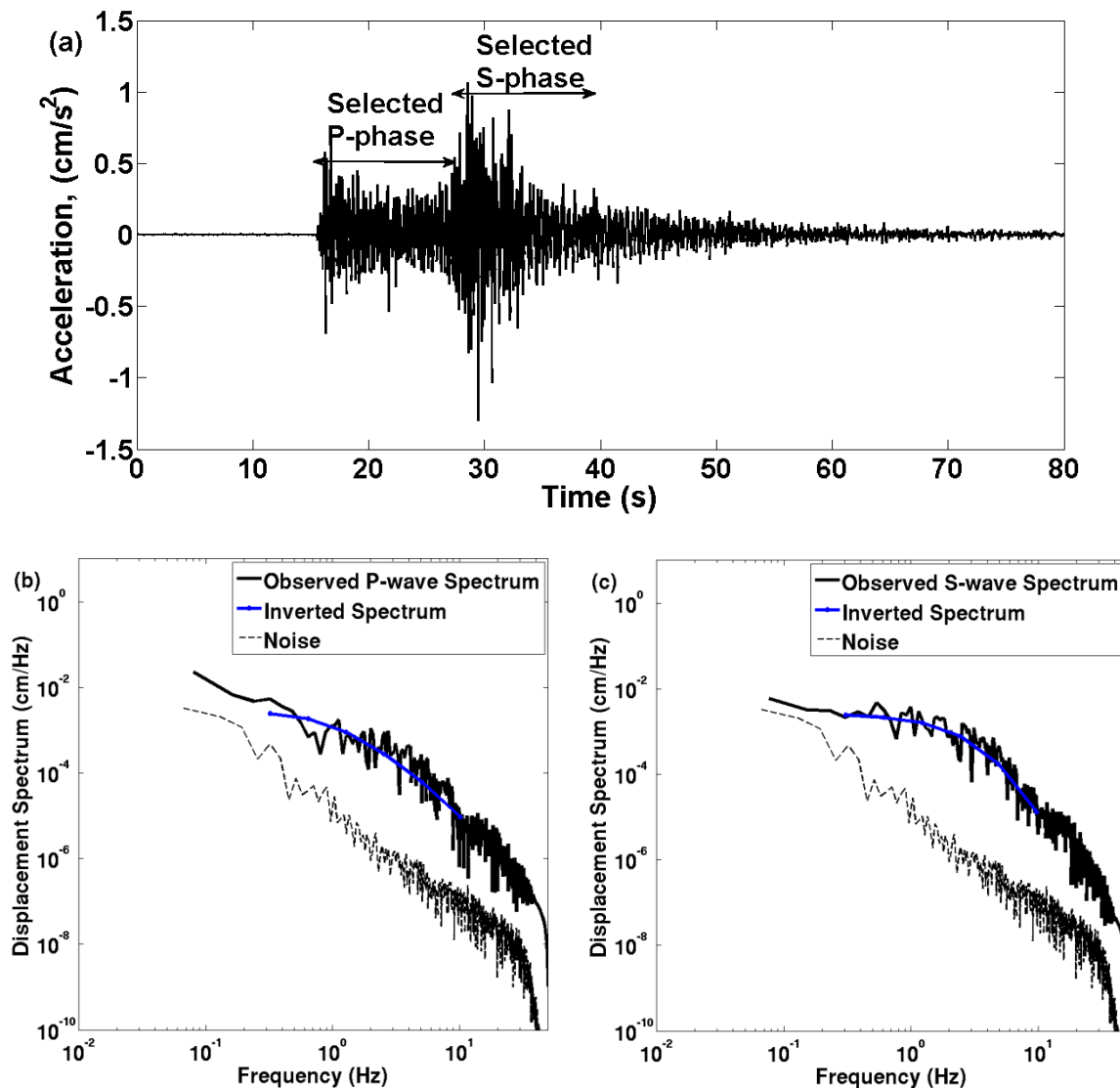


Figure 4.5 Example of observed and inverted spectra of P- and S-waves (vertical component) for the August 5, 2011 **M**4.9 event at 104.57 km hypocentral distance. (a) Vertical component of the acceleration time series from the IWTH02 KiK-net borehole station; black arrows show the selected P- and S- phase windows (12.45 and 13 sec respectively). (b) Observed and inverted P-wave spectra; **MP** and f_c are **M**5.2 and 0.99 (Hz) respectively and (c) observed and inverted S-wave spectra; **MS** and f_c are **M**4.7 and 2.5 (Hz) respectively.

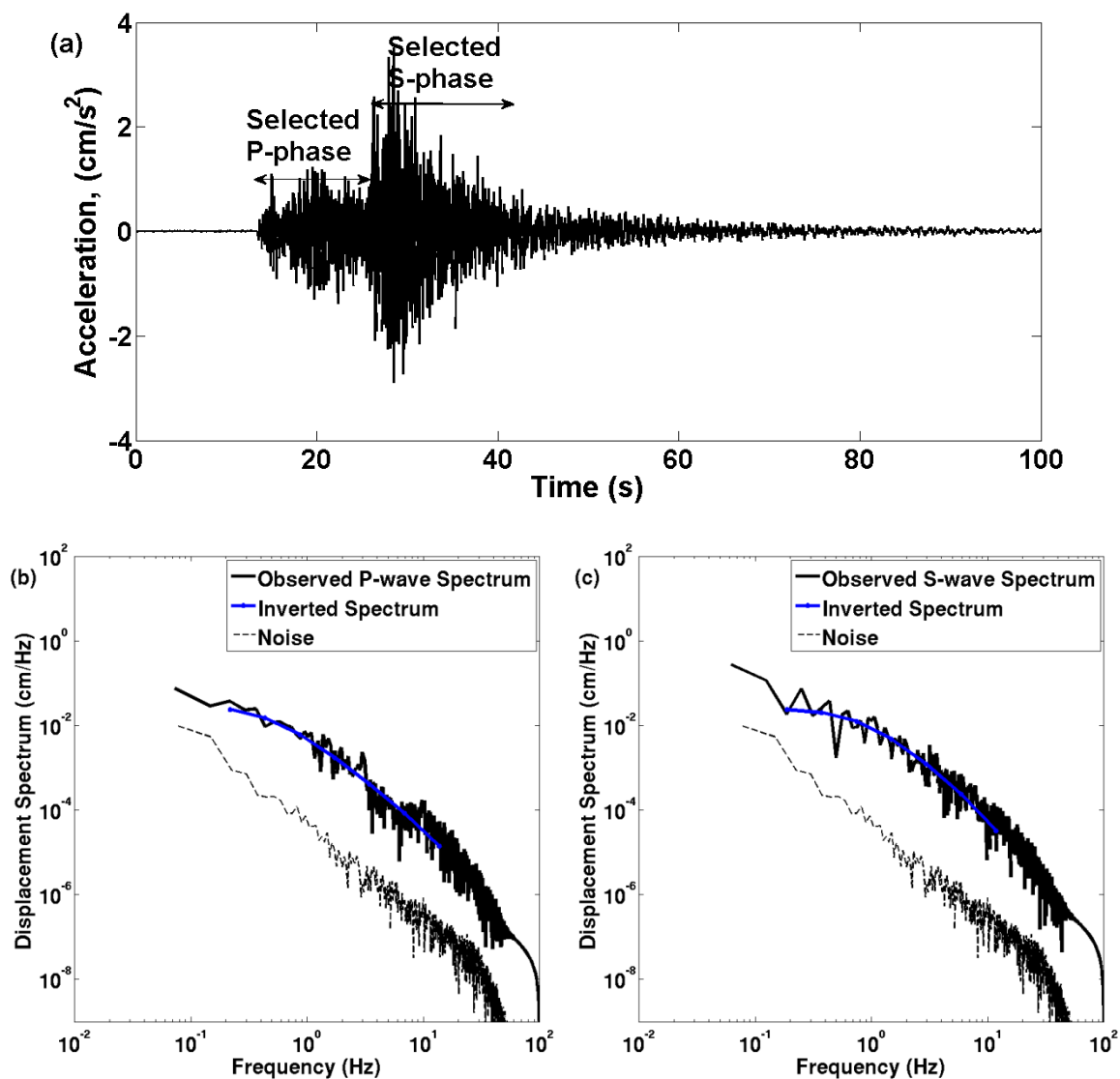


Figure 4.6 Example of observed and inverted spectra of P- and S-waves (vertical component) for the January 18, 2006 **M5.5** event at 115.4 km hypocentral distance. (a) Vertical component of the acceleration time series from the MYGH11 KiK-net borehole station; black arrows show the selected P- and S- phase windows (13.74 and 16 sec respectively). (b) Observed and inverted P-wave spectra; **MP** and f_c are **M5.7** and 0.46 (HZ) respectively and (c) observed and inverted S-wave spectra; **MS** and f_c are **M5.43** and 0.78 (Hz) respectively.

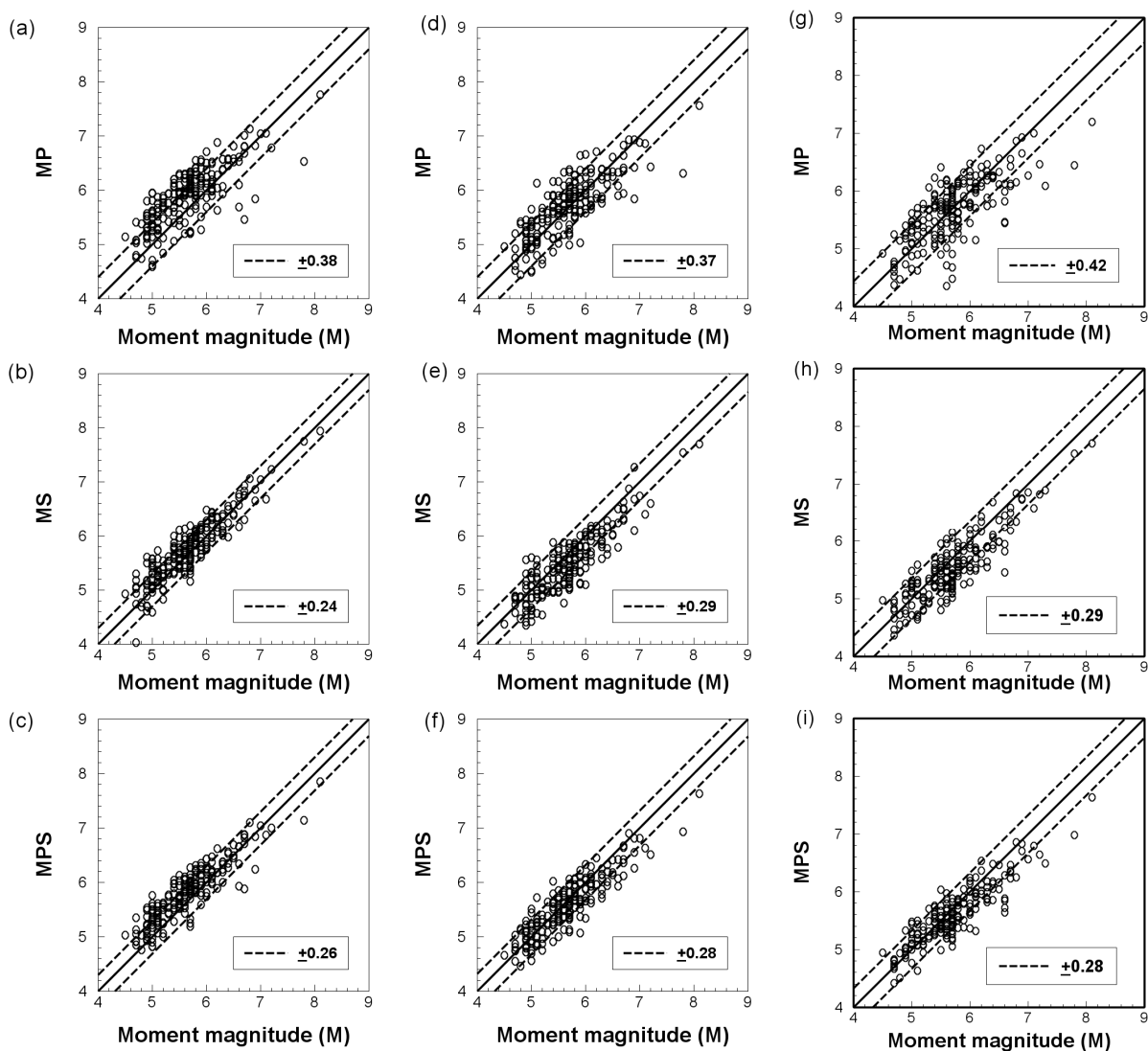


Figure 4.7 Ppredicted magnitude (**MP**, **MS** and **MPS**) versus **M** for the KiK-net borehole database (a, b and c), the KiK-net surface database (d, e and f) and the K-net database (g, h and i). The solid line is the 1:1 relation and dashed lines are one standard deviation.

Table 4.1 shows that, of the three magnitude estimates, **MP** has the largest standard deviation. **MS** from the KiK-net borehole and **MPS** from the KiK-net surface and K-net data have smaller standard deviations than the other estimates for those databases. The smallest standard deviation belongs to **MS** from the borehole recordings

(σ (**MS**) = 0.24) and **MP** from the K-net database has the largest standard deviation (σ (**MP**) = 0.42). Overall, we conclude that **MS** obtained using the borehole data provides the most accurate moment magnitude estimation with the smallest uncertainty among the methods tested.

Figure 4.8 illustrates the relationship between the magnitude residuals (for both **MP** and **MS**) and epicentral distance for the KiK-net borehole, KiK-net surface and K-net databases. As Figure 4.8 shows, **MP** underestimates the magnitude of the large events ($M > 6.0$) at very close distance, because at a station close to the source area, the S-P time window is very short (just few seconds), and so the final size of the event cannot be captured. For very large events ($M > 7.0$), **MS** provides better estimation in comparison to **MP** for all data types (Figure 4.8). As previously mentioned, overall we find that **MS** from borehole recordings (Figure 4.8d) provides the best moment magnitude estimation (with zero mean residuals and the smallest standard deviation).

Figure 4.9 shows the observed and inverted P- and S-waves spectra for the three largest events in our databases (**M7.8**, **M8.1**, and **M9.0**). Note that we chose the S-wave time windows by inspection to make sure that we capture the whole S-wave windows, in order to show how the estimation becomes stable through time. Our analysis shows that for larger events the magnitude updating needs to occur over a longer period of time, because the source duration is longer for larger events (Abercrombie, 1995). In real-time magnitude estimation, updating of the magnitude estimation can be performed for longer time windows after the first P-wave detection.

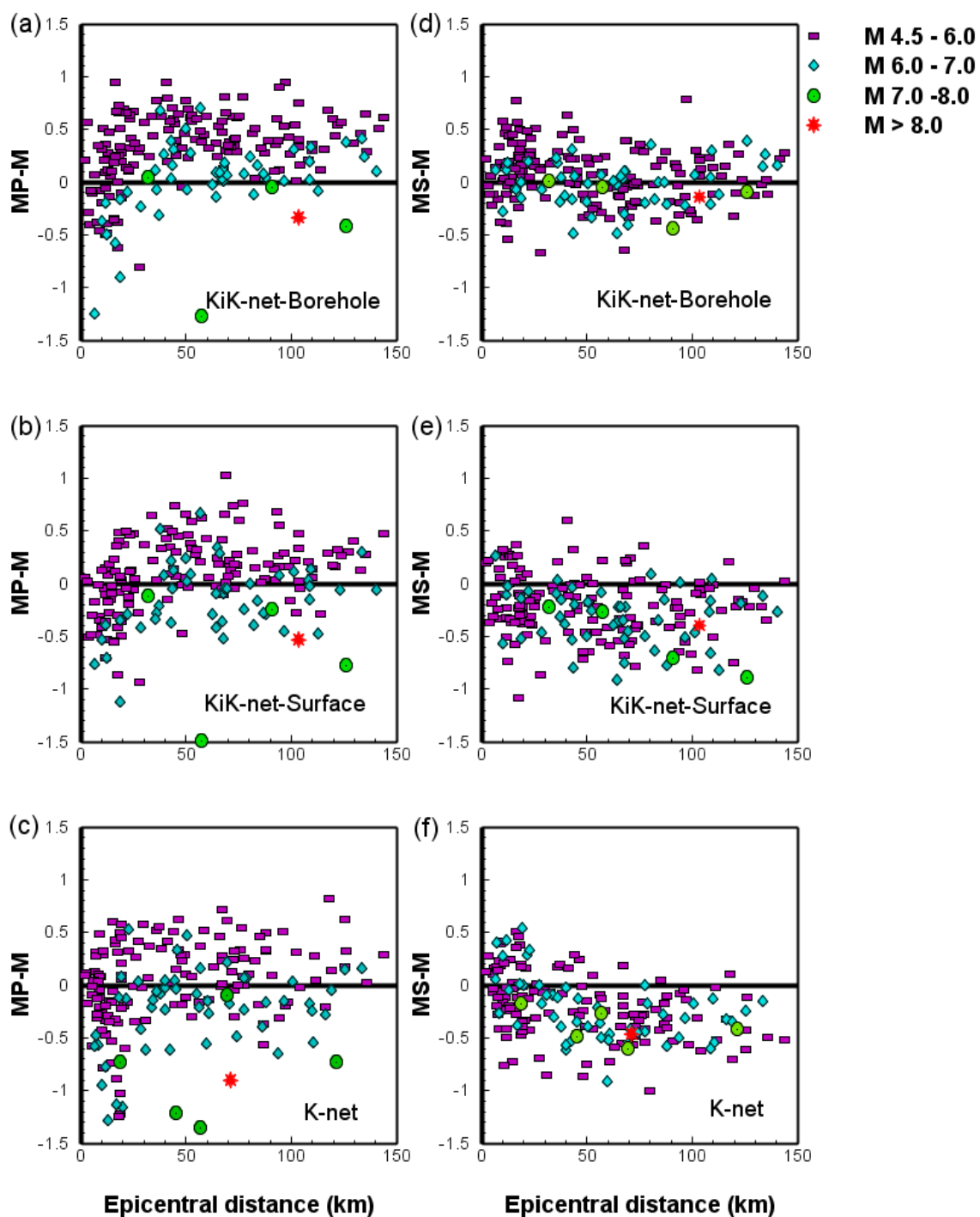


Figure 4.8 Distribution of magnitude residuals ($M_{\text{predicted}} - M_{\text{reported}}$) against epicentral distances. **MP** residuals vs. epicentral distance distribution for (a) KiK-net borehole, (b) KiK-net surface, and (c) K-net database. **MS** residuals vs. epicentral distance distribution for (d) KiK-net borehole, (e) KiK-net surface, and (f) K-net database.

Figure 4.10 shows the evolution of magnitude estimations (**MP** and **MS**) for the 26 September, 2003 **M8.1** Tokachi-Oki event. In Figures 4.10a and 4.10c, **MP** from KiK-net borehole and surface data converged to **M7.8** and **M7.6** approximately 13 seconds after the first P-wave arrival. **MS** from the KiK-net borehole and surface stations (Figure 4.10b and 10d) become stable approximately 15 seconds after the first S-wave arrival, which is about 28 seconds after the first P-arrival. The **MS** value converges to **M8.0** and **M7.8** for KiK-net borehole and surface data, respectively, 30 sec after the first S-arrival (43 sec after the first P-wave arrival). Figure 4.10e and 10f show that both **MP** and **MS** from the closest K-net station underestimated the final magnitude (**MP** = 7.2 and **MS** = 7.7).

The P-phase and S-phase portions of the vertical component of the strong motion recording from the March 11, 2011 Tohoku event (**M9.0**) at the closest KiK-net borehole, KiK-net surface, and K-net stations are shown in Figure 4.11. Previous studies have discussed this event (e.g. Aochi and Ide, 2011; Wang and Mori, 2011; Yoshida et al., 2011; Aochi and Ide, 2011; Meng et al., 2011; Kurahashi and Irikura, 2011; Eshaghi et al., 2013b) and suggested that the earthquake was complex and comprised of at least two phases. Note that there is some evidence for two fault segments that ruptured during the earthquake [Geospatial Information Authority of Japan (GSI), 2011; Maercklin et al., 2012], where the first and second segments generated a **M8.8** and a **M8.3** event respectively. The total energy of these two events produces a total moment magnitude of **M8.9**. Figure 4.11 clearly shows that the recordings from the closest station to the epicenter have at least two S-phase windows.

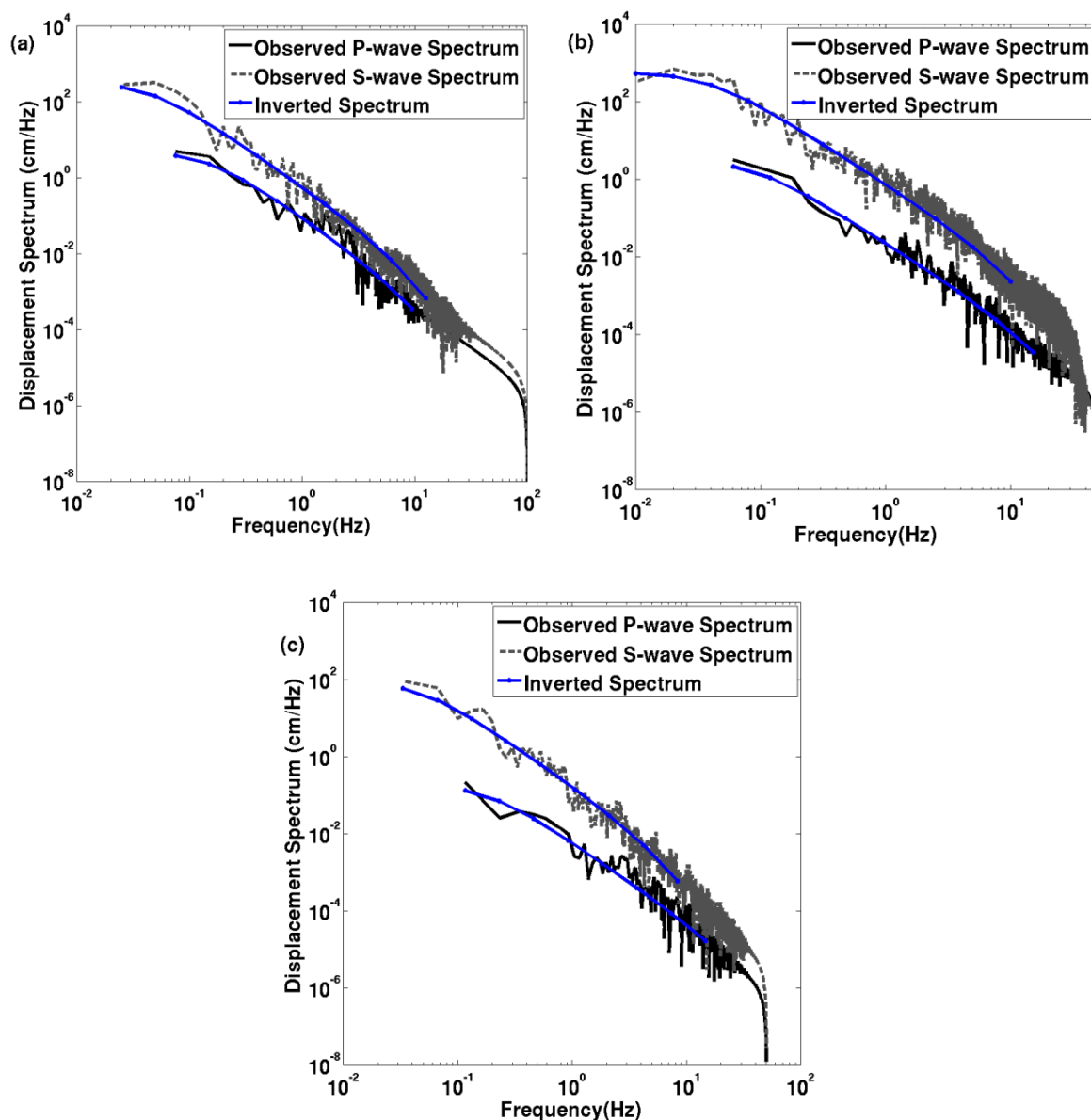


Figure 4.9 Observed and inverted spectra of P- and S-waves (vertical component) for the three largest events in this study. The P- and S-waves spectra from the KiK-net borehole stations for (a) the September 26 2003 **M8.1** Tokachi-Oki event, at 111.68 km hypocentral distance, (b) the 11 March 2011 **M9.0** Tohoku event, at 139.38 km hypocentral distance, and (c) the 11 March 2011 **M7.8** Tohoku aftershock event at 71.8 km hypocentral distance.

We chose the time window that includes both S-phases, 100 sec after the first S-phase arrival, approximately the same duration that the EEW system in Japan issued the estimated magnitude in real-time. **MP**, **MS** and the EEW magnitude (**EEW M**) estimation histories as a function of the time after the first P- and S-phase arrivals at the closest station, along with the reported **M** for the Tohoku event, are shown in Figure 4.12. Although **MP** underestimated the magnitude for all three types of data, most of the time it provides larger estimation than the **EEW M**. The **MS** estimation history for the borehole data starts with estimation of approximately **M5.0** and increases to **M7.8** almost 18 sec after the first S-arrival. At 30 sec after the first S-wave arrival, it converges to **M8.1** and remains stable at this value until the second S-phase reaches the station, 45 sec after the first S-phase arrival. The magnitude increases to **M8.5** about 60 sec after the first S-phase arrival and gradually converges to **M8.6**, approximately 116 sec after first the P-wave arrival.

The **MS** estimation histories for KiK-net surface and K-net data show a similar behavior but with smaller final estimates. For the first and second events, **MS** converges to **M7.9** and **M8.5** for KiK-net surface data and **M7.9** and **M8.4** for K-net data, respectively. Note that the **MS** histories show clearly that there are two levels of magnitudes. After receiving the second S-phase, the **MS** represents the magnitude of the second event, which is above the **EEW M** during that period of time, 45-100 sec after first S-phase arrival. Note that **EEW M** saturated at **M8.1**. In addition, the **EEW M** is obtained using information from more than one station (network-based approach), but here we use information from only one single station.

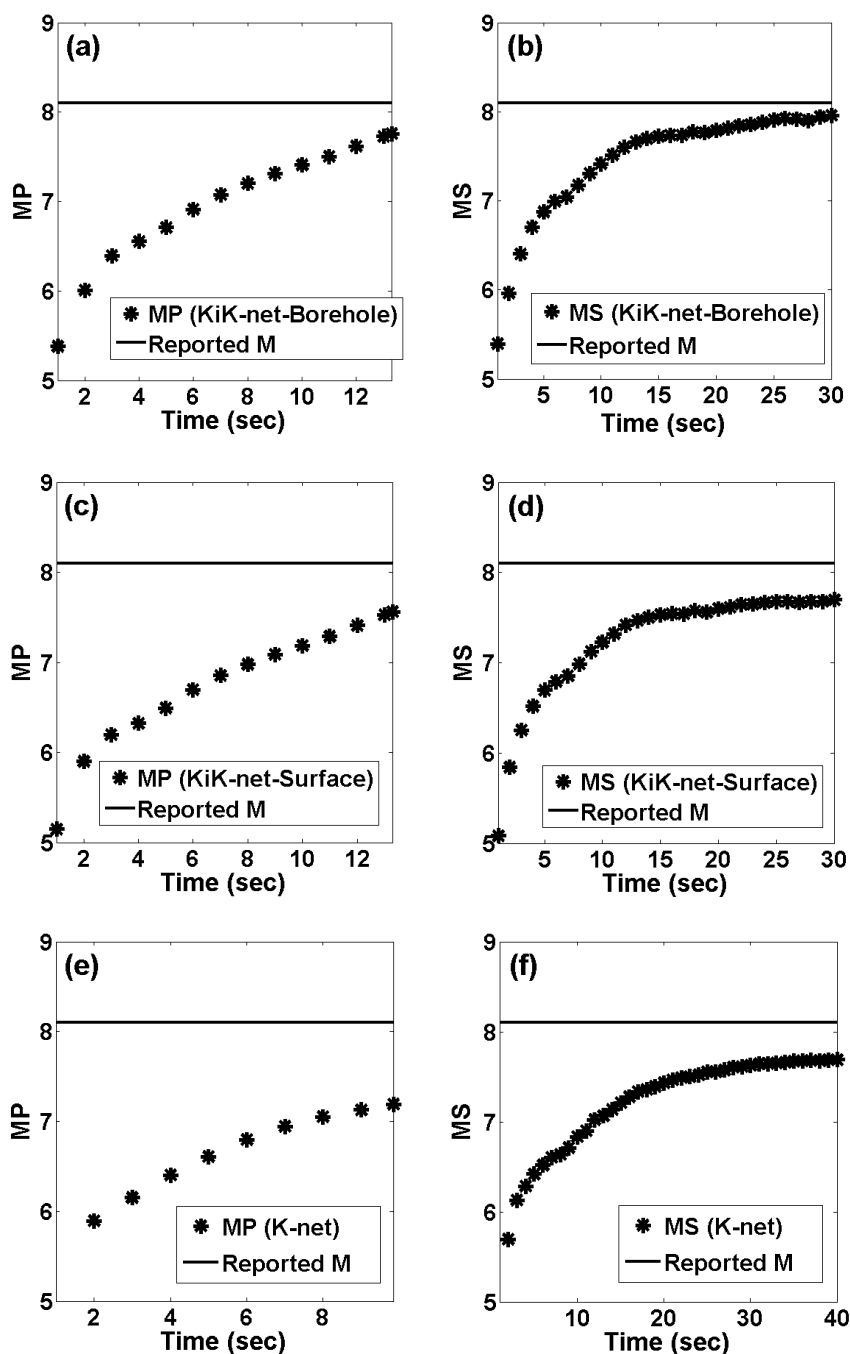


Figure 4.10 Predicted magnitude (**MP** and **MS**) versus time (seconds) after the first P- and S-wave arrivals for the September 26, 2003 **M8.1** Tokachi-Oki event. **MP** and **MS** versus time using the closest station for the KiK-net borehole stations (a and b); KiK-net surface stations (c and d); and K-net stations (e and f). The solid line represents the reported moment magnitude.

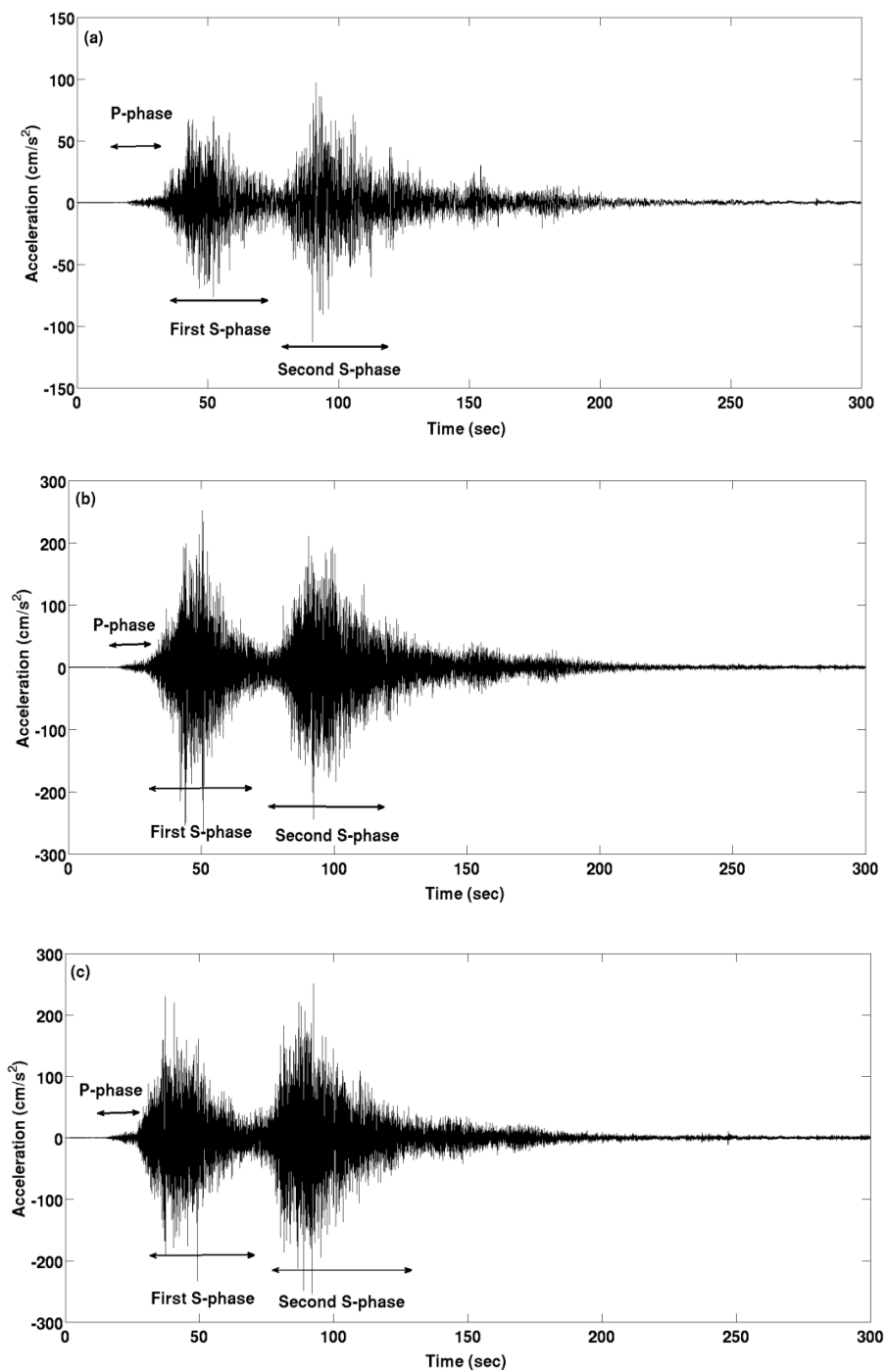


Figure 4.11 P-phase window and S-phase windows of the vertical component of the strong ground motion record at the closest (a) MYGH12 KiK-net borehole (b) MYGH12 KiK-net surface and (c) MYG011 K-net station to the epicenter of the March 11, 2011 M9.0 Tohoku event.

Figure 4.13 exhibits the evolution of magnitude prediction for the third largest event in our catalogues ($M7.8$, 11/03/2011) where **MP** underestimated the magnitude for all three types of data (KiK-net and K-net data). **MS** from the KiK-net borehole data (Figure 4.13b) converges to $M7.8$ about 30 sec after the first S-wave arrival, 38.6 sec after the first P-wave arrival. **MS** from the KiK-net surface (Figure 4.13d) and K-net data (Figure 4.13f) shows a similar behavior but with about 0.3 magnitude unit underestimation.

4.5 Discussion and Conclusions

In this study, we calculated the magnitudes for a large database for events with $M \geq 4.5$ that occurred in Japan based on the inversion of the displacement spectra. Displacement spectra inversion has not been used to calculate the magnitude of $M \geq 7.0$ earthquakes before in an EEW framework. Our results show that this method provides an accurate early estimation for the magnitude of these large events (Figures 4.10, 4.12 and 4.13). In this technique, the low frequency plateau is calculated using the three components of the available portion of strong motion time series (both P- and S-phases) and the moment magnitude is estimated from that low frequency plateau.

Magnitude determination begins one second after first P-wave detection and is updated every one second as more data become available. Note that information about the location of the event is required and the existing EEW system in Japan can provide this information approximately two seconds after the first P-wave detection (Odaka et al., 2003; Tsukada et al., 2004). Therefore in real-time EEW practice, we have to consider

the time required for location determination, the time needed for the data processing and calculation of the magnitude, and the telemetry delay.

In addition, we determined that more accurate results were produced for larger events if we did not first filter the ground motion recordings in the frequency domain, as doing so can remove bandwidth that is critical for estimating the magnitude of larger events. For example, we tested the application of a band-pass Butterworth filter with corner frequencies of 0.1-15 Hz to the all records, where 0.16 is the low cut corner of the filter used in the existing EEW system in Japan. The results were not significantly different for $M < 7.0$ events, but the magnitude estimation for the largest events ($M8.1$ and $M9.0$ events) underestimated the magnitude of those events (see Table B1 and Figure B1 in Appendix B). It is suggested that in real-time practice the system uses both filtered and unfiltered data, considering the signal/noise ratio for each component. Where we have a large event, such as an $M8.1$ or $M9.0$ event, the signal strength at long periods will allow a broader bandwidth, and result in improved magnitude determinations. The estimation from the filtered data will saturate, but the estimate from the unfiltered data will continue to grow with time, providing confirmation that a very large event is occurring.

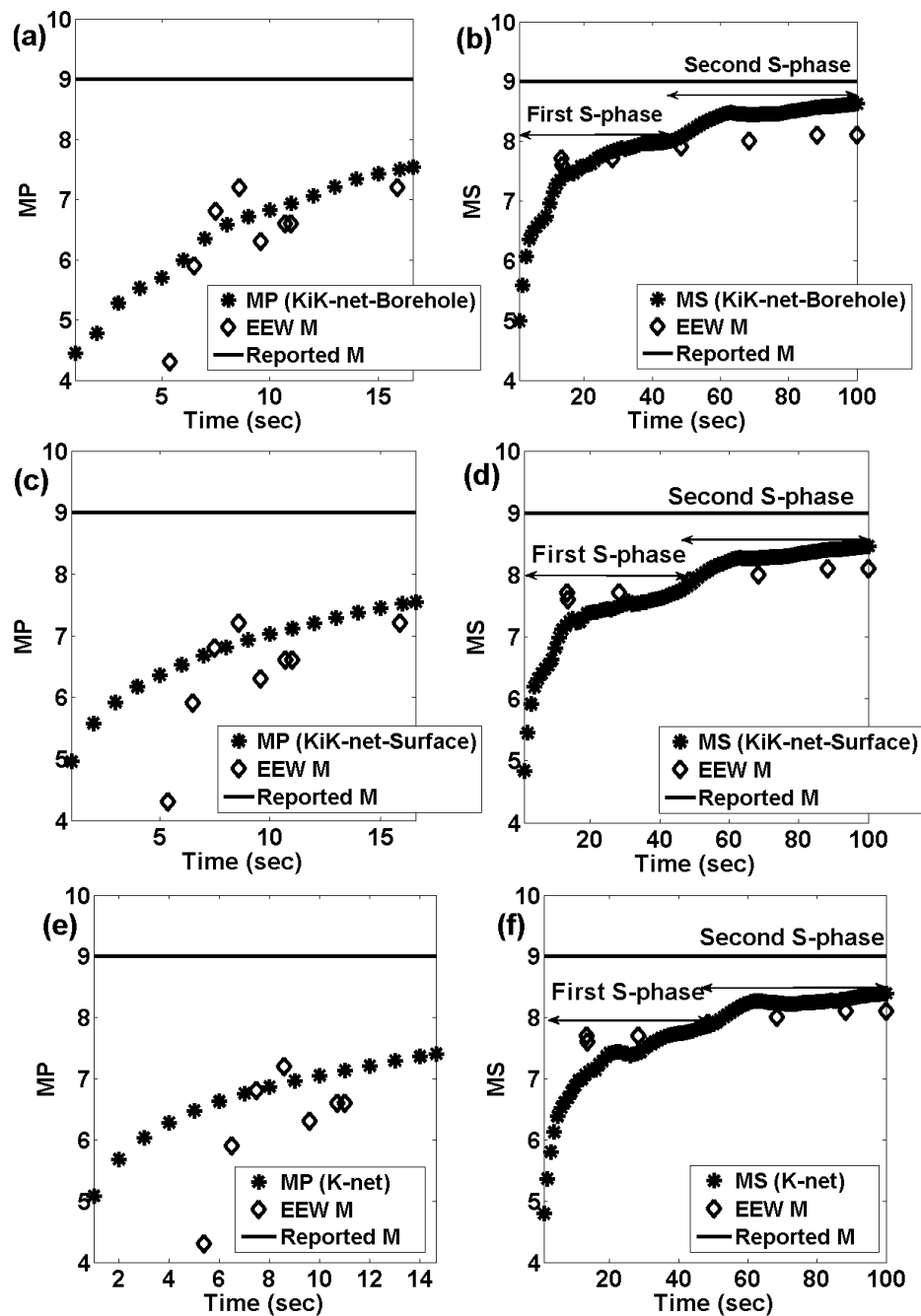


Figure 4.12 Predicted magnitude (MP and MS) and EEW M versus time (seconds) after the first P- and S-wave arrivals for the March 11, 2011 M9.0 Tohoku event. MP and MS versus time using the closest station for the KiK-net borehole stations (a and b); KiK-net surface stations (c and d); and K-net stations (e and f). The solid line represents the reported moment magnitude.

We conclude that, in general, borehole recordings allow for more accurate magnitude estimations with a smaller standard deviation for larger events. Borehole recordings, when used with our algorithm, tend to overestimate the magnitude of the smaller events (i.e. $M \leq 6.0$) but provide a better estimate of larger earthquakes and have the smallest standard deviation in comparison with results obtained from surface databases (Table 4.1). This suggests that the use of borehole recordings improves the performance of EEW systems, particularly for larger earthquakes.

Moreover, the results show that the single-station approach is able to provide useful estimates of earthquake magnitude from the earliest available information. This ability is significant for the application of EEW system in vulnerable areas exposed to seismic hazard with sparse seismic networks, such as the Cascadian subduction zone. A single-seismic station close to the seismic source can provide a low-cost tool to mitigate seismic hazards in these regions.

It also is observed that the first predictions generally underestimate the magnitude, but as more data is acquired the prediction converges to the reported M (Figures 4.9, 4.11, and 4.12). As previously mentioned, there is always a trade-off between time and accuracy of the predicted magnitudes. Therefore, early estimation can provide a minimum threshold for the final size of the event in real-time practice, and preliminary actions to reduce the earthquake hazard can be taken before a more precise estimation with less uncertainty is obtained.

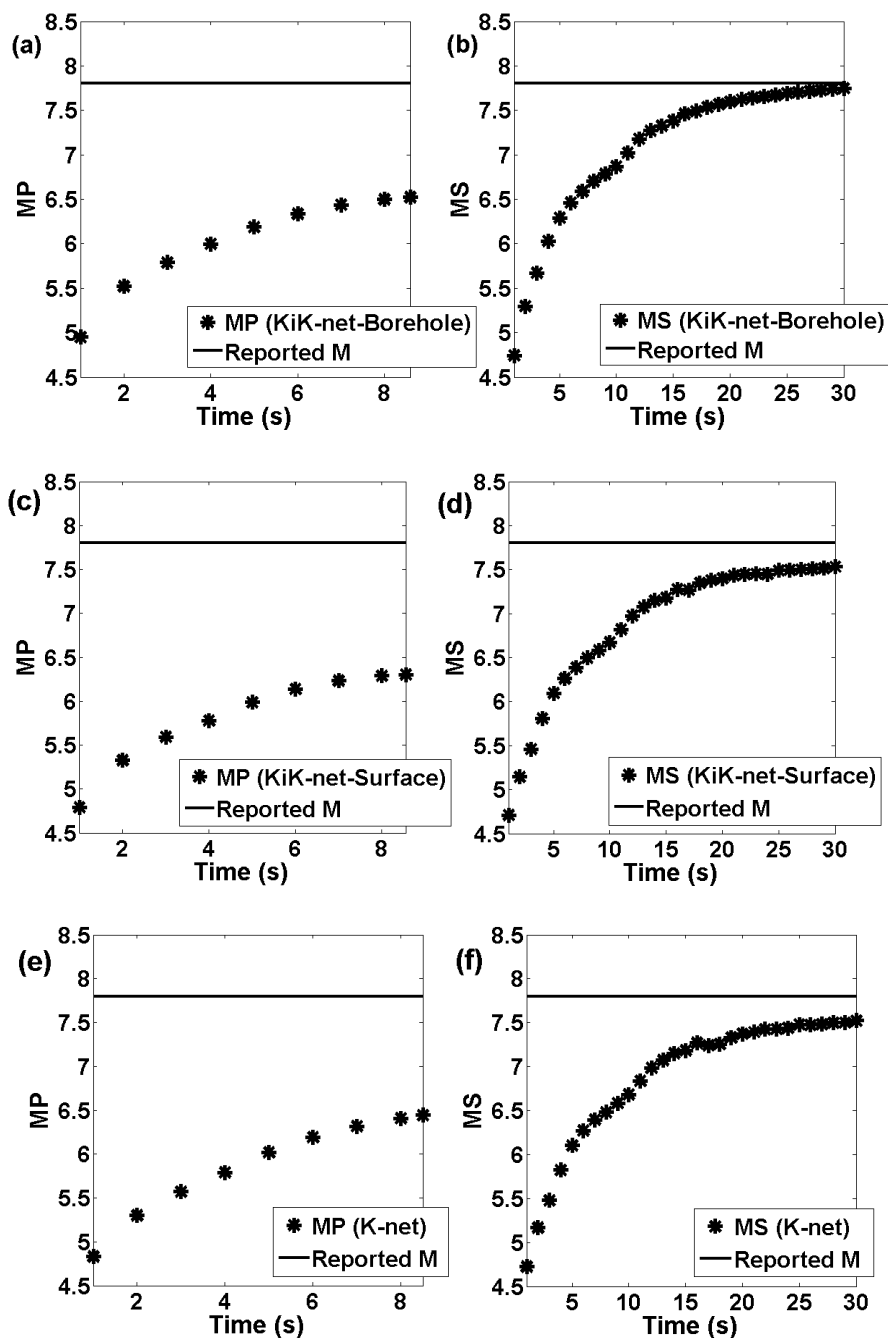


Figure 4.13 Predicted magnitude (MP and MS) versus time (seconds) after the first P- and S-wave arrivals for the March 11, 2011 M7.8 Tohoku aftershock event. **MP** and **MS** versus time using the closest station for the KiK-net borehole stations (a and b); KiK-net surface stations (c and d); and K-net stations (e and f). The solid line represents the reported moment magnitude. The solid line represents the reported moment magnitude.

Our results show that, although the **MP** provides a faster estimation for the magnitude, it has a larger standard deviation in comparison with **MS** and **MPS**. On the other hand, **MS** and **MPS** produce more stable and accurate estimates for larger events (Figures 4.7 and 4.8) but provide shorter warning time.

Note that due to the variety of contributing factors, estimation of the errors in the source parameters is not a simple task (Abercrombie, 1995). Possible sources of the scatter observed in our magnitude estimation would be the unaccounted site amplification effects, misdetermination of the radiation pattern and the fitting errors. Borehole recordings are less affected by the wave propagation through the surface layers; however, this is not the case for surface recordings (Abercrombie, 1995). As a result, accounting for site amplification effects would potentially improve the accuracy of the magnitude estimation particularly for surface data. Previous studies showed that the observed radiation pattern was not as variable as the theoretical radiation pattern (see Guo et al., 1992; Abercrombie 1995); however, the effect of focal mechanism and radiation pattern can not be neglected (Vidale, 1989). In this study we calculated the the mean value of **MP** and **MS**, as **MPS**. Because the node in radiation pattern of P-wave corresponds to the maximum in the S-wave, this averaging minimizes the effect of the radiation pattern (Abercrombie, 1995).

Finally, our research adds further evidence for the suitability of magnitude estimation based on the inversion of the displacement spectra for all types of regions. This method does not rely on previously derived empirical relationships (such as τ_c or τ_p -magnitude relationships) and directly estimates the quantities related to the moment magnitude. It would be straightforward to apply to other regions such as Cascadia, with

simple validation and calibration if necessary, which could be based on even a limited amount of regional data.

4.6 References:

Abercrombie, R. (1995). Earthquake source scaling relationships from -1 to 5 ML using seismograms recorded at 2.5-km depth, *J. Geophys. Res.*, 100, 24015–24036.

Aki, K., and P. Richards (2002). *Quantitative Seismology*, 2nd ed., Univ. Sci., Sausalito, Calif.

Alcik, H., O. Ozel, N. Apaydin, and M. Erdik (2009). A study on warning algorithms for Istanbul earthquake early warning system, *Gephys. Res. Lett.*, 36, L00B05.

Allen, R. V. (1978). Automatic earthquake recognition and timing from single traces, *Bull. Seismol. Soc. Am.*, 68, 1521–1532.

Allen, R. M., and H. Kanamori (2003). The potential for earthquake early warning in Southern California, *Science*, 300, 786–789, doi:10.1126/science.1080912.

Allen, R. M., P. Gasparini, O. Kamigaichi, and M. Böse (2009). The status of earthquake early warning around the world: An introductory overview, *Seismol. Res. Lett.*, 80, 682–693, doi:10.1785/gssrl.80.5.682.

Aochi, H. and S. Ide (2011). Conceptual multi-scale dynamic rupture model for the 2011 off the Pacific coast of Tohoku Earthquake, *Earth Planets Space*, 63, 761–765.

Aoi, S., T. Kungugi, and H. Fujiwara (2004). Strong-motion seismograph network operated by NIED: K-NET and KiK-net, special issue, *J. Japan Assoc. Earthq. Eng.* 4, no. 3 (special issue), 65–74.

Atkinson, G. M. and D. M. Boore (1995). Ground-motion relations for eastern North America, *Bull. Seismol. Soc. Am.* 85, 17-30.

Atkinson, G. M., and Silva, W., (2000). Stochastic modeling of California ground motions, *Bull. Seismol. Soc. Am.*, 90, 255-274.

Boatwright, J. A. (1980). A spectral theory for circular seismic sources: Simple estimates of source dimension, dynamic stress drop and radiated energy. *Bull. Seism. Soc. Am.*, 70, 1–27.

Boore, D. (2003). Simulation of ground motion using the stochastic method, *Puer Appl. Geophys.* 160, 636–676.

Boore, D. and S. Akkar (2003). Effect of causal and acausal filters on elastic and inelastic response spectra, *Earthquake Engng Struct. Dyn.* 32, 1729–1748, doi: 10.1002/eqe.299

Boore, D. M., K. W. Campbell, and G. M. Atkinson (2010). Determination of stress parameters for eight well-recorded earthquakes in eastern North America, *Bull. Seism. Soc. Am.* 100, 1632-1645.

Brune, J. N. (1970). Tectonic stress and the spectra of seismic shear waves from earthquakes, *J. Geophys. Res.*, 75, 4997–5009.

Caprio, M., M. Lancieri, G. B. Cua, A. Zollo, and S. Wiemer (2011). An evolutionary approach to real-time moment magnitude estimation via inversion of displacement spectra, *Geophys. Res. Lett.*, 38, L02301, doi:10.1029/2010GL045403.

Eshaghi, A., K. F. Tiampo, H. Ghofrani, G. M. Atkinson (2013a). Using borehole records to estimate magnitude for earthquake and tsunami early-warning systems, *Bull. Seismol. Soc. Am.* 103, 2216–2226, doi:10.1785/0120120319.

Eshaghi, A., K. F. Tiampo, H. Ghofrani, G. M. Atkinson (2013b). Magnitude estimation for the 2011 Tohoku-Oki earthquake based on ground motion prediction equations. *Pure Appl. Geophys.*, doi: 10.1007/s00024-013-0746-y

Geospatial Information Authority of Japan (2011). Crustal Deformation and Fault Model obtained from GEONET data analysis. Last accessed February 2014, <http://www.gsi.go.jp/cais/topic110422-index-e.html>.

Ghofrani, H., and G. M. Atkinson (2011). Forearc versus Backarc attenuation of earthquake ground motion, *Bull. Seismol. Soc. Am.*, 101, 3,032–3,045, doi: 10.1785/0120110067.

Ghofrani, H., G. M. Atkinson, and K. Goda (2012). Implications of the 2011 M 9.0 Tohoku Japan earthquake for the treatment of site effects in large earthquakes, *Bull. Earthq. Eng.*, doi: 10.1007/s10518-012- 9413-4.

Guo, H. A., A. Ierler-Lam, and S. E. Hough (1992). Empirical Green's function study of Loma Prieta aftershocks: Evidence for fault zone complexity (abstract), *Seimol. Res. Lett.*, 63, 76.

Hanks, T. C., and H. Kanamori (1979). A moment magnitude scale, *J. Geophys. Res.*, 84, 2,348–2,350.

Horiuchi, S., H. Nrgishi, K. Abe, A. Kaminuma, and Y. Fujinawa (2005). An automatic processing system for broadcasting earthquake alarms, *Bull. Seismol. Soc. Am.*, 95, 708–718.

Hoshiaba, M., O. Kamigaichi, M. S. Tsukada, and N. Hamada (2008). Earthquake Early Warning starts nationwide in Japan, *EOS Trans. AGU*, 89, 73-74.

Hoshiaba, Y., K. Iwakiri, N. Hayashimoto, T. Shimoyama, K. Hirano, Y. Yamada, Y. Ishigaki, and H. Kikuta (2011). Outline of the 2011 off the Pacific coast of Tohoku Earthquake (M9.0) Earthquake Early Warning and observed seismic intensity, *Earth Planets Space*, 63, 547–551.

Hoshiaba, M. (2013). Real-time prediction of ground motion by Kirchhoff-Fresnel boundary integral equation method: Extended front detection method for Earthquake Early Warning, *Journal of Geophysical Research: Solid Earth*, 118, 1038–1050, doi:10.1002/jgrb.50119.

Kanamori, H. (2005). Real-time seismology and earthquake damage mitigation, *Annu. Rev. Earth Planet Sci.*, 33, 195–214.

Kamigaichi, O., K. Ohtake, D. Nozaka, D. Hasebe, T. Odaka, S. Tsukada, K. Ashiya and S. Sato (2002). Focal parameters estimation method to be used in JMA nowcast earthquake information - 2 – Magnitude estimation, *Proceedings of 2002 Japan Earth Planetary Science Joint Meeting*, S045-P007.

Kamigaichi, O. (2004). JMA earthquake early warning. *Journal of the Japan Association for Earthquake Engineering* 4, 134– 137.

- Kamigaichi, O., M. Saito, K. Doi, T. Matsumori, S. Tsukada, K. Takeda, T. Himoyama, K. Nakamura, M. Kiyotomoto, and Y. Watanabe (2009). Earthquake early warning in Japan: Warning the general public and future prospects, *Seismol. Res. Lett.* 80, 717–726.
- Katsumata, A. (2004). Revision of the JMA displacement magnitude, *Quart. J. Seismol.*, 67, 1-10. (in Japanese with English abstract)
- Kurahashi, S., and K. Irikura (2011). Source model for generating strong ground motions during the 2011 off the Pacific coast of Tohoku Earthquake, *Earth Planets Space* 63, 571–576.
- Lagarias, J.C., J. A. Reeds, M. H. Wright, and P. E. Wright, (1998). Convergence properties of the Nelder-Mead simplex method in low dimensions, *SIAM Journal of Optimization*, 9, pp. 112-147.
- Luersen, M.A., R. Le Riche, and F. Guyon (2004). A constrained, globalized, and bounded Nelder–Mead method for engineering optimization, *Structural and Multidisciplinary Optimization*, 27, pp 43-54, doi: 10.1007/s00158-003-0320-9.
- Lin, T., and Y. M. Wu (2010). Magnitude determination using strong ground motion attenuation in earthquake early warning, *Geophys. Res. Lett.*, 7, L07304. doi:10.1029/2010GL042502.
- Lin, T., Y. M. Wu, D. Chen, N. Hsiao and C. Chang (2011). Magnitude Estimation in Earthquake Early Warning for the 2010 JiaSian, Taiwan, Earthquake, *Seismol. Res. Lett.* 82, 201-206.
- Maercklin, N., G. Festa, S. Colombelli, and A. Zollo (2012). Twin ruptures grew to build up the giant 2011 Tohoku, Japan, earthquake, *Sci. Rep.* 2, 709.

- Madariaga, R. (1976). Dynamics of an expanding circular fault, *Bull. Seismol. Soc. Am.*, 66, 639–666.
- Meng, L., I. Asaf and J.P. Ampuero (2011). A window into the complexity of the 2011 M_w 9 Tohoku-Oki earthquake, *Geophys. Res. Lett.*, 38. doi:10.1029/2011GL048118
- Nakamura, Y. (1988). On the urgent earthquake detection and alarm system (UrEDAS). In *Proceedings of the 9th World Conference on Earthquake Engineering VII*, 673–678.
- Nakamura, H., S. Horiuchi, C. Wu, S. Yamamoto, and P. A. Rydelek (2009). Evaluation of the real-time earthquake information system in Japan, *Geophys. Res. Lett.*, 36, L00B01.
- Nelder, John A., R. Mead (1965). A simplex method for function minimization, *Computer Journal* 7: 308–313. doi:10.1093/comjnl/7.4.308
- Odaka, T., K. Ashiya, S. Tsukada, S. Sato, K. Ohtake, and D. Nozaka (2003). A new method of quickly estimating epicentral distance and magnitude from a single seismic record, *Bull. Seismol. Soc. Am.*, 93, 526–532.
- Rydelek, P., and S. Horiuchi (2006). Is earthquake rupture deterministic? *Nature* 442, E5–E6.
- Rydelek, P., C. Wu, and S. Horiuchi (2007). Comment on “Earthquake magnitude estimation from peak amplitudes of very early seismic signals on strong motion records” by Aldo Zollo, Maria Lancieri, and Stefan Nielsen, *Geophys. Res. Lett.*, 34, L20302, doi: 10.1029/2007GL029387.
- Tsukada, S., S. Odaka, K. Ashiya, K. Ohtake, and D. Nozaka (2004). Analysis of the envelope waveform of the initial part of P waves and its application to quickly estimating the epicentral distance and magnitude, *Zisin* 2, 56, 351–361 (in Japanese).

Vidale, J. E., (1989). Influence of focal mechanism on peak ground accelerations of strong motions of the Whittier Narrows, California, earthquake and an aftershock. *J. Geophys. Res.*, 94, 9607-9613.

Wang, D., and J. Mori (2011). Rupture process of the 2011 off the Pacific coast of Tohoku Earthquake (M_w 9.0) as imaged with back-projection of teleseismic P-Wave, *Earth Planets Space*, 63, 603–607.

Wu, Y.M., and H. Kanamori (2005a). Experiment on an onsite early warning method for the Taiwan early warning system. *Bull. Seismol. Soc. Am.*, 95, 347–353.

Wu, Y.M., and H. Kanamori (2005b). Rapid assessment of damage potential of earthquakes in Taiwan from the beginning of P waves. *Bull. Seismol. Soc. Am.*, 95, 1181–1185.

Wu, Y.M., and H. Kanamori (2008). Exploring the feasibility of onsite earthquake early warning using close-in records of the 2007 Noto Hanto earthquake. *Earth Planets and Space.*, 60, 155–160.

Yamada, T., and S. Ide (2008). Limitation of the predominant-period estimator for earthquake early warning and the initial rupture of earthquakes, *Bull. Seismol. Soc. Am.*, 98, 6, 2739– 2745

Yamada, M., and J. Mori (2009). Using τ_c to estimate magnitude for earthquake early warning and effects of near-field terms, *J. Of Geophys. Res.* 114, B05301, doi:10.1029/2008JB006080, 2009

Yenier, E., and G. M. Atkinson (2014). Equivalent point-source modeling of moderate-to-large magnitude earthquakes and associated ground-motion saturation effects, *Bull. Seismol. Soc. Am.*, 104, doi:10.1785/0120130147.

Yoshida, K., K. Miyakoshi and K. Irikura (2011). Source process of the 2011 off the pacific mecoast of Tohoku Earthquake inferred from waveform inversion with long-period strong-motion records, *Earth Planets Space*, 63, 577–582.

Chapter 5

5 Conclusions and future studies

5.1 Summary and conclusions

The goal of this study was to examine alternative methods to estimate the correct magnitude of an earthquake using the earliest information from strong ground motion recordings for earthquake and tsunami early warning systems. An accurate early estimation of magnitude is critical during strong earthquakes, especially for those that are capable of causing tsunamis, such as the Tohoku earthquake of 2011. A faster and more reliable earthquake and tsunami early warning system in vulnerable areas can increase the warning time to evacuate people from hazardous areas and improve risk reduction actions and emergency response efficiency.

In Chapter 2, I presented a new application of GMPEs for magnitude estimation for EEW systems. Both borehole and surface databases recorded by KiK-net stations from (16/08/1998-11/08/2009) with $5.0 \leq M \leq 8.1$ were used to develop the new GMPEs. In total, 2160 borehole accelerograms with $PGA \geq 10 \text{ cm/s}^2$ and 890 surface accelerograms with $PGA \geq 80 \text{ cm/s}^2$ were used to derive GMPEs for both PGA and PGV in Japan. Later these estimated GMPEs were used as a basis for magnitude determination for those events that had 20 or more recordings in the databases. The results confirmed that using GMPEs provides a very good estimate of M for a large event approximately 40 seconds after the origin time without the problem of saturation. They also show that the magnitude estimates based on GMPEs from PGV values, M_{pgv} , provided a more stable

and accurate estimation when compared to the PGA values, M_{pga} . It is noted that the estimation based on the borehole database has a smaller standard deviation, which suggests borehole recordings in a seismic network can improve the EEW and tsunami warning systems' performances.

Estimation of the moment magnitude of the 2011 Tohoku-Oki event in Japan using real-time strong ground motion data was the subject of Chapter 3. The Tohoku event is the largest earthquake in the modern history of Japan, recorded by thousands of seismic stations across Japan. The wealth of strong motion recordings in 2011 provides a more complete strong motion database for an unprecedented range of magnitudes and distances. First, an offline test was performed to estimate the magnitude of the Tohoku event based on the GMPEs obtained in Chapter 2. Then, in order to improve the determination of attenuation parameters and magnitude scaling, I developed new GMPEs using the more complete database (16/08/1998–14/12/2011). To account for site effects for KiK-net surface stations, I explored the use of the common site variable, average shear-wave velocity in the uppermost 30 m, V_{s30} . The newly obtained GMPEs were used to estimate the magnitude of the Tohoku event, in addition to all the other events with at least 20 records in the new catalog. The values obtained for M_{pga} and M_{pgv} for the Tohoku event were compared with the real time magnitude estimates provided by the existing EEW system in Japan at that time. This comparison showed that, unlike the estimation provided by the existing EEW system in Japan, this magnitude estimate does not saturate. Instead, the robust estimates of moment magnitude for both catalogs could have been determined within 100 s after the earthquake onset.

It is noted that the use of V_{S30} improves the accuracy of magnitude estimates from surface recordings, especially for M_{pgv} . The analysis of the standard deviations of magnitude estimates confirms that the M_{pgv} from borehole recordings provides a more stable and accurate estimate for EEW systems. Again, the incorporation of borehole recordings into real-time EEW practice for vulnerable countries exposed to future great earthquakes and tsunamis is highly recommended. The results showed that in most cases the magnitude is over estimated at early times. With the addition of more data that estimate converges to the reported moment magnitude. Therefore, in real-time practice, it will be necessary to wait until the magnitude estimate become stable before using it for EEW purposes. This can be done by fitting a line to the estimates to determine the slope of the line. When that slope is close to zero then the estimation has stabilized. It should be mentioned that this method is not intended to replace very short term warning methods; rather it is able to better determine the ultimate size of an event rapidly, i.e. within about a minute. Therefore, information provided by this method complements the existing EEW system and also is important for tsunami warnings and post-event response.

Finally, in Chapter 4 the real-time strong ground motion displacement spectra from KiK-net and K-net stations, 03/06/2000 - 03/12/2011, were used in a single station approach to estimate the magnitude of the earthquakes that occurred in Japan, $4.5 \leq \mathbf{M} \leq 9.0$. In any network, the estimation obtained from each station also can be incorporated into a network-based approach to further improve performance. The source parameters were determined using the inversion of displacement spectra for available P- and S-waves windows. In the single station approach, magnitude is estimated based on the information

from the closest station to the epicenter. It is noteworthy that in this method the magnitude is directly calculated from the displacement spectra of the available strong motion recordings. Previous empirical EEW parameters-magnitude scaling relationships (such as magnitude vs. τ_p/τ_c relationships or GMPEs) are not necessary. As a result, this method is suitable for vulnerable regions exposed to seismic hazards where existing recordings of strong ground motion from potentially damaging earthquakes are sparse or unavailable (such as the Cascadia region of North America).

The magnitude of the Tohoku event was calculated using data from the station with smallest epicentral distance and these estimates were compared with the magnitude estimates provided by the existing EEW system in Japan (Figure 4.12). The results from both approaches support the hypothesis that the Tohoku event was complex and comprised of two events, with moment magnitude around **M8.3** and **M8.8** respectively, where their energy together equated to an **M9.0** event.

Additionally, the impact of applying a fixed low-cut filter for strong motion recordings on the final magnitude estimates was examined. Low-cut filters are used to remove the low-frequency noise that is present in many analog and digital strong-motion recordings (Trifunac, 1971; Boore et al., 2002). First I used a band-pass filter with corner frequencies of 0.1-15 Hz where previous studies showed that the lower frequency limit is suitable to produce well-shaped displacement time series, with a flat displacement spectra at low frequencies (Ghofrani and Atkinson, 2011; Ghofrani et al., 2011). The analysis showed that using the fixed low-cut filter can remove the corner frequency of large events and results in the underestimation of the final magnitude for those events. Hence, in order to keep the relevant part of the data, particularly for larger events (such as

Tohoku), I did not use a fixed low-cut filter. Instead, I used only that frequency bandwidth where the signal/noise ratio was greater than 3.0, within the range from 0.01 to 15 Hz. It is suggested that in real-time practice the system uses both filtered and unfiltered data, considering the signal/noise ratio for each component. Where there is a large event, such as an **M8.1** or **M9.0** event, the signal strength at long periods will result in improved magnitude determinations. For events with $M \leq 7$, the low-cut filter does not remove the corner frequency of the events and the filtered data provide estimates with smaller uncertainty. On the other hand, for very large events the estimation from the filtered data will saturate, but the estimate from the unfiltered data will continue to grow with time and confirm that a very large event is occurring.

The results from the single station approach indicate that **MP** presents a faster early estimate for the ultimate size of an earthquake, but these estimates also have a lower degree of precision. On the other hand, **MS** provides a less biased estimate with a smaller standard deviation, but a shorter warning time. The **MS** from the borehole database has the smallest standard deviation among the estimated magnitudes (Table 4.1). This again supports the conclusion that the use of borehole recordings can improve the EEW performance, particularly for the larger earthquakes.

5.2 Suggestions for future studies

Several factors including magnitude, distance, frequency, and site condition or a combination of these factors have strong effects on ground motion prediction equations. Therefore, it is a continuous task to develop new GMPEs based on updated uniform databases that include new earthquakes. In this study, very simple attenuation forms were

used to develop the GMPEs for PGA and PGV for all types of events. In-depth ground motion studies for specific regions will improve EEW performance. In addition, investigating the effects of earthquake focal mechanisms and location also would improve the accuracy of magnitude estimations.

Here, the GMPEs were developed for all three components of ground motion recordings, regardless of the orientation of the components. The next step to improve the GMPEs should include the study of different GMPEs for the horizontal and vertical components separately. Sensitivity tests should be conducted in order to determine if these result in more robust estimations with lower uncertainty. In addition, detailed studies of the variation in V_{S30} and the resulting confidence intervals of the GMPEs parameters could provide a better understanding of the effects of these parameters on the final magnitude estimation.

In the second part of this thesis, the source parameters were determined assuming a source model based on the Brune (1970) model, and the earthquake magnitude was estimated using the obtained source parameters from data recorded at a single station (station with smallest epicentral distance). Next steps should include testing of the performance of this method in a network-based approach. Additionally, more detailed analysis of the effects of various parameters in the model on the final results could help to determine which model provides more robust estimates with lower uncertainty.

Finally, application of this method to large earthquakes in other regions will provide additional insights into its ability to estimate the magnitude of large events worldwide.

5.3 References

Boore, D. M., C. D. Stephens, and W. B. Joyner (2002). Comments on baseline correction of digital strong-motion data: Examples from the 1999 Hector Mine, California, earthquake, *Bull. Seism. Soc. Am.* **92**, 1543–1560.

Brune, J. N. (1970). Tectonic stress and the spectra of seismic shear waves from earthquakes, *J. Geophys. Res.*, *75*, 4997–5009.

Ghofrani, H., and G. M. Atkinson (2011). Forearc versus Backarc attenuation of earthquake ground motion, *Bull. Seismol. Soc. Am.*, *101*, 3,032–3,045, doi: 10.1785/0120110067.

Ghofrani, H., G. M. Atkinson., and K. Goda (2012). Implications of the 2011 M 9.0 Tohoku Japan earthquake for the treatment of site effects in large earthquakes, *Bull. Earthq. Eng.*, doi: 10.1007/s10518-012- 9413-4.

Trifunac, M. D. (1971). Zero baseline correction of strong-motion accelerograms, *Bull. Seism. Soc. Am.* **61**, 1201–1211.

Appendices

Appendix A:

Tables A-1 and A-2 show the date, moment magnitude, Mpga, Mpgv, latitude, longitude and number of records used in the magnitude estimation for the borehole and surface recording database in Catalog 2.

Table A-1 Estimated magnitude for events with at least 20 records (borehole database, Catalog 2).

Date (dd/mm/yy)	Moment Magnitude	Mpga	Mpgv	Latitude	Longitude	Number of Records
06/10/2000	6.7	6.529	6.898	35.27	133.35	110
31/10/2000	5.5	5.3856	5.2528	34.28	136.34	23
03/11/2002	6.4	6.1617	5.9868	38.89	142.14	34
26/07/2003	6.1	5.9729	6.0869	38.4	141.17	55
26/09/2003	8.1	8.4382	8.596	41.78	144.08	205
26/09/2003	7.3	7.1483	7.3397	41.71	143.69	100
05/09/2004	6.9	6.5364	6.4891	33.03	136.8	37
05/09/2004	7.2	6.7817	6.9213	33.14	137.14	54
23/10/2004	6.6	6.6315	6.6702	37.29	138.87	95
23/10/2004	6.1	6.0013	5.9452	37.35	138.99	40
23/10/2004	5.7	5.9911	5.698	37.25	138.83	34
23/10/2004	6.3	6.3675	6.1338	37.3	138.93	82
25/10/2004	5.6	5.9745	5.5767	37.33	138.95	21
27/10/2004	5.8	6.2741	5.8682	37.29	139.03	51

08/11/2004	5.5	5.2927	5.5899	37.39	139.03	20
29/11/2004	7	7.4844	7.3838	42.94	145.28	76
06/12/2004	6.7	7.1809	6.9601	42.84	145.35	59
18/01/2005	6.2	6.4717	6.4292	42.88	145.01	37
20/03/2005	6.6	6.4046	6.7366	33.73	130.18	78
20/04/2005	5.4	5.6398	5.6921	33.67	130.29	29
16/08/2005	7.1	7.4722	7.1021	38.15	142.28	150
25/03/2007	6.7	6.8776	6.6555	37.22	136.69	48
16/07/2007	6.6	6.4934	6.7643	37.55	138.61	175
14/06/2008	6.9	6.6692	7.0168	39	140.9	135
11/08/2009	6.2	6.531	6.4239	34.8	138.5	96
14/03/2010	6.7	6.3154	6.1661	37.72	141.82	20
13/06/2010	6.2	6.5279	6.0655	37.39	141.8	31
09/03/2011	7.2	6.9106	7.1066	38.33	143.28	23
11/03/2011	7.8	7.1356	7.43	36.1	141.27	101
11/03/2011	9	9.0194	8.8604	38.1	142.86	409
11/03/2011	6.6	6.5431	6.2326	39.16	142.62	77
11/03/2011	7.4	7.0334	7.1242	39.84	142.78	76
12/03/2011	6.2	6.1276	6.3368	36.98	138.6	38
14/03/2011	5.7	5.8525	5.9149	36.45	141.13	25
15/03/2011	5.9	5.407	5.8623	35.3	138.72	45
19/03/2011	5.8	5.7351	5.7491	36.78	140.57	38
23/03/2011	5.4	5.5498	5.2844	37.06	140.77	21
24/03/2011	5.9	6.5688	5.971	39.07	142.36	32
28/03/2011	6.1	6.6958	6.3866	38.39	142.32	30

31/03/2011	6	5.7426	5.7005	38.87	142.09	21
11/04/2011	6.6	6.7872	6.8332	36.94	140.68	140
11/04/2011	5.5	5.5734	5.503	36.96	140.64	28
12/04/2011	5.9	6.0405	5.9101	37.05	140.65	60
23/06/2011	6.7	6.4121	6.5093	39.94	142.59	62
23/07/2011	6.3	6.0716	6.0307	38.87	142.09	32
01/08/2011	5.8	5.933	5.8579	34.7	138.55	33

Table A-2 Estimated magnitude for events with at least 20 records (surface database, Catalog 2).

Date (dd/mm/yy)	Moment Magnitude	Mpga	Mpgv	Latitude	Longitude	Number of Records
06/10/2000	6.7	6.75	6.85	35.27	133.35	53
26/09/2003	8.1	8.33	8.64	41.78	144.08	93
26/09/2003	7.3	6.91	7.41	41.71	143.69	24
23/10/2004	6.6	6.36	6.66	37.29	138.87	38
23/10/2004	6.3	6.34	6.21	37.30	138.93	39
27/10/2004	5.8	5.96	6.01	37.29	139.03	25
29/11/2004	7.0	7.16	7.27	42.94	145.28	36
06/12/2004	6.7	7.11	6.84	42.84	145.35	25
20/03/2005	6.6	6.47	6.63	33.73	130.18	25
16/08/2005	7.1	7.35	7.19	38.15	142.28	64
16/07/2007	6.6	5.88	6.59	37.55	138.61	25
14/06/2008	6.9	6.78	6.80	39.00	140.90	58
11/08/2009	6.2	6.61	6.65	34.80	138.50	40
11/03/2011	7.8	7.25	7.22	36.10	141.27	96
11/03/2011	9.0	9.18	9.05	38.10	142.86	217
11/03/2011	6.6	6.73	6.36	39.16	142.62	34
11/03/2011	7.4	7.04	6.99	39.84	142.78	58
12/03/2011	6.2	6.11	6.43	36.98	138.60	38
14/03/2011	5.7	6.18	6.12	36.45	141.13	26
15/03/2011	5.9	5.82	5.60	35.30	138.72	40

19/03/2011	5.8	5.81	5.78	36.78	140.57	58
23/03/2011	5.4	5.58	5.40	37.06	140.77	30
24/03/2011	5.9	6.03	5.80	39.07	142.36	34
28/03/2011	6.1	6.26	6.20	38.39	142.32	20
11/04/2011	6.6	6.66	6.66	36.94	140.68	154
11/04/2011	5.5	5.50	5.55	36.96	140.64	32
12/04/2011	5.9	6.18	5.89	37.05	140.65	82
23/06/2011	6.7	6.67	6.36	39.94	142.59	44
23/07/2011	6.3	6.02	5.94	38.87	142.09	24
01/08/2011	5.8	5.70	5.88	34.70	138.55	30
21/09/2011	5.1	5.26	5.06	36.73	140.58	20

Appendix B

Table B-1 compares the mean residuals and standard deviations of the predicted magnitude (moment magnitude) using filtered and unfiltered data. Figure A1 shows the predicted magnitude versus moment magnitude for filtered databases.

Table B-1. Mean residuals for the predicted magnitude (moment magnitude) using filtered and unfiltered data.

		$M < 6.5$			$M \geq 6.5$		
		KiK-net	KiK-net	K-net	KiK-net	KiK-net	K-net
		Borehole	Surface		Borehole	Surface	
Filtered data	MP*	0.23±0.34	0.01±0.34	-0.06±0.36	-0.37±0.45	-0.56±0.43	-0.78±0.35
	MS*	0.09±0.27	-0.24±0.31	-0.21±0.31	-0.4±0.28	-0.69±0.30	-0.71±0.30
	MPS*	0.12±0.26	-0.1±0.27	-0.13±0.26	-0.39±0.33	-0.63±0.34	-0.75±0.28
Unfiltered data	MP*	0.28±0.33	0.06±0.34	0.02±0.37	-0.23±0.49	-0.39±0.42	-0.61±0.41
	MS*	0.09±0.24	-0.18±0.30	-0.15±0.28	-0.04±0.19	-0.38±0.23	-0.37±0.27
	MPS*	0.19±0.24	-0.06±0.28	-0.06±0.24	-0.14±0.32	-0.39±0.28	-0.49±0.28

* Range represents one standard deviation.

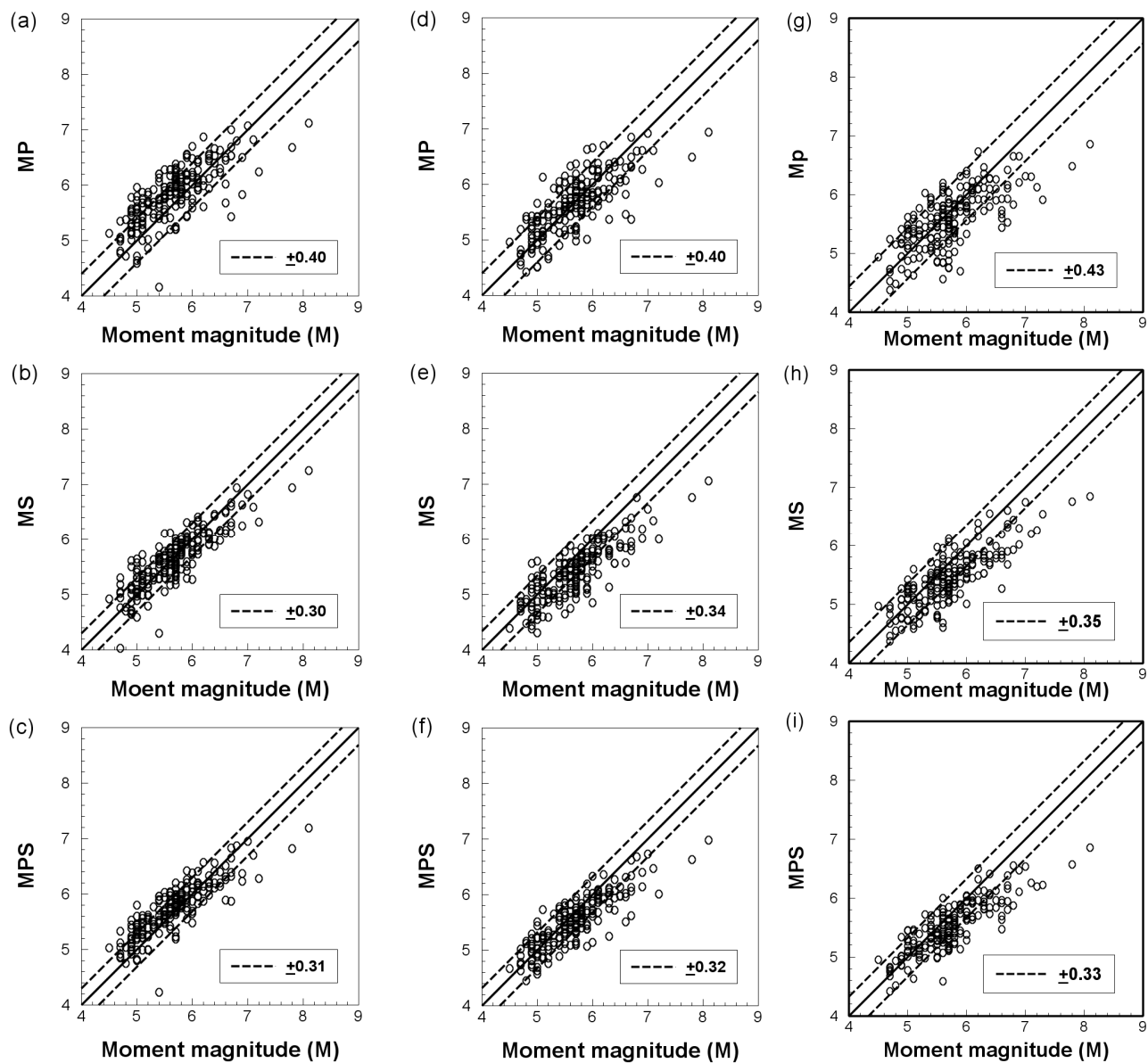


Figure B-1. M versus predicted magnitude (MP, MS and MPS) for the filtered KiK-net borehole database (a, b and c), the filtered KiK-net surface database (d, e and f) and the filtered K-net database (g, h and i). The solid line is the 1:1 relation and dashed lines are one standard deviation.

Appendix C: The computer code

Codes that were used in chapters 1 and 2.

```
% This code reads the PGA and PGV values from borehole recordings of
all events and calculate the Mpga and Mpgv for events with at least 20
records.

clc; clear all; close all
fid=fopen('mw_inp.txt','r'); % borehole data from kiknet from 1998-2011
with pga>10 gal

a          = textscan(fid,'%s %s %f %f %f %f %f %f %f %f
%f',[11,inf]);
dat1.odate1 = a{1};
dat1.fileName1 = a{2};
dat1.depth1   = a{3};
dat1.epil     = a{4};           % epicenter in Km
dat1.mag1     = a{5};           % magnitude
dat1.pga1     = a{6};           % peak ground acceleration in
cm/s2(gal)
dat1.pgv1     = a{7};           % peak velocity in cm/s
dat1.lat1     = a{8};           % event latitude
dat1.long1    = a{9};           % event Longitude
dat1.stlat1   = a{10};          % station latitude
dat1.stlong1  = a{11};          % station Longitude

A=[dat1.mag1 dat1.lat1 dat1.long1 dat1.depth1 dat1.epil dat1.pga1
dat1.pgv1...
dat1.stlat1 dat1.stlong1];%dat1.ta dat1.tv
st1=char(dat1.fileName1);
st=st1(:,1:6);
%station=dat1.fileName1;
ind  = 1;
index = 0;
ne   = 0;           % gives the number of earthquake
that we will use in our calculation for std
nd   = 0;           % gives the earthquake number
nr   = 0;
k    = 0;
while ind ~= 0

    index = index + 1;           % index gives number of
earthquakes

    %
    -----
    indmm = find(A(:,1) == A(1,1) & A(:,2) == A(1,2) & A(:,3) ==
A(1,3) & A(:,4) == A(1,4));
    k = k+indmm(end);
    l= indmm(end);
    lats=unique(dat1.lat1(k-l+1:k)); longs=unique(dat1.long1(k-
l+1:k));mm=unique(dat1.mag1(k-l+1:k));
```

```

ev_dat = unique(dat1.odate1(k-1+1:k));
name=char(ev_dat); name=[name(1:2), '-',name(4:5), '-',name(7:10)];
if size(ev_dat,2) > 1
    indm = strmatch(ev_dat(1),dat1.odate1(indmm));
else
    indm = indmm;
end
% disp(['indm:' num2str(length(indm)) ' - #repeat:'
num2str(size(ev_dat,2))])
%

```

```

no_sta(index,1) = length(indm); % gives number of records
nd = nd + 1;
nn = no_sta(index,1); % +nn;
station=st(1:nn,:);
nr = nr + nn; % gives the number of record for
the earthquake in loop
latlong(nd,1:4)=[ev_dat,lats,longs,mm]; %gives the date,lat, lonf
of the all events

if (nn >= 20)
    ne = ne + 1;
    mag = A(indm,1); lat = A(indm,2); long = A(indm,3); depth =
A(indm,4);
    epi = A(indm,5); pga = A(indm,6); pgv = A(indm,7); stlat =
A(indm,8); stlong = A(indm,9);

    logpga = log10(pga); % logarithm of peak ground motion
    logpgv = log10(pgv);
    logepi = log10(epi); % logarithm of epicentral distance

%%%%%%%%%%%%%%%%%%%%%%%%%%%%%%%%%%%%%%%%%%%%%%%%%%%%%%%%%%%%%%%%%%%%%%%%
dat = inverspga2('mw_inp.txt');
m1 = dat.m1;
mv1 = dat.mv1;
for ii=1:nn
    code(ii,1:6) = station(ii,1:6);
end
magal = zeros(nn,1);
magv1 = zeros(nn,1);
for i = 1:nn
    magal(i,1) = (logpga(i) - m1(1)*logepi(i) - m1(3))
/m1(2) ;
    magv1(i,1) = (logpgv(i) - mv1(1)*logepi(i) - mv1(3))
/mv1(2);
end

epimagal = [epi, magal];
epimagv1 = [epi, magv1];
[ss ,index1] = sortrows(epimagal,1);
[vv1, index3] = sortrows(epimagv1,1);

for i = 1:length(index1)
    ema_sort1(i,:) = epimagal(index1(i,1),:);

```

```

        emv1_sort(i,:) = epimagv1(index3(i,1),:);
    end

    %calculating the average value of magnitude with adding each
record
    for i=1:length(maga1)
        mavel(i,1)=mean(ema_sort1((1:i),2));%mag from acc with 3
variables
        mavev1(i,1)=mean(emv1_sort((1:i),2));%mag from velocity
with 3 variables
    end
    s = size(mag);
    ss = round((s(1)/5));
    j = 1;
    %
%%%%%%%%%%%%%%%%%%%%%%%%%%%%%%%%%%%%%%%%%%%%%%%%%%%%%%%%%%%%%%%%%%%%%%%%
    x = 0;
    %
%%%%%%%%%%%%%%%%%%%%%%%%%%%%%%%%%%%%%%%%%%%%%%%%%%%%%%%%%%%%%%%%%%%%%%%%

    m51 = zeros(ss - 1,1);
    m53 = zeros(ss - 1,1);
    x = zeros(ss - 1,1);
    for i = 1:ss - 1
        m51(i,1) = mean(ema_sort1((1:j + 4), 2));
        m53(i,1) = mean(emv1_sort((1:j + 4), 2));
        x(i,1) = mean(j:j + 4);
        j = j + 5;
    end
    mpa(ne).mp=mavel;
    mpv(ne).mp= mavev1;
    jx(ne).mp=x;
    mw(ne).mp=mag;
    mpre1(ne,1) = mavel(end);
    mpre3(ne,1) = mavev1(end);
    err1(ne,1) = mag(1) - mpre1(ne);
    err3(ne,1) = mag(1) - mpre3(ne);

    out(ne,1:9) =
[mag(1),mpre1(ne),mpre3(ne),lat(1),long(1),ne,nn,nr,index];
    info(ne,1:8) = [mag(1),mpre1(ne),mpre3(ne),ne,nn,nr,index, (nr-
nn)];
    % in output, ne gives the ith earthquake that can inter the
loop
    % calculation, nn gives the number of record for that event nr
gives the number of last record, index gives the number of eq in
catalogue)
    date(ne)=ev_dat;
    mmm=num2str(mag(1));
    name1=[name, '-', mmm];%, 'Mpga'
    clear maga1 maga2 magv1 magv2 m51 m52 m53 m54
    clear long lat mag mavev1 mavel

end
A(indm,:) = []; % delet the readed data to not include them again
if ~isempty(A) % testin if we finishe reading of A

```


Function to find the attenuation parameters.

```

function dat = inverspga(filename)

fid = fopen(filename, 'r');
a = textscan(fid, '%s %s %f %f %f %f %f %f %f %f %f', [11, inf]);
dat.odate      = a{1};
dat.fileName   = a{2};
dat.depth      = a{3};
dat.epi        = a{4};           % epicenter in Km
dat.mag        = a{5};           % magnitude
dat.pga        = a{6};           % peak ground acceleration in
cm/s2(gal)
dat.pgv        = a{7};           % peak velocity in cm/s
dat.lat        = a{8};           % event latitude
dat.long       = a{9};           % event Longitude
dat.stlat      = a{10};          % station latitude
dat.stlong     = a{11};          % station Longitude

logpga         = log10(dat.pga); % logarithm of peak ground motion

%
%%%%%%%%%%%%%%%%%%%%%%%%%%%%%%%%%%%%%%%%%%%%%%%%%%%%%%%%%%%%%%%%%%%%%%%%
%%
%
%%%%%%%%%%%%%%%%%%%%%%%%%%%%%%%%%%%%%%%%%%%%%%%%%%%%%%%%%%%%%%%%%%%%%%%%
%%

logpgv         = log10(dat.pgv);
logepi         = log10(dat.epi);           % logarithm of
epicentral distance
n              = length(dat.mag);
G              = [logepi, dat.mag, ones(n,1)]; % the matrix
with 3 Coefficient [logr, mag, 1]
%G2           = [dat.epi, logepi, dat.mag, ones(n,1)]; % the matrix
with 4 Coefficient [r, logr, mag, 1]
d              = logpga;                 % known
acceleration data
d1            = logpgv;                 % known velocity
data
% calculate the model
m1 = G\d;
dat.prel = G*m1;
dat.err1 = d - dat.prel;
dat.m1   = m1;

%inversion for velocity data
mv1      = G\d1;
dat.mv1  = mv1;
dat.pv1  = G*mv1;
dat.errv1 = d1 - dat.pv1;
dat.stdpgal = sqrt((1/length(dat.err1)*sum((dat.err1).^2)));
dat.stdpgv1 = sqrt((1/length(dat.errv1)*sum((dat.errv1).^2)));

fclose(fid);

```


Codes that were used in Chapter 4.

This code calculates the magnitude from displacement spectra.

```
#!/bin/csh
#2 October 2013, this code will read the records of closest station (kik-net stations) for
each event and will calculate the magnitude using the full P- and S-waves time windows.

set inp=`cat first_KiKB.txt`

foreach i($inp) #1loop

set station=`echo $i | cut -c 1-6`

set folder=`echo $i | cut -c 7-16`

set year=`echo $i | cut -c 17-24`

set year1=`echo 20$year`

set month=`echo $i | cut -c 25-32`

set day=`echo $i | cut -c 33-40`

set time=`echo $i | cut -c 41-48`

set Mw=`echo $i | cut -c 49-56`

set name=`echo $i | cut -c 57-64`

set UDfile=`ls $name*UD*nfil`

set epi=`sacst kuser1 f $UDfile lawk '{print $2}'`

set depth=`sacst kuser2 f $UDfile lawk '{print $2}'`

set lat=`sacst EVLA f $UDfile lawk '{print $2}'`

set long=`sacst EVLO f $UDfile lawk '{print $2}'`

set dt=`sacst delta f $UDfile lawk '{print $2}'`
```

```

set ppk=`sac1st a f $UDfile | awk '{print $2}'`

cd /home/data/Attieh2/Japan/KiK-NET/dir_$_year1

cd $month*

cd 20$folder*

pwd

matlab -nojvm -nosplash << END_matlab

addpath /home/data/Attieh2/Japan/KiK-NET/dir_2000/10-October/20001008131700

clc;clear

fido = fopen('/home/data2/Attieh/Mw-project3/new_method/KiKB/mag_KiKB.txt','a');
fid = fopen('/home/data2/Attieh/Mw-project3/new_method/KiKB/mag $name.txt','w');

lf1=-2; %it is log10(0.01)or min frequency that we want to have fft on that

dlf=0.1; %

lf2=1.18; %max of the log10 (15 hz)

w=10.^(lf1:dlf:lf2); %the ponis where we want fft values on it

ww=10.^(lf1-dlf/2:dlf:lf2+dlf/2);

alt=1/20;%the taping percentage

%%%%%%%%%%%%%%%%%%%%%%%%%%%%%%%%%%%%%%%%%%%%%%%%%%%%%%%%%%
%%%%%%%%%%%%%%%%%%%%%%%%%%%%%%%%%%%%%%%%%%%%%%%%%%%%%%%%%%

R = 6371;

roh = 2700; %density in kg/m3

alpha = 6*1000; %P-wave velocity m/s

beta = 3.5*1000; %(m/s) Shear wave velocity

kp = 0.32;

```

```
ks = 0.21;

dt1=$dt;

epi=$epi;

depth=$depth;

mag=$Mw;

ppk = $ppk;

c0 = [0.1,400,0.1]; % This is my first guess for search parameters

ufp=0.52;

ufs=0.63;

flp = 0.1; fhi=15;

F = 1; %for borehole recordings, 2 for surface recordings
data= dir('$name*1');

x=size(data);

p=x(1);

xx=size(data(1).name);

q=xx(2);

%%%%%%%% find the event information (depth, hypocenter,..)

for ii=1

    [FileName(ii,1:q)]=data(ii).name;

    filename=FileName(ii,1:q);

    dat = Atti_Read(filename);

    time1 = dat.Time_Record;

    depth = dat.Depth;
```

```

odate=dat.Date_Origin;

hight = dat.Station_Height;

depth = depth -(hight*0.001);

h=sqrt(epi^2+depth^2);

hypo = h;

% travel time of the wave being considered

tp = h*1000/alpha;%travel time of P-wave
ts = h*1000/beta; %travel time of S-wave
td = ts-tp; %P-wave window

len = length(dat.Acc);

fs = dat.Sampling_Freq;

dt = 1/fs;

% geometrical spreading

if h>= 50

    h = 1/((1/50)*((50/h).^0.5));

end

end

pw = floor(td);

pk = floor(ppk*fs);

% This part will smooth the spectra for signal and noise, and will find the min frequency
that the signal to noise ratio is higher than 3

%% Define Signal

for ii = 1:p

```

```

[FileName(ii,1:q)]=data(ii).name;

Filename = FileName(ii,1:q);

dat = Atti_Read(filename);

ac = dat.Acc;

len = length(dat.Acc);

fs = dat.Sampling_Freq;

dt = 1/fs;

pk = floor(ppk*fs);

time = 0:dt:(len - 1)*dt;

Acc(ii).sigs = ac(pk:end);%pp+pw*sps

Acc(ii).sigs_l = length(Acc(ii).sigs);

Acc(ii).sigs_t = time(pk:end);

%tapper the signal

Acc(ii).sigs = Acc(ii).sigs.*tukeywin(Acc(ii).sigs_l,alt*2);

Acc(ii).fft_sigs = fft (Acc(ii).sigs, dt, ww,fs);

l(ii)=length(Acc(ii).sigs_t);

for i=1:l

    Acc(ii).freq(i) = (i-1).*fs./l(ii);

end

%% define Noise

Acc(ii).nois = ac(1:pk);

Acc(ii).nois_t = time (1:pk);

Acc(ii).nois_l = length(Acc(ii).nois);

```

```

%tapering should be done before fft is done.

Acc(ii).nois = Acc(ii).nois.*tukeywin(Acc(ii).nois_1,alt*2); % tukeywin is the function
% that matlab has to apply cosine shape to the signal, ns(1) is the length
% of the signal (or noise).

Acc(ii).fft_nois= fft(Acc(ii).nois,dt,ww,fs)*sqrt(Acc(ii).sigs_1/Acc(ii).nois_1);

Acc(ii).fft_noisD= Acc(ii).fft_nois./(2*pi*w).^2;

Acc(ii).nois=dtrend(Acc(ii).nois);

Acc(ii).nois_v = cumtrapz(Acc(ii).nois)*dt;

Acc(ii).nois_v = dtrend(Acc(ii).nois_v);

Acc(ii).nois_d = cumtrapz(Acc(ii).nois_v)*dt;

%Acc(ii).diff = floor((Acc(ii).sigs_1-Acc(ii).nois_1)/2);

Acc(ii).nois_fftD = abs(fft(Acc(ii).nois_d));

Acc(ii).nois_fftD =
Acc(ii).nois_fftD(1:ceil(Acc(ii).nois_1/2))*sqrt(Acc(ii).sigs_1/Acc(ii).nois_1);

for i=1:Acc(ii).nois_1

    Acc(ii).f_nois(i)= (i-1).*fs./Acc(ii).nois_1;

end

%% Signal/Noise ratio

Acc(ii).ratio = Acc(ii).fft_sigs./Acc(ii).fft_nois;

%find the index that the ratio is higher than 2 from that

k(ii) = length(Acc(ii).ratio);

for i=k(ii):-1:1

    if(Acc(ii).ratio(i)>=3)

```

```

        k(ii)=k(ii)-1;
    else
        break
    end
end
end
if k(ii)==0
    k(ii) =1;
    f_min(ii)= floor(1/l(ii));
else
    f_min(ii) = w(k(ii));
end

%find the min freq that the ratio is higher than 3
f_ind(ii) = find(Acc(ii).freq>=f_min(ii), 1 );

num = find(Acc(ii).freq>=15, 1 );

Acc(ii).f = Acc(ii).freq(k(ii):num);

end

%% cut the data for each second coming for P-wave

num = 1;
lb1 = 0.0001;
if (pw>=1)
    for j=1:pw        %1 for
        for ii=1:p    %2 for
            [FileName(ii,1:q)] = data(ii).name;
        end
    end
end

```

```

Filename = FileName(ii,1:q);
dat = Atti_Read(filename);
accf = dat.Acc;
accf = dtrend(accf);
len = length(dat.Acc);
npts = len; delt = dt;
time = 0:dt:(len - 1)*dt;
window(j) = j;
acc(j,ii).tt = time(pk:pk+fs*j);
acc(j,ii).ac = accf(pk:pk+fs*j);
acc(j,ii).l=length(acc(j,ii).tt);
acc(j,ii).ac = acc(j,ii).ac.*tukeywin(acc(j,ii).l,alt*2);
i=1:acc(j,ii).l;
acc(j,ii).freq(i) = (i-1).*fs./acc(j,ii).l;%frequency vector
acc(j,ii).n = find(acc(j,ii).freq>15, 1 );%floor(acc(j,ii).l/2);
indp(ii) = find(acc(j,ii).freq>f_min(ii), 1 );
acc(j,ii).f = (acc(j,ii).freq(indp(ii):acc(j,ii).n))';%frequency vector up to the
Nyquist frequency
l1 = log10(acc(j,ii).f(1));
dlf2 = 0.3;
f = 10.^(l1:dlf2:lf2);
ff = 10.^(l1-dlf2/2:dlf2:lf2+dlf2/2);
acc(j,ii).v = cumtrapz(acc(j,ii).ac)*dt;

```



```

acc(j,ii).v = dtrend(acc(j,ii).v);

%compute the displacment vector

acc(j,ii).disp = cumtrapz(acc(j,ii).v)*dt;

acc(j,ii).fdisp = sm_ftt(acc(j,ii).disp,dt,ff);

ub1 = max(acc(j,ii).fdisp);%Max baound

acc(j,ii).obs_spectra = log10((acc(j,ii).fdisp));

% Find the best-fitting parameter using Nelder-Mead simplex algorithm
[acc(j,ii).cparams] = fit_spectralmodel(acc(j,ii).obs_spectra ,f,tp,c0,lb1,ub1);

% Simulate the best-fitting model

acc(j,ii).sim_spectra = spectralmodel(acc(j,ii).cparams,f,tp);

% Find the best-fitting parameter using Nelder-Mead simplex algorithm
[acc(j,ii).cparams] = fit_spectralmodel(acc(j,ii).obs_spectra ,f,tp,c0,lb1,ub1);

% Simulate the best-fitting model

acc(j,ii).sim_spectra = spectralmodel(acc(j,ii).cparams,f,tp);

%% plot the spectra

%   figure(1)

%   loglog(f,10.^(acc(j,ii).obs_spectra),'ko-','LineWidth',2)

%   hold on

%   loglog(f,10.^(acc(j,ii).sim_spectra),'b','LineWidth',2)

%   loglog(w2,10.^(acc(j,ii).smoot), '*k')

%   hold on

%   loglog(w2,10.^(acc(j,ii).sim_smooth),'g')

%   title(filename)

```



```
\n','Pwave',filename,$year1,$month,$day,$time,mag,epi,depth,$lat,$long>window(j),cpar
m(j).omega,cparm(j).QQ,cparm(j).Fc,rp(j),M0p(j),Mp(j));
```

```
end          %end for 1

if td > floor(td)    %if 1

    delta = td-pw;

    j=j+1;

    for ii=1:p        %for 3

        [FileName(ii,1:q)]=data(ii).name;

        filename=FileName(ii,1:q);

        %[time,accf,p1]=readsac(filename);

        dat = Atti_Read(filename);

        accf = dat.Acc;

        accf = dtrend(accf);

        len = length(dat.Acc);

        fs = dat.Sampling_Freq;

        dt = 1/fs;

        time = 0:dt:(len - 1)*dt;

        window(j) = j;

        window(j) = j-1+(delta);

        acc(j,ii).tt = time(pk:pk+floor(fs*td));%pt

        acc(j,ii).ac = accf(pk:pk+floor(fs*td));

        acc(j,ii).l=length(acc(j).tt);

        acc(j,ii).ac = acc(j,ii).ac.*tukeywin(acc(j,ii).l,alt*2);
```

```

i=1:acc(j,ii).l;

acc(j,ii).freq(i) = (i-1).*fs./acc(j,ii).l;%frequency vector

acc(j,ii).n = find(acc(j,ii).freq>15, 1 );

indp(ii) = find(acc(j,ii).freq> f_min(ii), 1 );

acc(j,ii).f = (acc(j,ii).freq(indp(ii):acc(j,ii).n))';%frequency vector up to the
Nyquist frequency

l1 = log10(acc(j,ii).f(1));

dlf2 = 0.3;

f = 10.^(l1:dlf2:lf2);

ff=10.^(l1-dlf2/2:dlf2:lf2+dlf2/2);

%compute the velocity vector

acc(j,ii).v = cumtrapz(acc(j,ii).ac)*dt;

acc(j,ii).v = dtrend(acc(j,ii).v);

% compute the displacement vector

acc(j,ii).disp = cumtrapz(acc(j,ii).v)*dt;

acc(j,ii).fdisp = sm_ftt(acc(j,ii).disp,dt,ff);

ub1 = max(acc(j,ii).fdisp);

acc(j,ii).obs_spectra = log10(abs(acc(j,ii).fdisp));

% Find the best-fitting parameter using Nelder-Mead simplex algorithm

[acc(j,ii).cparams] = fit_spectralmodel(acc(j,ii).obs_spectra ,f,tp,c0,lb1,ub1);

% Simulate the best-fitting model

acc(j,ii).sim_spectra = spectralmodel(acc(j,ii).cparams,f,tp);

```

```

        % Compute the RMS
        acc(j,ii).rms = Error1(acc(j,ii).cparams,f, tp, acc(j,ii).obs_spectra);

        % low frequency plateau in meter
        acc(j,ii).omega0= acc(j,ii).cparams(1);
        acc(j,ii).Q = acc(j,ii).cparams(2);
        acc(j,ii).fc = acc(j,ii).cparams(3);
    end          %end for 3

    cparm(j).omega =
    sqrt((acc(j,1).omega0.^2)+(acc(j,2).omega0.^2)+(acc(j,3).omega0.^2))*0.01;

    %M0 should be in N.meter which is kg.(m2/s2)

    %mean radiation pattern for p-wave is 0.52 and for s-wave is 0.63
    cparm(j).Fc = (acc(j,1).fc+acc(j,2).fc+acc(j,3).fc)/3;
    cparm(j).QQ = ( acc(j,1).Q+ acc(j,2).Q+ acc(j,3).Q)/3;
    M0p(j) =(4*pi*roh*cparm(j).omega*h*1000*(alpha).^3)/(ufp*F);
    Mp(j) = (log10(M0p(j))-9.05)/1.5;
    Mpfinal(j) = Mp(j);
    rp(j) = (3*kp*beta)/(3*cparm(j).Fc);
    rpfinal (j)= rp(j);

    fprintf(fid,'%s \t %s \t %g \t %g \t %g \t %g \t %g \t %g \t %g \t %g \t %g \t %e \t
    %6.2f \t %6.2f \t %e \t %e \t %g
    \n','Pwave',filename,$year1,$month,$day,$time,mag,epi,depth,$lat,$long>window(j),cpar
    m(j).omega,cparm(j).QQ,cparm(j).Fc,rp(j),M0p(j),Mp(j));

end    %end if

elseif (pw<1)
%When P-wave window is smaller than 1 sec
    j=1;

```

```

for ii = 1:p          %for a
    [FileName(ii,1:q)]=data(ii).name;
    filename=FileName(ii,1:q);
    dat = Atti_Read(filename);
    accf = dat.Acc;
    accf = dtrend(accf);
    len = length(dat.Acc);
    fs = dat.Sampling_Freq;
    dt = 1/fs;
    time = 0:dt:(len - 1)*dt;
    window (j) = (td);
    acc(j,ii).tt = time(pk:pk+ceil(fs*td));
    acc(j,ii).ac = accf(pk:pk+ceil(fs*td));
    acc(j,ii).l = length(acc(j).tt);
    acc(j,ii).ac = acc(j,ii).ac.*tukeywin(acc(j,ii).l,alt*2);
    acc(j,ii).l = 4*acc(j,ii).l;
    l1 = log10(acc(j,ii).f(1));
    dlf2 = 0.3;
    f = 10.^(l1:dlf2:l1); %noghati ke tush fft ra mikhahim
    ff=10.^(l1-dlf2/2:dlf2:l1+dlf2/2);
    i=1:l(j);
    acc(j,ii).freq(i) = (i-1).*fs./acc(j,ii).l;%frequency vector
    acc(j,ii).n = find(acc(j,ii).freq>15, 1 );

```

```

indp(ii) = find(acc(j,ii).freq> f_min(ii), 1 );
acc(j,ii).f = (acc(j,ii).freq(indp(ii):acc(j,ii).n))';

% computes the velocity vector
acc(j,ii).v = cumtrapz(acc(j,ii).ac)*dt;
acc(j,ii).v = dtrend(acc(j,ii).v);

% computes the displacement vector
acc(j,ii).disp = cumtrapz(acc(j,ii).v)*dt;
acc(j,ii).fdisp = sm_ftt(acc(j,ii).disp,dt,ff);
acc(j,ii).obs_spectra = log10(abs(acc(j,ii).fdisp));

% Find the best-fitting parameter using Nelder-Mead simplex algorithm
[acc(j,ii).cparams] = fit_spectralmodel(acc(j,ii).obs_spectra ,f,tp,c0,lb1,ub1);

% Simulate the best-fitting model
acc(j,ii).sim_spectra = spectralmodel(acc(j,ii).cparams,f,tp);

    % Compute the RMS
acc(j,ii).rms = Error1(acc(j,ii).cparams,acc(j,ii).f, tp, acc(j,ii).obs_spectra);

% low frequency plateau in meter
acc(j,ii).omega0= acc(j,ii).cparams(1);
acc(j,ii).Q = acc(j,ii).cparams(2);
acc(j,ii).fc = acc(j,ii).cparams(3);

end          %end for 3

cparm(j).omega =
sqrt((acc(j,1).omega0.^2)+(acc(j,2).omega0.^2)+(acc(j,3).omega0.^2))*0.01;

%M0 should be in N.meter which is kg.(m2/s2)

```

```

%mean radiation pattern for p-wave is 0.52 and for s-wave is 0.63

cparm(j).Fc = (acc(j,1).fc+acc(j,2).fc+acc(j,3).fc)/3;

cparm(j).QQ = ( acc(j,1).Q+ acc(j,2).Q+ acc(j,3).Q)/3;

M0p(j) =(4*pi*roh*cparm(j).omega*h*1000*(alpha).^3)/(ufp*F);

Mp(j) = (log10(M0p(j))-9.05)/1.5;

Mpfinal(j) = Mp(j);

rp(j) = (3*kp*beta)/(3*cparm(j).Fc);

rpfinal (j)= rp(j);

fprintf(fid,'%s \t %s \t %g \t %g \t %g \t %g \t %g \t %g \t %g \t %g \t %g \t %e \t
%6.2f \t %6.2f \t %e \t %e \t %g
\n','Pwave',filename,$year1,$month,$day,$time,mag,epi,depth,$lat,$long>window(j),cpar
m(j).omega,cparm(j).QQ,cparm(j).Fc,rp(j),M0p(j),Mp(j));

    end

S_win1 = ceil((2/cparm(j).Fc)+0.1*hypo);

%the S-wave window starts here

st = pk+ceil(fs*pw);

i = 1;clear time accf p1

%from here we calculate the magnitude for each second of S-wave coming
lb1 = 0.001; % lower bound

for i = 1:S_win1 %for 5

    for ii=1:p %for 6

        [FileName(ii,1:q)]=data(ii).name;

        filename=FileName(ii,1:q);

        dat = Atti_Read(filename);

        accf = dat.Acc;

```



```

accf = dtrend(accf);

len = length(dat.Acc);

fs = dat.Sampling_Freq;

dt = 1/fs;

% accf = bandpass_filter(accf,flp,fhi,len,dt);

time = 0:dt:(len - 1)*dt;

win(i) = i;

accs(i,ii).ac = accf(st:st+fs*(i));

accs(i,ii).tt = time(st:st+fs*(i));

accs(i,ii).l = length(accs(i,ii).tt);

accs(i,ii).ac = accs(i,ii).ac.*tukeywin(accs(i,ii).l,alt*2);

%define the frequency vector

kk = 1:accs(i,ii).l;

accs(i,ii).freq(kk) = (kk-1).*fs./accs(i,ii).l;%frequency vector

accs(i,ii).n = find(accs(i,ii).freq>15, 1 );

inds(ii) = find(accs(i,ii).freq> f_min(ii), 1 );

accs(i,ii).f = (accs(i,ii).freq(inds(ii):accs(i,ii).n))';%frequency vector up to 15 Hz

l1 = log10(accs(i,ii).f(1));

dlf2 = 0.3;

f = 10.^(l1:dlf2:lf2);

ff=10.^(l1-dlf2/2:dlf2:lf2+dlf2/2);

% Compute the velocity vector

accs(i,ii).v = cumtrapz(accs(i,ii).ac)*dt;

```

```

accs(i,ii).v = dtrend(accs(i,ii).v);

%compute the displacement vector

accs(i,ii).disp = cumtrapz(accs(i,ii).v)*dt;

accs(i,ii).fdisp = sm_ftt(accs(i,ii).disp,dt,ff);

ub1 = max(accs(i,ii).fdisp); %upper bound

accs(i,ii).obs_spectra = log10(abs(accs(i,ii).fdisp));

% Find the best-fitting parameter using Nelder-Mead simplex algorithm
[accs(i,ii).cparams] = fit_spectralmodel(accs(i,ii).obs_spectra,f,ts,c0,lb1,ub1);

% Simulate the best-fitting model

accs(i,ii).sim_spectra = spectralmodel(accs(i,ii).cparams,f,ts);

    % Compute the RMS

accs(i,ii).rms = Error1(accs(i,ii).cparams,f,ts,accs(i,ii).obs_spectra);

% low frequency plateau in meter

accs(i,ii).omega0=accs(i,ii).cparams(1);

accs(i,ii).Q =accs(i,ii).cparams(2);

accs(i,ii).fc =accs(i,ii).cparams(3);

end          %end for 6

cparams(i).omega =
sqrt((accs(i,1).omega0.^2)+(accs(i,2).omega0.^2)+(accs(i,3).omega0.^2))*0.01;

cparams(i).Fc = (accs(i,1).fc+accs(i,2).fc+accs(i,3).fc)/3;

cparams(i).QQ = (accs(i,1).Q+accs(i,2).Q+accs(i,3).Q)/3;

M0s(i) =(4*pi*roh*cparams(i).omega*h*1000*(beta).^3)/(ufs*F);

Ms(i) = (log10(M0s(i))-9.05)/1.5;

```

```

Msfinal(i) = Ms(i);

rs(i) = (3*kp*beta)/(3*cparms(i).Fc);

rsfinal(i)= rs(i);

fprintf(fid,'%s \t %s \t %g \t %g \t %g \t %g \t %g \t %g \t %g \t %g \t %g \t %e \t
%6.2f \t %6.2f \t %e \t %e \t %g
\n','Swave',filename,$year1,$month,$day,$time,mag,epi,depth,$lat,$long,win(i),cparms(i)
.omega,cparms(i).QQ,cparms(i).Fc,rs(i),M0s(i),Ms(i));

W = win(i)+window(end);

end %end for 5

Mf = (Mpfinal(end)+Msfinal(end))/2;

rf = (rpfinal(end)+rsfinal(end))/2;

fprintf(fid,'%s \t %s \t %g \t %g \t %g \t %g \t %g \t %g \t %g \t %g \t %g \t %e \t
%g \t','final',filename,$year1,$month,$day,$time,mag,epi,depth,$lat,$long,W,rf,Mf);

fprintf(fido,'%s \t %g \t %g \t %g \t %g \t %g \t %g \t %g \t %g \t %g \t %s \t %g \t %e \t
%g \t %s \t %g \t %e \t %g \t %s \t %g \t %e \t %g
\n',filename,$year1,$month,$day,$time,mag,epi,depth,$lat,$long,'Pwave',window(j),rpfinal
al(end),Mpfinal(end),'Swave',win(i),rsfinal(end),Msfinal(end),'final',W,rf,Mf);

END_matlab

cd /home/data2/Attieh/Mw-project3/new_method/KiKB

end #end foreach i(`cat UDlist.txt`)

```

Functions used in the main code for Chapter 4.

```

%%%%%%%%%%%%%%%%%%%%%%%%%%%%%%%%%%%%%%%%%%%%%%%%%%%%%%%%%%%%%%%%%%%%%%%%
Function to find the parameter that produces the best fit to the observed spectra

function [cparams]=fit_spectralmodel(obs,f,t,c0,lb1,ub1)
%%%%%%%%%%%%%%%%%%%%%%%%%%%%%%%%%%%%%%%%%%%%%%%%%%%%%%%%%%%%%%%%%%%%%%%%
% function [cparams]=fit_spectralmodel(obs,f,t,c0)
% fminsearchbnd3 is FMINSEARCH (that finds minimum of unconstrained
multivariable function using derivative-free method (with Nelder-Mead
simplex direct search algorithm), but with bound constraints by
transformation

%%%%%%%%%%%%%%%%%%%%%%%%%%%%%%%%%%%%%%%%%%%%%%%%%%%%%%%%%%%%%%%%%%%%%%%%

lb=[lb1 0 0.001]; %lower band
ub=[ub1 1000 5]; %uper band

    opts = optimset('TolFun', 1.0e-8);
    cparams = fminsearchbnd3(@Error1,c0,lb,ub,opts,f,t,obs);
end
%%%%%%%%%%%%%%%%%%%%%%%%%%%%%%%%%%%%%%%%%%%%%%%%%%%%%%%%%%%%%%%%%%%%%%%%

function rms = Error1(c, f, t, obs)
% usage: rms = Error(c, f, t, obs)
%
% Calculates the error as the weighted sum of the difference squared.
%
% INPUT
%   c = Model parameters as vector
%   f, t = Data to fit (f is frequency, t is time
%   obs = observations which is displacement for iueh spectra)
%
% OUTPUT
%   rms = Sum of the squared error

    predictedvalues=spectralmodel(c,f,t);
    err = obs-predictedvalues;      % define error as the distance from
the data
    rms = sqrt(sum(err.^2)/length(f)); % sum the error squared

end

```

Curriculum Vitae

Name:	Attieh Eshaghi
Post-secondary Education and Degrees:	Isfahan University of Technology, Isfahan, Iran 2000-2005 B.Sc.
	University of Tehran Tehran, Iran 2005-2008 M.Sc.
	The University of Western Ontario London, Ontario, Canada 2009-2014 Ph.D.
Honors and Awards:	Western Graduate Research Scholarships (WGRS) 2009-2013 Canadian Exploration Geophysical Society (KEGS) Award, 2012 Robert and Ruth Lumsden Graduate Award in Earth Sciences, 2013 Society of Graduate Student (SOGS) Bursary, 2013 Michael A. King award (SOGS), 2014
Related Work Experience	Teaching Assistant, Western University, Canada 2009-2013 Research Assistant, Western University, Canada 2009-2014

Affiliations/Memberships

Student Membership in the Association of Professional Geoscientists of Ontario (APGO),

Student and Prospectors & Developers Association of Canada (PDAC).

Member of Graduate Teaching Assistants (GTA) union, Western's Society of Graduate Students (SOGS) and GGS (Graduate Geosciences Society) at the University of Western Ontario.

Publications:

Eshaghi, A., K. F. Tiampo, H. Ghofrani, G. M. Atkinson, P. Gonsales (2014). Real-Time Moment Magnitude Estimation from Displacement spectra Inversion. Submitted to *Bull. Seism. Soc. Am.* (in review)

Eshaghi, A., K. F. Tiampo, H. Ghofrani, and G. M. Atkinson (2013). Magnitude Estimation for the 2011 Tohoku-Oki Earthquake Based on Ground Motion Prediction Equations, *Pure Appl. Geophys.* doi: 10.1007/s00024-013-0746-y

Eshaghi, A., K. F. Tiampo, H. Ghofrani, G. M. Atkinson (2013). Using Borehole Records to Estimate Magnitude for Earthquake and Tsunami Early-Warning Systems, *Bull. Seism. Soc. Am.* 103. doi:10.1785/0120120319.